The Thesis Committee for Jonathan William Driver
Certifies that this is the approved version of the following thesis:

Tailoring Polymer Molecular Weight Distribution to Pore Size Distribution using Filtration and Mechanical Degradation

APPROVED BY
SUPERVISING COMMITTEE:

Supervisor:

Gary A. Pope

Matthew T. Balhoff

Tailoring Polymer Molecular Weight Distribution to Pore Size Distribution using Filtration and Mechanical Degradation

by

Jonathan William Driver

Thesis

Presented to the Faculty of the Graduate School of

The University of Texas at Austin

in Partial Fulfillment

of the Requirements

for the Degree of

Master of Science in Engineering

The University of Texas at Austin

August 2017

Dedication

To my parents, grandparents and sister.

Acknowledgements

As someone who changed careers, I have a long list of people to thank who helped me along the way. My adviser, Dr. Pope, is at the top of the list. He saw my potential despite my unconventional background and extended the opportunity to me for a funded education, and had a direct hand in paving the way for me into an industry position. My parents, family and I will always be grateful to him.

Speaking of my parents, they have been unwaveringly supportive of me throughout this process, giving of their time, energy, and occasional financial assistance. One of the many reasons I made a change was so that I could have the opportunity to live and work near my family. That has been a true joy these past two years, and it looks to continue. I am also thankful for the continued love of my grandparents who live near Austin. Seeing more of them has been a gift, and they have repeatedly offered to help me if I ever needed it. I would also like to acknowledge anyone who lent me their advice over the course of this transition, including, but by no means limited to, my friends Matthew Zimmerman and Kenneth Jamison.

I would be remiss if I did not mention my previous, postdoctoral adviser, Dr. Charles "Chip" Asbury of the University of Washington department of Physiology and Biophysics. He was extremely kind and supportive of me making a move that is both unusual and difficult to make. His letter of support for my application to the University of Texas was undoubtedly helpful. By the same token, I would like to thank my other letter writers: my previous graduate adviser, Dr. Michael Diehl, and my co-adviser, Dr. Anatoly Kolomeisky, both of Rice University. All of these past mentors have helped shape my future.

Abstract

Tailoring Polymer Molecular Weight Distribution to Pore Size Distribution using Filtration and Mechanical Degradation

Jonathan William Driver, M. S. E.

The University of Texas at Austin, 2017

Supervisor: Gary A. Pope

High molecular weight polymers are used for mobility control during oil recovery operations. The cost effectiveness of polymer solutions improves as the molecular weight of the polymer increases, but very high molecular weight polymers can be as large in solution as the throats of the pores that support transport. An envelope exists in pore size and permeability that marks the limits of transport without plugging for polymers of different sizes. The concept of a polymer's "size" is a complicated one; polymers adopt non-spherical shapes in solution, a distribution of molecular weights is present in any given solution, and the exact relationship between a polymer's apparent size and the size of pores as inferred from mercury injection capillary pressure is unclear. This study contends that filter plugging is the most practical measurement of the sizes of polymers in a polymer solution, and builds a quantitative theory to maximize the quality of the information extracted. Specifically, the most effective size characterization method is the filtration pore size assay, in which plugging of a polymer solution is measured on filters across a range of pore sizes. The utility of this assay is demonstrated in comparisons of polymer shearing, variations in salinity, post-hydrolysis, and filtration processing. It is shown that mechanical

degradation of polymer solutions shifts the high molecular weight tail of the polymer size distribution without appreciably reshaping it, that swelling by salinity and hydrolysis has a differential effect on plugging at large and small pore sizes, and that serial filtration can produce high-quality, high-viscosity polymer solutions that cannot be produced from a single filtration. Furthermore, mechanical degradation and serial filtration can be used in combination to produce polymer solutions that can be filtered at extremely small pore sizes, down to one tenth of a micrometer in diameter, with surprising retention of viscosity that makes them suitable for chemical EOR core floods. Single phase core floods with HPAM and scleroglucan are used to assay the limits of transport without plugging, while a successful surfactant flood in a seventeen millidarcy reservoir carbonate core proves the power of the optimized tight-filtration technique.

Table of Contents

List of Tables

List of Figures

1 Introduction

1.1 Background

Hydrocarbons are oxidizable chemical species derived from plant, algal and planktonic matter preserved from ancient depositional environments (e.g. deltas, turbidites, anoxic lakes). Though typically sourced in impermeable rocks (shales), buoyancy forces induce hydrocarbons to migrate toward the surface. Along the way, they migrate through the pore spaces of higher permeability sedimentary rocks (typically sandstones and limestones) until they encounter another impermeable rock or some other seal, such as a fault. They can thus remain trapped for some time in rocks that will permit rapid flow, the setting of a conventional oil and gas reservoir. The same buoyancy forces that cause the hydrocarbons to initially migrate toward the surface cause a buildup of pressure in the reservoir that is harnessed during primary recovery to drive hydrocarbons laterally toward the wellbore and then up the well.

Naturally, conservation of energy dictates that the pressure declines as the recovery operation proceeds. Often the first consideration that halts primary recovery is that the bubble point of the liquid hydrocarbons is reached, below which a third, gaseous phase will emerge and adversely affect the fractional flow behavior of the water and oil. Primary recovery typically nets ~20% of oil initially in place (OIIP). To maintain pressure, water is injected into the reservoir at separate injection wells (secondary recovery), displacing the oil. Unfortunately, this displacement is sometimes unstable, meaning that the more mobile water macroscopically channels through and bypasses the oil as it migrates to the

production well. The displacement is also inefficient at the pore level when the mobility of the water is higher than the oil. Water cut at the production well can thus increase quickly after secondary recovery begins, resulting in an economic limit for secondary recovery that typically amounts to around another 20% of OIIP.

To economically (quickly) produce more oil, the mobility of the water injected can be reduced by adding large, water-soluble polymers that increase solution viscosity many fold. This can be done alone or in conjunction with other elements of enhanced recovery process such as surfactants. Like most chemicals used in tertiary oil recovery, polymers are susceptible to retention in the reservoir. Retention refers simply to polymer that remains in the reservoir after injection, and it occurs by more than one mechanism. The polymers can non-covalently adsorb onto the rock as a result of chemical attractions between the polymer and the surface-exposed minerals. This must be kept below a certain threshold for economically viable recovery. Polymer can also become trapped in the pore throats of the rock if the hydrodynamic size of the polymer is similar to or larger than that of the throat. This produces a conundrum: higher molecular weight makes a polymer more efficient as a viscosifying agent and therefore more economical, but more prone to retention by the plugging mechanism. The optimal polymer flood is one that uses the highest molecular weight polymer that will not plug the reservoir rock.

1.2 Objective

The objective of this research was to delineate guidelines and procedures for the selection and preparation of polymers for enhanced oil recovery. Preparation principally refers to filtration and mechanical degradation processes. The idea is that pore size information derived from measurements such as mercury intrusion capillary pressure (MICP) can be used to predict the maximum size of the polymer that can be injected, and that filters can be used to remove polymer that is too large. Custom sized polymers that will filter without excessive loss of mass can be created by shearing commercially-available products. The process entails optimizing the size of the polymer to the required filter. The success of the procedure is validated using core floods.

2 Literature Review

2.1 Polymers for EOR

2.1.1 Partially-hydrolyzed Polyacrylamide (HPAM)

The most commonly used polymer in enhanced oil recovery is partially-hydrolyzed polyacrylamide, a semi-random co-polymer of acrylamide and acrylic acid (Sorbie, 1991). A typical commercial product is synthesized from mixtures of both monomers (~70% acrylamide, 30% acrylic acid) using radical chain growth polymerization chemistry (Figure 2-1).

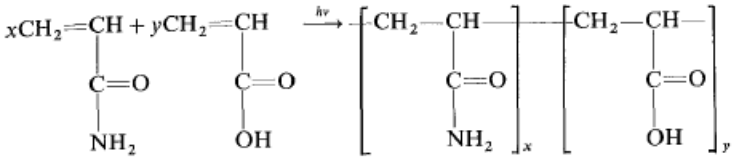

Figure 2-1: Radical Copolymerization of HPAM (Sorbie, 1991)

In such a synthesis scheme, monomers add one at a time to the ends of growing chains, each of which is started by an initiator molecule that is distinct from the monomers. The average molecular weight of product polymer chains is easily controlled by adjusting the ratio of monomers to initiators; if there are 1000 monomers for each molecule of initiator, the average chain will contain 1000 monomers (neglecting side reactions and incomplete initiation), and the average molecular weight will be 1000 times the mass of the monomer.

$$\bar{M}_n = \sum_i x_i M_i = \frac{[M]_o}{[I]_o} \qquad [2\text{-}1]$$

The distribution of molecular weights depends upon the mechanism by which termination occurs. For termination by combination (desirable), the mole fraction of *i*-mers in the molecular weight distribution can be written as a function of the degree of polymerization, *p* (Hiemenz & Lodge, 2007).

$$x_i = (i-1)(1-p)^2 p^{i-2} \qquad [2\text{-}2]$$

Plots of mole fraction of *i*-mer for various values of *p* are shown in Figure 2-2.

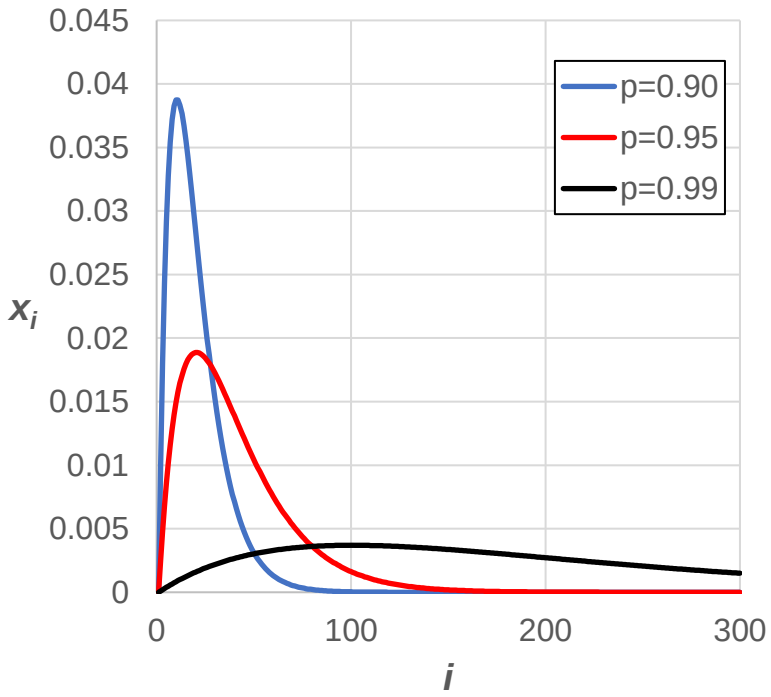

Figure 2-2: Mole fraction of i-mers from radical polymerization terminated by combination

The weight-averaged molecular weight of a polymer is defined below, from which a polymer solution's polydispersity index is derived. The polydispersity index (*I*) is a measure of the width of the molecular weight distribution.

$$[\,2\text{-}3\,] \qquad \bar{M}_w = \sum_i x_i M_i^2$$

$$[\,2\text{-}4\,] \qquad I = \frac{\bar{M}_w}{\bar{M}_n} = \frac{\sum_i x_i M_i^2}{\sum_i x_i M_i}$$

For radical polymerization terminating by combination, as $p \rightarrow 1$, $I \rightarrow 1.5$ (Hiemenz & Lodge, 2007). This provides an easily-defined limit on the narrowness of the molecular weight distribution produced by the chain growth polymerization. The polydispersity index for other termination mechanisms (e.g. disproportionation) is higher. Irreducible polydispersity of the synthesized polymer explains why plugging may occur during filtration or transport in porous media, even though the nominal (average) size of the polymer would indicate that none should occur.

As a material in solution, HPAM is a hydrophilic, flexible chain. The degree to which it swells is a function of the ionic species present in solution (e.g. Na^+, K^+, Ca^{++}, Mg^{++}) and the degree of hydrolysis, both discussed later in this literature review. The more the polymer swells, the more viscous the solution. As a result of its flexibility, HPAM is a highly viscoelastic material (considerable Hookean character) at higher molecular weights and greater degrees of swelling. It is also prone to mechanical shear degradation by scission of the polymer backbone, with significant loss of viscosity from the surface to the reservoir observed in the field (Morel, Vert, Jouenne, & Nahas, 2008). As divalent cations interact with the acidic groups within the co-polymer, susceptibility to precipitation

is an increasing function of the degree of hydrolysis of the polymer. Hydrolysis-resistant analogues of HPAM (AMPS and NVP) have been devised to address this problem for chemically challenging polymer applications (Levitt & Pope, 2008).

2.1.2 Scleroglucan

Scleroglucan is a glucose-derived biopolymer produced by the fungus *Sclerotium rolfsii* during fermentation (Rehm, 2009). Its primary structure is a linear chain of β-1,3-D-glucopyranose residues with a β-1,6 residue as a side chain on every third main chain unit (Figure 2-3) (Zentz, Verchere, & Muller, 1992). This primary structure is identical to that of schizophyllan, which is produced by a different fungus and is also used in EOR.

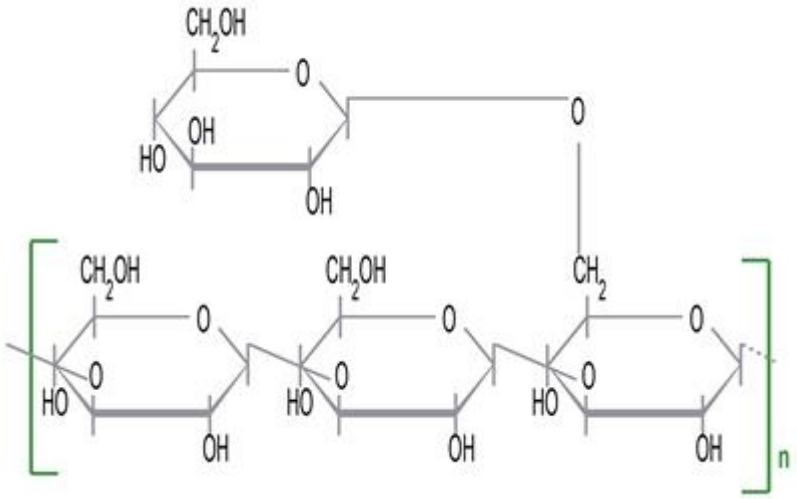

Figure 2-3: Scleroglucan molecular structure (Cargill)

The polymer is rod-like in structure, and forms a triple helix in solution under most conditions. It is used in the cosmetics and personal care industries in addition to its use in

the oil and gas industry as an EOR polymer. Scleroglucan is non-ionic, and as a result, the swelling of the polymer is not affected significantly by brine composition or pH (Rivenq, Donche, & Noik, 1992). Among over 140 candidate polymers tested in a study in the early 1980s, scleroglucan was deemed the most promising for application in the North Sea because of its combination of viscosifying power, brine and temperature tolerance (Davison & Mentzer, 1982). It is therefore being marketed for polymer floods using high-salinity and/or hard brines. The molecular weight of the scleroglucan triple helix manufactured by Cargill and used in this study is 3 MDa. Scleroglucan is resistant to mechanical shear degradation and very (reversibly) shear thinning owing to the semi-rigid-rod structure of the molecule in solution. Scleroglucan is very susceptible to free radical degradation at high temperature because the acetal carbon (connected to the bridging oxygen) is able to stabilize the product species through resonance (Kalpakci, Jeans, Magri, & Padolewski, 1990). As such, care must be taken during experiments to purge all oxygen from the polymer solution, and cores must be reduced with a strong reducing agent like sodium dithionite (Wellington, 1983). Since reservoirs are oxygen-depleted, reducing environments, this is less of an issue in the field.

The primary difficulty with scleroglucan has been filterability and transport (Kulawardana, et al., 2012). Even very recent attempts with scleroglucan polymer solutions that filter well have plugged medium permeability reservoir cores (Lee, 2015). This lack of correspondence has been puzzling, perhaps owing to the large disparity in the shear rates experienced by a polymer solution during filtration versus during a core flood.

An inverse relationship between plugging behavior and filtration rate was reported long ago for another biopolymer, xanthan gum (Kohler & Chauveteau, 1981).

2.2 Polymer Rheology

2.2.1 Origins of Polymer Solution Viscosity

Polymer solutions can be extraordinarily viscous despite consisting of less than 1% polymer by weight. The polymer swells with water in solution, but water cannot flow through the swollen polymer, so shearing flows must travel between polymer molecules. This accounts for the outsized effect relative to the dry weight of polymer; its effect is governed by its swollen volume fraction in solution.

Albert Einstein investigated the rheological effect of rigid spheres in liquid from 1906-1911, developing his famous viscosity equation that relates the viscosity of a solution to the solvent viscosity (η_S) and the volume fraction of suspended spheres (φ) (Hiemenz & Lodge, 2007).

$$\eta = \eta_S(1 + 2.5\,\phi + 4\,\phi^2 + \cdots) \qquad [\,2\text{-}5\,]$$

Because the coefficients are known constants, this equation is quite useful for determining the effective size of a polymer in solution. One can write an analogous power series relation in polymer concentration with a new quantity, $[\eta]$, known as the polymer's *intrinsic viscosity*. The intrinsic viscosity is a measure of its size in solution relative to its mass, and therefore has dimensions of L^3/M.

$$\eta = \eta_S(1 + [\eta]\,c + k_h\,[\eta]^2 c^2 + \cdots) \qquad [\,2\text{-}6\,]$$

Intrinsic viscosity is typically defined from the equation above, taken to the limit of zero concentration.

$$[\eta] = \lim_{c \to 0} \frac{\eta/\eta_S - 1}{c} = \lim_{c \to 0} \eta_{red} \qquad [2\text{-}7]$$

Comparing the two formulations of Einstein's viscosity equation, it is clear that intrinsic viscosity relates to volume fraction directly through the linear terms. Volume fraction, in turn, can be generally written in terms of mass concentration, molecular weight, and hydrated volume.

$$\phi = \frac{c}{M} N_{av} V_h \qquad [2\text{-}8]$$

This yields an expression for hydrated volume in terms of intrinsic viscosity.

$$V_h = \frac{2\,[\eta] M}{5\,N_{av}} \qquad [2\text{-}9]$$

We can also use a spherical description of the polymer to derive an expression for its radius of gyration.

$$R_g = \sqrt[3]{\frac{3\,[\eta] M}{10\,\pi\,N_{av}}} \qquad [2\text{-}10]$$

Alternatively, this can be arranged to qualitatively relate intrinsic viscosity to molecular weight (Hiemenz & Lodge, 2007).

$$[\eta] \propto \frac{{R_g}^3}{M} \sim \frac{M^{3\nu}}{M} \sim M^{3\nu - 1} \qquad [2\text{-}11]$$

The parameter *v* is an indicator of the actual shape of the polymer in solution. It should be 1/3 for a rigid sphere and 1 for a rigid rod, with intermediate values indicating intermediate conformations. This relation is the basis of the phenomenological Mark-Houwink Equation (Sorbie, 1991).

$$[\eta] = kM^{\alpha} \qquad [2\text{-}12]$$

Information about the shape of the polymer is now embedded in the parameter α, which should be 0 for a sphere and 2 for a rod.

2.2.2 Modeling the Rheological Behavior of Polymer Solutions

Polymer solutions are viscoelastic, owing both to elastic deformation of individual polymer molecules and the existence of temporary linkages between molecules. Popular models of polymer solutions and melts are founded on descriptions of the time evolution of linkages in response to stresses, yielding testable predictions of solution responses to a large number of qualitatively different stress tests. The most popular model was developed by Pierre J. Carreau (Carreau, 1972). The polymer solutions used in this study and EOR in general are above the entanglement threshold for polymer concentration, so these temporary linkage models are likely to be mechanistically accurate.

The most basic rheological test of importance is the steady shear stress test. Under constant flow and saturation, injected polymer is subject to temporally (though not spatially) invariant shear stress in a core or reservoir. This viscous response is typically modeled with a modified power law.

$$\eta_{eff} = \eta_{\infty} + \frac{\eta_o - \eta_{\infty}}{1 + (\lambda \dot{\gamma}_{eff})^n} \qquad [2\text{-}13]$$

The viscosity approaches η_o in the limit of zero shear rate and η_∞ (solvent viscosity) in the limit of infinite shear rate. Measurements of intrinsic viscosity utilize η_o. The sensitivity to shear rate, captured by the parameters λ and n, is related to the shape of the polymer in

solution, its molecular-level deformation in response to shearing flows, and the rate of temporary linkage formation and rupture.

Numerous models of the shear stress imposed on solutions flowing through porous media have been developed. This brief review is restricted to a semi-mechanistic description known as the effective capillary tube model, in which a porous medium is described as a single effective capillary tube with an apparent shear rate (Cannella, Huh, & Seright, 1988).

$$\dot{\gamma}_{app} = C\left(\frac{3n+1}{4n}\right)^{\frac{n}{n-1}} \frac{u}{\sqrt{k\phi}} \qquad [\,2\text{-}14\,]$$

Remarkably, this simple model is quite effective, though determination of the fit parameter *C* requires steady state pressure measurements with polymer solution at multiple flow rates.

2.2.3 Ion Effects

Salts reduce the swelling of HPAM in solution, presumably by cation coordination with hydrolyzed, acidic side chains. Unscreened negative charges on polymer require hydration, a phenomenon analogous to clay swelling in porous media. Divalent cations are particularly effective as they can associate with two acidic residues at once, exponentially increasing the overall persistence in time. The thermodynamics of polymer mixing with a solvent can be written as a sum of ideal and non-ideal terms (Hiemenz & Lodge, 2007).

$$\frac{\Delta G_m}{RT} = \phi_1 \ln \phi_1 + \frac{\phi_2}{N} \ln \phi_2 + \phi_1 \phi_2 \chi \qquad [\,2\text{-}15\,]$$

Here, components 1 and 2 are the solvent and polymer, respectively, φ is the volume ratio of a component and N is ratio of the molar volume of the polymer to the solvent. The first two terms are entropic and always negative (favorable). The third term with the parameter χ reflects the enthalpic contribution of polymer-solvent interaction. When $\chi < 0$, enthalpy favors mixing. An "ideal" solvent is a solvent for which mixing is purely entropically driven ($\chi = 0$). A solvent's deviation from ideality is reflected in the polymer's shape in solution and therefore in its Mark-Houwink exponential parameter, α. A polymer in an ideal solvent has a spherical shape ($\alpha = 0.5$). As the enthalpic interaction between the polymer and the solvent strengthens, the polymer adopts an ever more rod-like shape ($\alpha >$ 0.5, tending towards 2). HPAM solutions under common brine conditions can have α in the 0.6-0.8 range, while α is around 1 for scleroglucan. High salinity HPAM solutions approximate enthalpically neutral mixing.

With swelling comes an increase in the radius of gyration of a polymer, and therefore an increase in solution viscosity. Innumerable papers and dissertations have elucidated the effect of common salts on viscosity. Qualitatively, viscosity decreases rapidly as a salt is added to fresh water, after which a plateau is reached where charge screening within the polymer is satisfied. The amount of the salt required to achieve this varies depending on the cation. Quantitatively, the effect of salts can be described by a power law dependence with respect to effective salinity, with model fit parameters that capture the potency of the screening effect (Flory, 1953).

2.2.4 Hydrolysis

Hydrolysis (proportion of acrylate moieties) of an HPAM polymer promotes swelling of the polymer much as the presence of cations reduces swelling. Higher degrees of hydrolysis mean a higher density of negative charges which, unless screened, repel one another (Martin & Sherwood, 1975). The degree of hydrolysis also governs precipitation of the polymer in response to divalent cations that coordinate with the hydrolyzed (acrylate) side chains.

Hydrolysis of the amide side chains proceeds spontaneously at both low and high pH and elevated temperature. High or low pH promotes hydrolysis because, like many hydrolysis reactions in organic chemistry, it can be either acid- or base-catalyzed. Low pH drives protonation of the amide, while high pH drives nucleophilic attack of the carbonyl. As hydrolysis of the polymer proceeds, the kinetics at high pH become self-retarding because acrylate moieties that are formed repel hydroxide attacks on neighboring amide groups, making a degree of hydrolysis greater than 67% difficult to achieve in the laboratory (Levitt, Pope, & Jouenne, 2011). The opposite is true at low pH, where further hydrolysis is promoted by neighboring groups. Hydrolysis can also proceed to completion at high temperature (100ºC) and neutral pH over the course of months. The initial rate of hydrolysis in any case is a complex function of the initial degree of hydrolysis, the ordering of hydrolyzed and unhydrolyzed residues in the polymer, pH/buffering, and temperature. The degree of hydrolysis of HPAM can be measured directly using NMR (Levitt, 2009); quantitative inference through viscosity is not recommended, as differing, sometimes non-monotonic trends are observed depending on salt conditions.

2.3 Shear Degradation of Polymers

High molecular weight polymers are widely known to be susceptible to irreversible mechanical shear degradation, a phenomenon observed both in the laboratory and in the field. In the field, degradation occurs primarily in surface equipment, chokes, and perforations. Morel et al. (2008) measured the degradation of 18 MDa HPAM in seawater through a field choke, and observed a 50% loss of viscosity at high polymer concentration. Mechanical degradation has also been studied in laboratory cores and blenders. Degradation in cores requires extremely high flow rates, and is therefore only pertinent in the near wellbore region. While generally thought of as deleterious, mechanical degradation can improve polymer filterability and can therefore be desirable in some contexts.

During mechanical degradation, polymer undergoes scission of its backbone to produce two radical species. The force required to break the bond is thus directly related to the strength of the bonds that make up the backbone, i.e. the energy required for heterolytic cleavage. While the degradation is generally called “shear degradation”, there is good evidence that a major cause of degradation is extensional flows that exist in most shearing devices (Al Hashmi, et al., 2013; Jouenne, Chakibi, & Levitt, 2015; Maerker, 1975; Southwick & Manke, 1988). Polymer elongation in extensional flows has been observed by birefringence, and scission has been shown to occur around the midpoint where hydrodynamic forces are highest, with resultant molecular weight distributions consistent with this hypothesis (Horn & Merrill, 1984).

Mechanical degradation is widely reported to vary with polymer molecular weight, concentration, and brine conditions. A weakness in the current literature is that when polymer degraded under condition X (concentration, brine) is compared to polymer degraded under condition Y, the pre- and post-degradation samples are not compared under the same conditions. A more transparent study could be conducted in which both samples are diluted to the same condition Z for rheological comparison, so that the only difference between the two samples is molecular weight. With that said, degradation is almost universally reported to increase in the presence of high salt, particularly divalent cations like Ca^{++} and Mg^{++} (Maerker, 1975; Noik, Delaplace, & Muller, 1995; Zaitoun, et al., 2012). The exact mechanism by which this occurs remains elusive. It could be that divalent cations directly chemically promote cleavage somehow. It might also be of interest that divalent cations precipitously reduce the elastic modulus of a polymer solution. This elastic modulus is what resists the development of sharp extensional flows that seem to be an important cause of degradation. At low salinity and hardness, modified HPAMs exhibit greater resistance to mechanical degradation at equal solution viscosity (Zaitoun, et al., 2012).

Empirically, mechanical degradation is asymptotic in time. That is, the observed loss of viscosity as a function of the amount of time that a polymer solution spends in a blender or the number of passes through a valve appears to approach a plateau below which the device cannot degrade (Jouenne, Chakibi, & Levitt, 2015; Mansour, Al-Maamari, Al-Hashmi, Zaitoun, & Al-Sharji, 2014). The higher the shear rate through the device, the lower this viscosity plateau is. For the experiments in this thesis, polymer solutions are

deliberately sheared to improve filterability, and blender time and speed are calibrated for reproducible viscosity and filtration behavior.

2.4 Filtration of Polymers

Filtration of polymers is used in the laboratory and in the field to measure the quality of a polymer solution, and to condition it for transport. In the field, filtration is often used to remove large microgels and impurities, whereas in the laboratory filtration is used for both microgel removal and for shaping the molecular weight distribution of monodisperse polymer.

The idea of using analytical filtration to measure polymer size is a common and old one (Gogarty, 1967). Fang et al. (2015) identify what they term to be the "inflection" in polymer effluent and viscosity data for various weights of HPAM polymer in different brines, yielding a positive trend in the apparent size on paper with polymer molecular weight and a negative trend with increasing salinity. The method for identifying the inflection is not explained, and it is worth noting that unacceptable plugging by polymer solutions likely occurs before the inflection.

In order to use filtration as a tool and technique that produces interpretable results, we must embrace a quantitative theory that describes what it does. The UT filtration ratio test has been the empirically validated metric in our laboratory for decades, but it is inflexible in the sense that very specific volumes are required for the measurement. It is also unclear as to exactly what the ratio measures, besides some normalized, accumulated resistance. In his UT master's thesis, Dana Wreath states that classical theory would

predict that a plot of filtered volume versus the square root of time should be linear (Wreath, 1989). This is nearly but not precisely correct, and a careful treatment of the theory shows what the true dependence should be.

It is experimentally observable that the plugging of a filter occurs in stages. During the first stage, the resistance of the filter increases linearly with the filtered volume; thereafter, the loss of permeability accelerates. Our purpose is to characterize the first, *linear* plugging regime, and to relate that to plugging in porous media. A theory to describe the initial, linear plugging of filters was developed within the water quality industry many years ago, and it begins by expressing the permeability of the filter as a linear function of the filtered volume (Dillon, Pavelic, Massmann, Barry, & Correll, 2001).

$$\kappa = L/\left(R_f + R_{plug}\right) = L/\left(R_f + V\,I/A\right) \qquad [\,2\text{-}16\,]$$

Permeability is inversely proportional to the total resistance to flow, which is taken as the sum of an intrinsic resistance of the filter and a resistance due to plugging, which is proportional to the filtered volume and inversely proportional to the filter area. The parameter *I*, which has units of inverse area, is an intensive quantity that describes plugging. Using Eq. [2-16], we can add a description of plugging to Darcy's Law, which can be easily rearranged and integrated to relate cumulative time to filtered volume.

$$Q = \frac{dV}{dt} = \frac{\kappa\,A\,\Delta P}{\mu\,L} \qquad [\,2\text{-}17\,]$$

$$\frac{dt}{dV} = \frac{\mu\,L}{\kappa\,A\,\Delta P} \qquad [\,2\text{-}18\,]$$

$$\int_0^T dt = \int_0^V \frac{\mu}{A\,\Delta P}\left(R_f + \frac{V\,I}{A}\right) dV \qquad [\,2\text{-}19\,]$$

[2-20] $$t[s] = \frac{\mu[cP]\, V[cm^3]}{A[cm^2]\, \Delta P[atm]} \left(R_f[cm^{-1}] + \frac{1}{2} \frac{I[cm^{-2}]}{A[cm^2]} V[cm^3] \right)$$

[2-21] $$t[s] = \frac{\mu[cP]\, H[cm]}{\Delta P\ [atm]} \left(R_f[cm^{-1}] + \frac{1}{2} I[cm^{-2}]\, H[cm] \right)$$

Equation [2-21] is equivalent to [2-20] with $H = V/A$ (the height of the head is equal to the volume divided by the filter area), which would be more useful when relating results from different diameter filters (or rocks). Both of these equations are simple quadratic functions in V. If one fits the filtration data to a quadratic equation of the form $t = ½\ a\ V^2 + b\ V + c$, the quantity 2a/b, named β here, is (using [2-20]):

[2-22] $$\beta[cm^{-3}] = \frac{I[cm^{-2}]}{A[cm^2]\, R_f[cm^{-1}]}$$

This parameter is a function of I, the true plugging parameter, and R_f, the original resistance of the filter. To gain some insight into its meaning, we can rearrange [2-16]:

[2-23] $$\kappa = \frac{L}{R_f + V\, I/A} = \frac{L/R_f}{1 + V\, I/(A\, R_f)} = \frac{\kappa_o}{1 + \beta V}$$

The parameter β therefore straightforwardly quantitates the fall in permeability in the linear plugging regime.

Examining the quadratic relationship for t, it should be clear that $\sqrt{t} \propto V$ for large V, but not for small V. At small V, the time course is dominated by the initial, unplugged resistance of the filter (R_f) to the polymer solution. This is the likely source of the deviation from prediction in Wreath's plots and reconciles the theory with the data presented in this thesis.

For low pressure drop data, it may be desirable to correct for the loss of hydrostatic head through the filter. This can be accomplished by substituting for the pressure drop in the integrand in the derivation of [2-20].

$$[\ 2\text{-}24\ ] \qquad \int_0^T dt = \int_0^V \frac{\mu}{A\,\Delta P_o - G*V}\left(R_f + \frac{V\,I}{A}\right) dV$$

The hydrostatic gradient is G. This can be integrated to yield:

$$[\ 2\text{-}25\ ] \qquad t = \mu\left(\frac{I\,\Delta P_o + G R_f}{G^2}\ ln\frac{A\,\Delta P_o}{A\,\Delta P_o - G\,V} - \frac{I\,V}{A\,G}\right)$$

Expressed in terms of the fitting variables (a, b) from before, and defining $F_o = A\,\Delta P_o$:

$$[\ 2\text{-}26\ ] \qquad t = \frac{b\,{F_o}^2 + G\,a\,F_o}{G^2}\ ln\frac{F_o}{F_o - G\,V} - \frac{b\,F_o\,V}{G}$$

In practice, this correction has little effect when the applied pressure is over 1 psi.

This filtration theory can be applied to filtration ratio measurements. Filtration ratio is defined as the interval time from 180 mL to 200 mL divided by the interval time from 60 mL to 80 mL. This can be related to β in our model using [2-20].

$$[\ 2\text{-}27\ ] \qquad FR_\beta = \frac{\frac{\mu\,200\ mL}{A\,\Delta P}\left(R_f + \frac{1I}{2A}200\ mL\right) - \frac{\mu\,180\ mL}{A\,\Delta P}\left(R_f + \frac{1I}{2A}180\ mL\right)}{\frac{\mu\,80\ mL}{A\,\Delta P}\left(R_f + \frac{1I}{2A}80\ mL\right) - \frac{\mu\,60\ mL}{A\,\Delta P}\left(R_f + \frac{1I}{2A}60\ mL\right)}$$

$$[\ 2\text{-}28\ ] \qquad FR_\beta = \frac{200\ mL\left(1 + \frac{1}{2}\beta\ 200\ mL\right) - 180\ mL\left(1 + \frac{1}{2}\beta\ 180\ mL\right)}{80\ mL\left(1 + \frac{1}{2}\beta\ 80\ mL\right) - 60\ mL\left(1 + \frac{1}{2}\beta\ 60\ mL\right)}$$

This can also be estimated from the average filtration rate in each interval:

$$[\ 2\text{-}29\ ] \qquad FR_\beta = \frac{\left\langle\frac{dt}{dV}\right\rangle_{180\ mL}^{200\ mL}}{\left\langle\frac{dt}{dV}\right\rangle_{180\ mL}^{200\ mL}} = \frac{1 + \beta\ 190\ mL}{1 + \beta\ 70\ mL}$$

This simple relation gives excellent experimental agreement with the standard filtration ratio for filtration ratios between 1 and 2. Thereafter, the estimated filtration ratio is less

than the true filtration ratio because the linear plugging assumption no longer holds. One can see from [2-29] that as β becomes large, FR_β approaches 190/70 = 2.71. FR can, of course, be much higher.

2.5 Retention in Porous Media

Polymer is retained in porous media by two qualitatively different mechanisms: adsorption and mechanical entrapment. Adsorption refers to the deposition of polymer from the aqueous phase onto the solid rock, while mechanical entrapment refers to physical restriction of the polymer molecules in pore throats. Farajzadeh et al. (2016) provide an excellent, contemporary overview and theoretical treatment of adsorption and deep-bed filtration in porous media. A third, less understood mechanism called "hydrodynamic entrapment" has been delineated in the literature, but will not be treated in this thesis.

2.5.1 Adsorption

Adsorption (or sometimes "sorption") of polymer is driven by molecular attractions between the polymer and the rock surface. This attraction is influenced by surface lithology, polymer chemistry, temperature, pH, etc. (Sodeifian, Daroughegi, & Aalaie, 2015). The amount of polymer that adsorbs generally increases with the injected concentration, but has been observed experimentally to exhibit plateaus in the low and high concentration regimes (Zhang & Seright, 2014; Sodeifian, Daroughegi, & Aalaie, 2015). According to Langmuir theory, a plot of adsorbed polymer concentration versus injected concentration ought to be concave down and asymptotic. Zhang and Seright (2014) argue that the practical irreversibility of adsorption would indicate that the change in the adsorbed

mass stems from crowding of polymer at higher concentrations that prevents full contact of each adsorbed polymer molecule with the surface of the rock. They also advance the idea that pre-flooding with a slug of dilute polymer can reduce overall polymer retention.

While there is some confusion in the literature, pure adsorption should not cause a measurable loss of permeability in a porous medium, which is to say that the thickness of the adsorbed layer of polymer has a negligible effect on flow. Permeability reduction was a commonly observed phenomenon with previous generations of polymers, and theories of polymer adsorption layers as thick, impermeable coatings proportional to the swollen molecular size of the polymer were developed in line with experimental evidence (Hirasaki & Pope, 1974; Smith, 1970). However, currently available high-quality HPAM polymers with appropriate preparation do not suffer from this problem (Koh, Lee, & Pope, 2017; Qi, Ehrenfried, Koh, & Balhoff, 2017; Yerramilli, Zitha, & Yerramilli, 2013).

Adsorption does delay breakthrough of the polymer, usually by a small fraction of a pore volume, though in some cases it is more significant. High polymer adsorption is undesirable because a larger mass of polymer must be injected to achieve the desired incremental oil recovery of a polymer flood. Also, high adsorption substantially delays the arrival of the oil bank (Zhang & Seright, 2014; Pope, 1980). Adsorption inferred from breakthrough time can be underestimated due to the confusingly named phenomenon of "inaccessible pore volume" (the tendency of polymer to run ahead of a tracer because it only explores a sub-portion of each pore), but methods based on mass balance such as used in this study are perfectly valid. In this work, the polymer concentration needed in the mass balance was estimated from the effluent viscosity.

Polymer adsorption is typically reported as a dimensionless mass fraction relative to the mass of rock, ω_{4s} [μg/g]. For prediction of flood performance using fractional flow theory, this is converted into a dimensionless adsorption, D_4, (Pope, 1980).

$$D_4 = \frac{(1-\phi)\rho_s\,\omega_{4s}}{\phi\, c_{41}} \qquad [\,2\text{-}30\,]$$

The dimensionless velocity of the polymer front (ignoring "inaccessible pore volume") is given by

$$v_4 = \frac{f_1^*}{S_1^* + D_4} \qquad [\,2\text{-}31\,]$$

where (S_1^*, f_1^*) is the saturation and fractional flow at the point where the velocity of the polymer front is equal to the velocity of the polymer saturation shock. The breakthrough time in pore volumes is the inverse of this velocity, so adsorption increases breakthrough time by approximately D_4 pore volumes.

2.5.2 Mechanical Entrapment

Swollen high-molecular weight polymers can reach a hydrodynamic size of nearly a micron, on the order of the size of some pores in typical reservoir rocks. Thus, some polymer molecules can become lodged in the throats of pores that are too small to pass through. Indeed, some polymer solutions have been known to damage both laboratory cores and oil field wells; the permeability of the porous medium falls, and in the case of laboratory cores, the polymer concentration in the effluent does not return to its injected concentration. The rock therefore mirrors the behavior of a filter, and the proposed mechanism is sometimes referred to as deep-bed filtration. This phenomenon is the primary concern of the work undertaken in this thesis project.

Mechanical entrapment is an extremely complicated subject. As has already been discussed, polymer solutions are polydisperse. The same is true of pore networks, where pore throat sizes within a single rock sample vary over orders of magnitude that interconnect in an unknown way. Polymer chains have a flexibility that could allow them to reptate through constrictions that seem to be too small, judging from their average size in solution (de Gennes, 1971). It has been proposed that, in marginal cases of deep bed filtration, a small number of pores may be susceptible to plugging and that filtration and permeability loss should cease after this subcritical set of pores is plugged (Gogarty, 1967). To elucidate the mechanisms of mechanical entrapment, meticulous, pertinent measurements must be combined with a quantitative theory and language.

As was alluded to in the previous section, fractional flow theory has been extended to polymer flooding, with an explicit treatment of polymer mass transport. This theory can be further extended fractional flow theory to handle deep bed filtration, and to develop an analytical solution to the problem when a constant filtration coefficient applies, i.e. when plugging of the pores is constant and linear, as in the case of filters considered earlier (Farajzadeh, Bedrikovetsky, Lotfollahi, & Lake, 2016). Filtration by a medium of considerable thickness is more complicated than that by a thin filter because mass removed in an upstream section of the rock cannot be filtered again downstream. The spatiotemporal nature of deep bed filtration therefore requires careful mathematical bookkeeping.

Farazadeh et al. (2016) develop their theory in dimensionless coordinates, with new variables for entrapped polymer (S) and filtration coefficient (Λ). A linear relationship between polymer concentration and viscosity is assumed for simplicity, so the theory will

be inaccurate for large filtration coefficients. To minimize error, the linear approximation should be centered around the concentration of polymer used, not 0. Four physical relations are considered: (1) filtered mass in time, (2) mass balance, (3) Darcy's Law, and (4) Langmuir adsorption.

$$\frac{\partial S}{\partial t_D} = \Lambda C \qquad [\ 2\text{-}32\ ]$$

$$\frac{\partial (C+\hat{C}+S)}{\partial t_D} + \frac{\partial C}{\partial x_D} = 0 \qquad [\ 2\text{-}33\ ]$$

$$1 = -\frac{1}{(1+MC)(1+R\phi c_o \hat{C}+\beta\phi c_o S)}\frac{\partial P}{\partial x_D} \qquad [\ 2\text{-}34\ ]$$

$$\hat{C} = \frac{bC}{1+bC}\hat{C}_{max} \qquad [\ 2\text{-}35\ ]$$

Even unfiltered HPAM polymer solutions can transport through cores of Darcy permeability with very little permeability reduction ($R_k \approx 1$), and carefully hydrated and filtered HPAM solutions like those used in this thesis leave permeability unaffected unless plugging ensues (Koh, Lee, & Pope, 2017; Yerramilli, Zitha, & Yerramilli, 2013; Qi, Ehrenfried, Koh, & Balhoff, 2017). It is therefore reasonable to simplify [2-34] by assuming that the sensitivity of permeability to adsorbed polymer concentration, *R*, is 0. No discussion of the validity of the Langmuir adsorption model is discussed by the authors, though the work of Zhang and Seright (2014) is referenced in the text. The parameter β is introduced as a pressure sensitivity to the concentration of mechanically entrapped polymer in units of volume per unit mass. The equations for filtration and mass balance are easily combined, and have a solution that obeys a pair of characteristic equations.

$$\frac{dC}{dx_D} = -\Lambda C \qquad [\ 2\text{-}36\ ]$$

$$\frac{dt_D}{dx_D} = 1 + \frac{d\hat{C}}{dC} \qquad [\ 2\text{-}37\ ]$$

The Langmuir adsorption equation is simple to differentiate in polymer concentration, which [2-36] dictates is a decaying exponential in x_D. The second characteristic equation ([2-37]) can thereby be written explicitly in x_D.

$$\frac{dt_D}{dx_D} = 1 + \frac{b\hat{C}_{max}}{\left(1+be^{-\Lambda x_D}\right)^2} \qquad [\ 2\text{-}38\ ]$$

The solution to the above equation contains a shock front satisfying the Hugoniot-Rankine condition of mass balance, which yields an equation that is slightly simpler than the characteristic above.

$$\frac{dt_{Df}}{dx_{Df}} = 1 + \frac{b\hat{C}_{max}}{1+be^{-\Lambda x_D}} \qquad [\ 2\text{-}39\ ]$$

This can be integrated in x_{Df} to yield a final relation between the position of the front as a function of pore volumes injected.

$$t_{Df} = x_{Df}\left(1 + b\hat{C}_{max}\right) + \frac{b\hat{C}_{max}}{\Lambda} ln\left(\frac{1+be^{-\Lambda x_{Df}}}{1+b}\right) \qquad [\ 2\text{-}40\ ]$$

By definition, polymer solution concentration ahead of the front is 0. Behind the front, polymer concentration exponentially decays in x_D. An expression for dimensionless time can be obtained from integration of the previous characteristic equation ([2-38]), which I reproduce in terms of t_{Df}.

$$t_D = t_{Df} - \frac{b\hat{C}_{\max}}{\Lambda}\left(\frac{1}{1+be^{-\Lambda x_D}} - \frac{1}{1+b}\right)$$

The filtered polymer mass equation can be integrated from t_{Df} to t_D to yield a final expression for S.

$$S = \Lambda\left(t_D - t_{Df}\right)e^{-\Lambda x_D}$$

The pressure drop is obtained from integration of Darcy's Law ([2-34]) with respect to x_D from 0 to x_{Df}. I reproduce here the expected pressure drop after polymer breakthrough, assuming a resistance factor R = 0.

$$[\text{ 2-41 }] \qquad \boldsymbol{\Delta P = 1 + \left[\frac{M}{\Lambda} + \beta\phi c_0 t_D - \frac{\beta\phi c_0}{\Lambda}\left(1 + \frac{M\hat{C}_{max}}{2}\right)\right](1 - e^{-\Lambda}) + \frac{\beta\phi c_0 \hat{C}_{max}}{\Lambda}\left[1 + be^{-\Lambda} + \frac{M}{2}\left(be^{-2\Lambda} - \frac{1}{b}\right)\right] ln\left(\frac{1+be^{-\Lambda}}{1+b}\right) + \beta\phi c_0\left[\left(1 + b\hat{C}_{max}\right)\left(1 + \frac{M}{2}e^{-\Lambda}\right)e^{-\Lambda} + \frac{M}{2}(1 - e^{-2\Lambda})\left(t_D - \frac{1}{2\Lambda}\right)\right]}$$

This relationship is extremely complicated. To gain some insight, notice that we can differentiate [2-41] with respect to t_D to get something much simpler.

$$[\text{ 2-42 }] \qquad \boldsymbol{\frac{d(\Delta P)}{dt_D} = \beta\phi c_0\left[(1 - e^{-\Lambda}) + \frac{M}{2}(1 - e^{-2\Lambda})\right]}$$

The derivative above is a measurable quantity, as is the concentration at the outlet, which can be used to infer the filtration parameter, Λ, from [2-36].

$$[\text{ 2-43 }] \qquad \boldsymbol{\Lambda = -\ln C_{x_D=1}}$$

We can make this substitution in [2-42] and solve for β to get a very tractable result.

$$[\text{ 2-44 }] \qquad \boldsymbol{\beta = \frac{\frac{d(\Delta P)}{dt_D}}{\phi c_0\left[(1 - C_{x_D=1}) + \frac{M}{2}\left(1 - C_{x_D=1}{}^2\right)\right]}}$$

There are now two physical parameters, Λ and β, determined by two simple and independent experimental observables, the steady state concentration of polymer in the effluent and the slope of the pressure drop versus pore volumes data after full satisfaction of adsorption of the polymer. The filtration parameter is the most readily interpretable vis-à-vis the interaction between the polymer solution and the core material, but the pressure

sensitivity is very practically important. It is also necessary to validate the deep bed filtration hypothesis with pressure data from taps along the core.

2.6 Capillary Pressure and Inferred Permeability

Capillary pressure arises from contact between two immiscible fluids, e.g. oil and brine or air and mercury. The pressure is a function of the interfacial tension between the two fluids (σ), the wetting angle in the solid matrix (θ), and the radius of the aperture where the contact exists (R). In an idealized equilibrium, the capillary pressure can be written as a simple expression.

$$P_c = \frac{2\,\sigma\cos\theta}{R} \qquad [\,2\text{-}45\,]$$

Since capillary pressure, interfacial tension, and contact angle are all physical quantities that are measurable in the laboratory, they are used to infer the pore throat radius. For mercury injection capillary pressure (MICP) experiments, the volume of mercury injected (in pore volumes) into the rock sample is measured as the injection pressure is increased, constructing a relationship between P_c and S and, therefore, r and S (Purcell, 1949). Practically, this is interpreted as a cumulative distribution of pore throat radius versus non-wetting phase saturation (the incremental distribution follows trivially). This can also be translated into a permeability distribution, which is helpful for understanding which pore throats actually contribute to flow, using a bundle-of-capillary-tubes model (Purcell, 1949). One begins with the Hagen-Poiseuille equation for flow rate in a cylindrical tube.

$$Q = \frac{\pi R^4 \Delta P}{8 \mu L} \qquad [\,2\text{-}46\,]$$

The volume of the cylindrical tube can be factored out, and R can be replaced with the expression inferred from [2-45].

$$[\,2\text{-}47\,] \qquad \boldsymbol{Q = \frac{(\sigma\ cos\,\theta)^2\ V\ \Delta P}{2\ \mu\ L^2\ {P_c}^2}}$$

Of course, flow rate is also determined from Darcy's Law. A facile rearrangement yields an expression for permeability.

$$[\,2\text{-}48\,] \qquad \boldsymbol{\frac{\kappa\ A\ \Delta P}{\mu\ L} = \frac{(\sigma\ cos\,\theta)^2\ V\ \Delta P}{2\ \mu\ L^2\ {P_c}^2}\ \therefore\ \kappa = \frac{(\sigma\ cos\,\theta)^2\ V}{2\ A\ L\ {P_c}^2}}$$

This expression applies to each capillary tube (i) in the bundle, so the composite permeability of the bundle is a summation.

$$[\,2\text{-}49\,] \qquad \boldsymbol{\kappa = \frac{(\sigma\ cos\,\theta)^2}{2\ A\ L}\sum_i \frac{V_i}{{P_{c_i}}^2}}$$

Typically, we have measures of volume fraction (S) and porosity (φ), so it helps to recast this permeability relation as follows, noting that AL is the bulk volume.

$$[\,2\text{-}50\,] \qquad \boldsymbol{\kappa = 0.5\ (\sigma\ cos\,\theta)^2\ \phi \sum_i \frac{S_i}{{P_{c_i}}^2}}$$

Permeability may now be estimated from measured quantities. In practice, this permeability relation ([2-50]) must be multiplied by a lithology factor (F) that accounts for the interconnectedness of the pores. This is not dissimilar from the shear correction factor mentioned previously ([2-14]). In this application, F is between 0 and 1. It should be noted that the lithology factor is irrelevant to the prediction of the *relative* contribution of pores of various sizes to composite permeability. That prediction derives entirely from the bundle-of-capillary tubes model described above. One unstated assumption in this model is that each of the tubes in the bundle is of equal length (tortuosity). The model can

be reformulated to accommodate a radius-dependent length factor, determined by an empirical relationship (Burdine, Gournay, & Reichertz, 1950). That is, one substitutes $L_i = x_i\, L$, and x_i appears in the denominator of the summation in the permeability formula, where x_i is defined in terms of R_i, which of course is determined by $P_{c\,i}$, σ, and θ.

$$x_i = 5\, e^{-0.4\, R_i} + 1.83 \qquad [\ 2\text{-}51\ ]$$

3 Materials and Methods

3.1 Polymer Procedures

3.1.1 Storage

Partially hydrolyzed polyacrylamide (HPAM) is received as a powder and stored at room temperature in vacuum containers to avoid absorption of water by the polymer, which can render mass measurements inaccurate and degrade the polymer. Lot numbers and dates of receipt are catalogued for quality tracking. Scleroglucan is received as either a powder or a paste, both of which are stored at room temperature in sealed containers. The paste contains volatile liquid components that evaporate from an open container and thus must be sealed tightly between uses.

3.1.2 Hydration

HPAM

HPAM solutions are hydrated in low-salinity, mildly-buffered brines (e.g. 1,000 ppm NaCl + 400 ppm $NaHCO_3$, pH ~8) for 24-72 hours with gentle stirring. Low salinity, zero hardness, and buffering help to ensure that stock solutions hydrate fully and are of consistent quality, while also providing plenty of flexibility in the final brine conditions for the diluted polymer. HPAM is hydrated at 5,000 ppm polymer in brine unless experimental demands dictate that a higher stock concentration (e.g. 10,000 ppm by weight) is needed. Stock solutions are typically prepared at the 500-gram scale.

Hydration buffer is weighed into a flat-bottomed plastic polymer container (Figure 3-1) using a balance with a nominal precision of ±0.01 g (Sartorius). A large magnetic stir bar is used to stir the brine at a speed sufficient to create a vortex ¾ of the height of the liquid (~375 rpm). Polymer powder is weighed using a balance with a nominal precision of ±0.0001 g (OHAUS) and is then steadily poured into the stirring brine over the course of 30 to 60 seconds to avoid clumping of the powder. For hydrations lasting longer than 24 hours (typically a very high molecular weight HPAM polymer like FP3630S from SNF), an argon blanket is poured over the polymer to displace the oxygen rich air in the container, which is subsequently sealed using parafilm. The stir speed is reduced to 150 rpm after addition of the polymer, as prolonged high-speed stirring has been shown to damage high molecular weight HPAM.

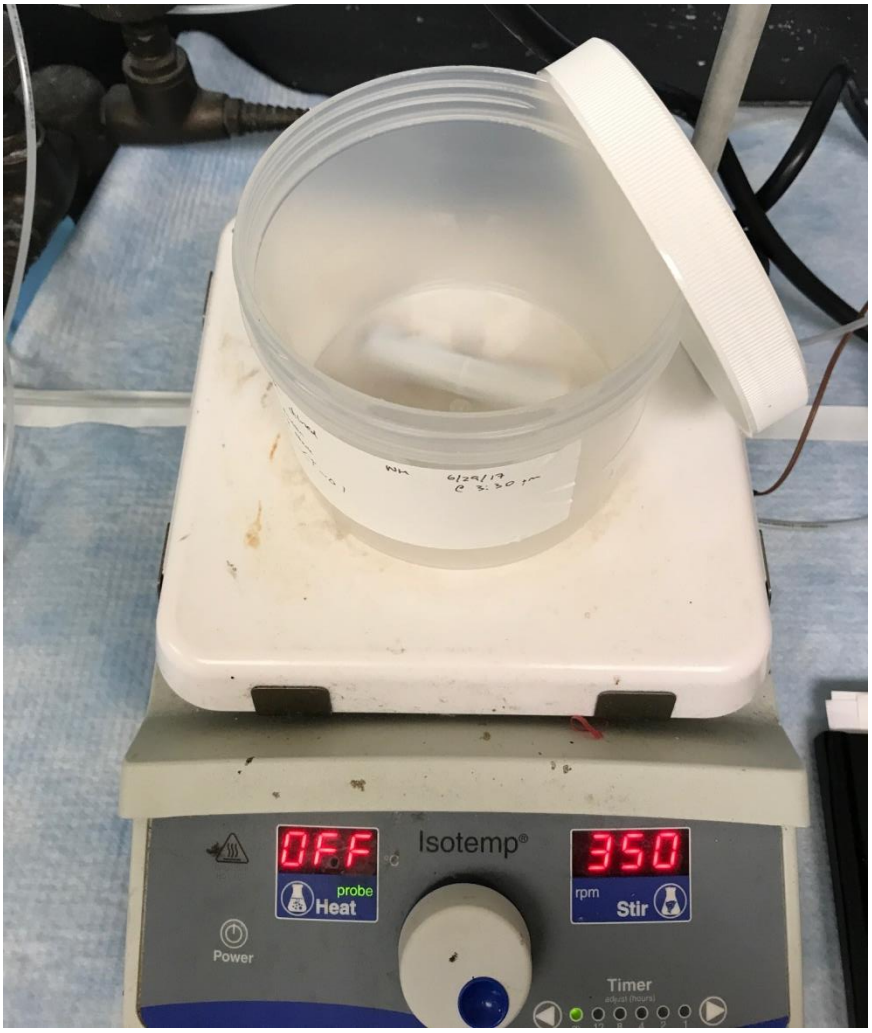

Figure 3-1: Polymer container with stir bar on stir plate

Scleroglucan

Scleroglucan (SG) paste and powder are typically hydrated and homogenized at the concentration and brine conditions at which they are ultimately to be used (in other words, no polymer "stock" is made). The polymer is weighed using a balance with a nominal precision of ±0.0001 g (OHAUS) and added to vigorously-stirred brine (stirring will not

degrade the polymer). After a few minutes of stirring, the polymer solution must be homogenized using the IKA magic LAB mixer (Figure 3-2). The blade speed is set to 20,000 rpm and the polymer is passed through the device twice.

Figure 3-2: IKA magic Lab mixer

The homogenized solution is typically opaque due to the suspension of air bubbles by the shearing device; these bubbles leave the polymer solution over the course of an hour or so, depending on the solution viscosity. One should wait for the suspended air bubbles to leave the solution before measuring viscosity or filterability. Heating of the solution before argon bubbling is not recommended, as it accelerates oxygen-based radical degradation. This polymer solution cannot be stored at room temperature for more than about a day, as bacteria that invariably contaminate the solution will feed on the polymer and grow. The polymer can be argon bubbled for an hour or more and then stored at 70-80ºC (to prevent bacterial growth) for approximately a week. The best practice is to wait to prepare an SG solution until it is needed.

3.1.3 Filtration

Polymer solutions are filtered through 90 mm mixed cellulose filter paper (Millipore) loaded into OFITE stainless steel filter bells. The cellulose filters from Millipore are paper-like, hydrophilic membranes with a heterogeneous mesh structure, as shown below (Figure 3-3, left).

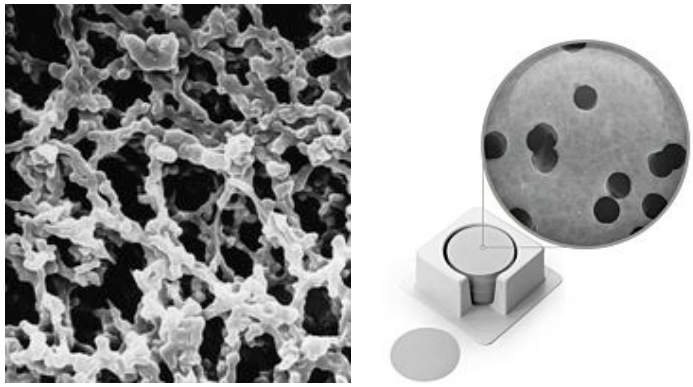

Figure 3-3: Cellulose (left) and polycarbonate (right) filter microstructures

The filters vary in thickness (L) from 0.105 mm to 0.150 mm and are highly porous ($\phi \approx 0.8$). They have a maximum operating temperature of 75°C, or 167°F. Their "pore size" is derived from their bubble point pressure, the pressure required to begin to drive air through them when saturated with water. The pore size reported is therefore best understood as the effective size of the *largest* pores, which would transmit air before the others.

Sterlitech offers polycarbonate filters in hydrophilic and hydrophobic varieties. As all of the polymers used for EOR are hydrophilic, only hydrophilic membranes should be used. One of their selling points is that they have a well-defined pore size (Figure 3-3,

right). The percentage of filter area occupied by the pores varies between papers, but is around 10%. They have an extremely high maximum operating temperature of 140°C, but are only recommended for pH 4-8, and have a quoted "burst strength" of 10 psi. This is likely better understood as a maximum recommended operating pressure. Paper thickness also varies, but is on the order of 0.01 mm in most cases.

Filtration is done at a constant pressure applied at the head through a regulator / manifold by an argon tank and measured by a mechanical gauge (Figure 3-4). The pressure at the gauge should be checked at least once during the filtration to ensure that it is stable. Upon the application of head pressure, a timer is started to mark the elapsed time. The filtered polymer is collected in a graduated cylinder that varies in size depending on the volume of polymer to be filtered and the aggressiveness of the plugging anticipated. For a standard filtration ratio test, > 200 mL of filtered polymer is required, and a 250-mL cylinder is used. The standard filtration ratio is defined as the ratio of the 180-200 mL and 60-80 mL interval times.

$$FR = \frac{t_{200\ mL} - t_{180\ mL}}{t_{80\ mL} - t_{60\ mL}} \qquad [\ 3\text{-}1\ ]$$

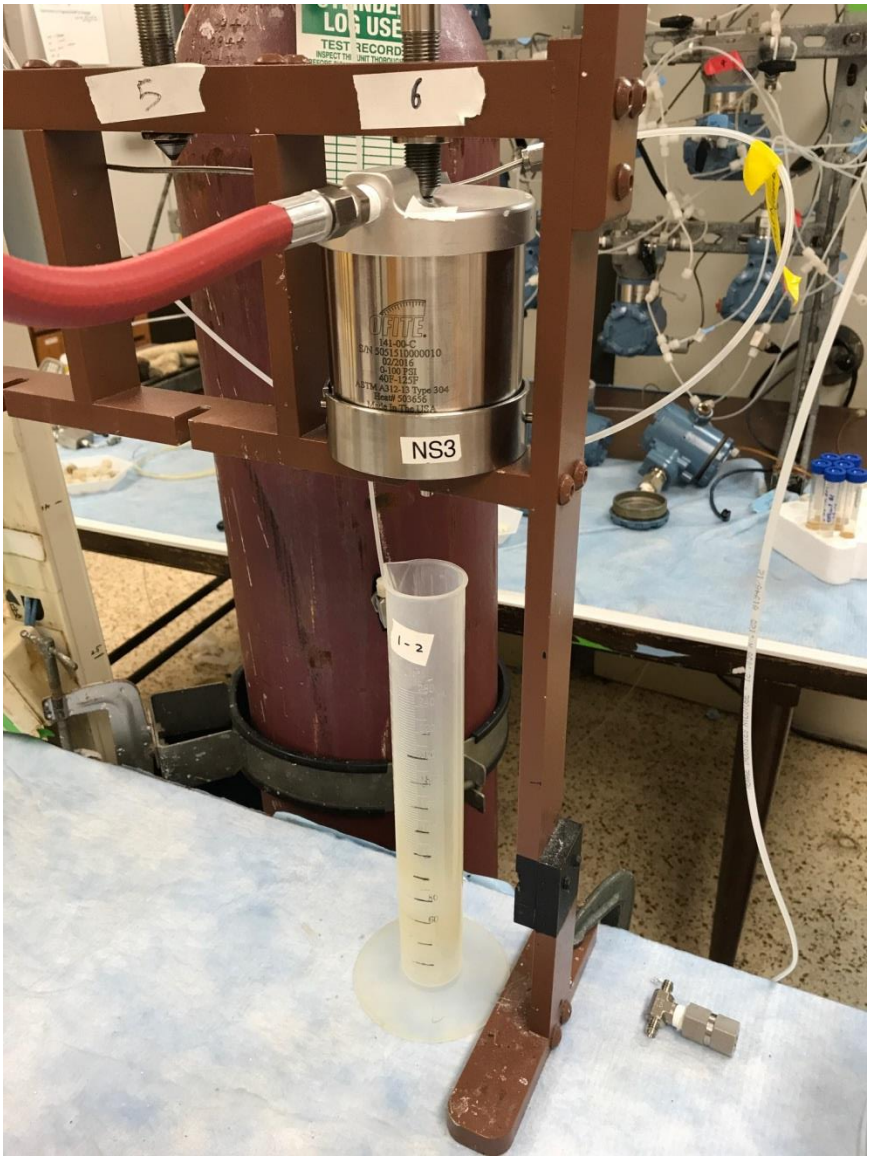

Figure 3-4: OFITE filter bell on manifold with graduated cylinder

The standard UT filtration ratio test requires FR < 1.2 at 15 psig head pressure on 1.2 µm filter paper. This quality control metric is generalized to the study of the hydrodynamic size of polymers by fitting the full volume time course to a second order polynomial to extract the plugging coefficient, β, as a ratio of the quadratic and linear coefficients of the

fit. A macro-enabled Excel workbook was created for this task (Figure 3-5). Plotting the full time course allows the experimentalist to exclude data from later, nonlinear plugging if it is encountered.

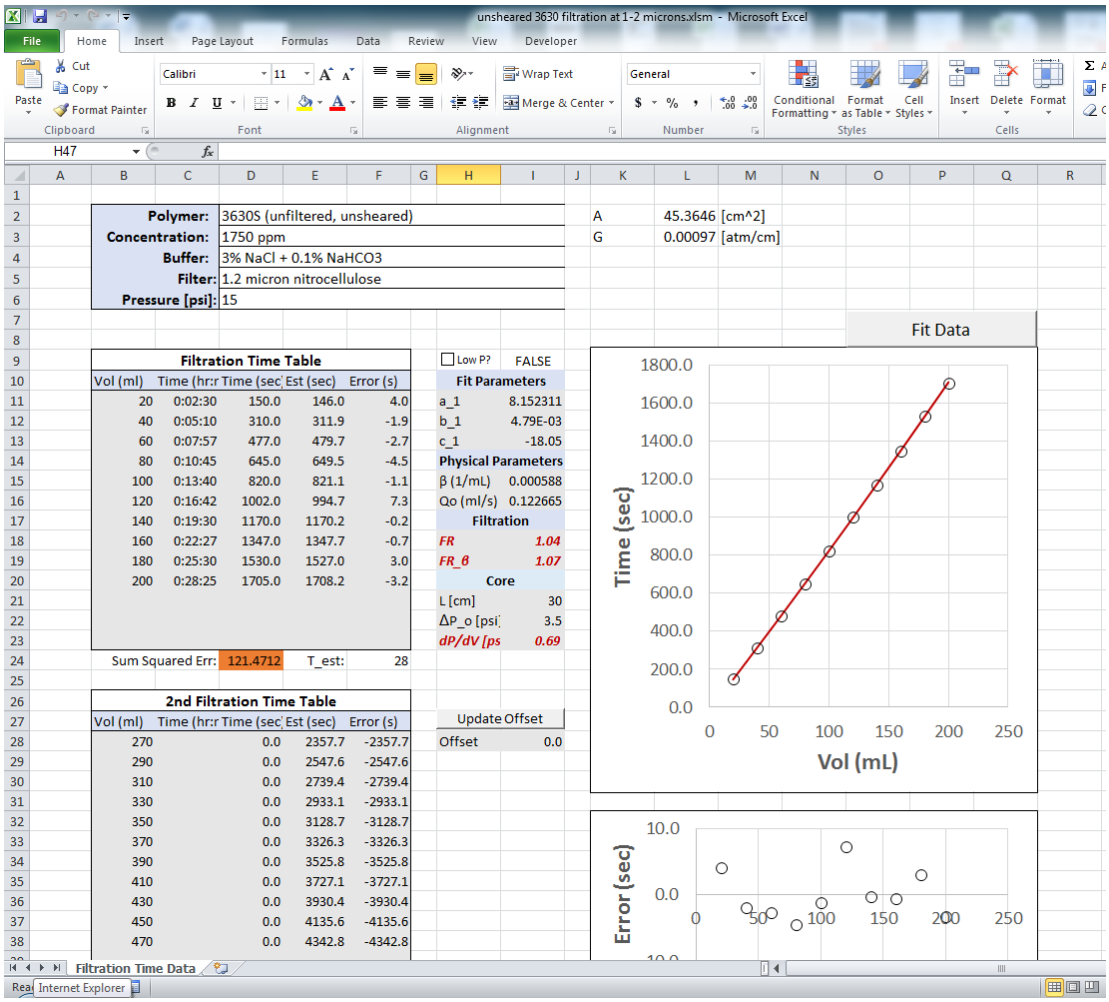

Figure 3-5: Filtration analysis spreadsheet

The plugging coefficient can be translated into a β-estimated filtration ratio, FR_β, even if the standard filtration ratio intervals are not recorded. The correspondence between FR and FR_β is very close for FR < 2.0 (Figure 3-6).

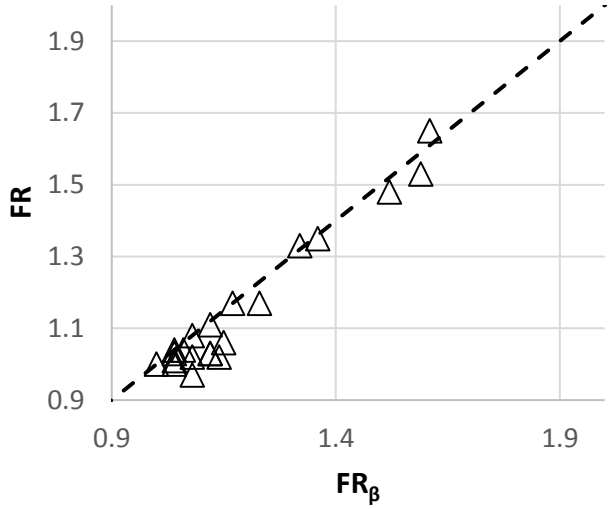

Figure 3-6: Comparison of FR and beta-estimated FR

All HPAM solutions that were used in core flood experiments were filtered at 15 psig head pressure, though lower pressure testing was conducted. Scleroglucan solutions used in core flood experiments were filtered at 2.5 psig to reduce throughput, as SG solutions pass most filters too quickly for accurate measurement at 15 psig, and plugging may be artificially suppressed at extraordinarily high flow rates.

3.1.4 Shearing of HPAM solutions

HPAM solutions can be shear degraded using any number of devices, including overhead mixers, pumps/valves, and (most commonly) blenders. Each device must be calibrated for the duration of shearing (or number of passages for a valve) and the strength of shearing (i.e. the speed setting or flow rate).

To shear polymer solutions with a needle valve, polymer is pumped through the valve at a constant rate using a water-filled ISCO pump. The polymer is loaded into an accumulator and separated from the water from the ISCO pump using a synthetic piston with o-rings. The valve is flanked by t-junctions with leads to a pressure transducer to measure pressure drop across the valve during flow. Water or brine is used to calibrate the valve setting and to ensure that the needle valve is the dominant source of resistance (pressure drop) by comparison with the fully open state.

In the case of a laboratory blender, this means that for any given polymer solution, a speed setting on the blender must be chosen and timepoint samples of the polymer solution must be taken for viscosity measurements. The temporal decay of the Newtonian plateau viscosity should be plotted and interpolated to target a particular viscosity in future batches. It is desirable to choose a shearing device and speed setting that requires a relatively long shearing time (~1 min) to degrade the polymer by the required amount, so that small changes in manual timing have negligible impact on the product solution. The mass of polymer solution in the blender must also be standardized (e.g. 250 g), as the shearing time is essentially shared within the volume of the blender between solution in the proximity of the blades and that which lies above. It is not safe to assume that polymer solutions of different mass, polymer type or molecular weight, concentration, salinity, hardness, or degree of hydrolysis can be sheared for the same amount of time to yield an equal percentage loss of viscosity, as all of these factors affect degradation.

Deliberate shearing of HPAM solutions is used in this study to reduce plugging of polymer solutions on filter paper and in cores. Changes in filterability are measured using

the procedures delineated in the previous section, using a succession of filters with different pore sizes (e.g. 0.80, 0.65, 0.45 microns).

3.1.5 Hydrolysis of HPAM solutions

Fast hydrolysis of HPAM and some of its derivatives is possible at either low or high pH and elevated temperature. To prevent oxygen-mediated free-radical degradation, HPAM solutions are argon bubbled for 1 to 2 hours in a Pyrex jar (provided pH < 12) before tight capping and transferring to an oven or water bath for incubation. A gas cap of around 50% of the container volume should be left to prevent burst. The incubation temperature varies (78-95ºC) depending on the temperature at which the subsequent core flood is to be carried out. Hydrolysis initially results in an increase in solution viscosity, the extent and speed of which is dependent on pH and temperature. For the core flood in this thesis in which hydrolyzed HPAM was used (SAMA-13R), the polymer was hydrolyzed for 24 hours at 80ºC prior to filtration.

3.1.6 UV-Vis Assay for Polymer Concentration

Polymer concentration can be detected by assaying solution absorbance at 520 nm after treatment with acetic acid and bleach. The assay requires standard solutions ranging from 0 to ~500 ppm polymer for calibration of the signal, which is linear in this regime. Samples are prepared by mixing polymer solution, acetic acid (5N), and bleach (1.3%) in equal proportions. The acetic acid is added first and incubated with the polymer with mixing for 3 minutes, after which the bleach is added and incubated for 5 minutes. The bleaching time is important to standardize for repeatability, as the precipitated polymer does not

remain suspended for very long. Mixing with a pipette is helpful to homogenize the sample before measurement.

The laboratory UV-Vis instrument (Agilent Technologies, Cary 100) can measure sample absorbance across a range of discrete light frequencies during a frequency scan (Figure 3-7). Measurements are background subtracted using a blank (polymer free) sample with buffer (polymer buffer + acetic acid + bleach in this case) loaded in a separate cell. While plastic cuvettes are available, quartz cuvettes (Fisher Scientific #14-385-902C) can be used for greater measurement accuracy.

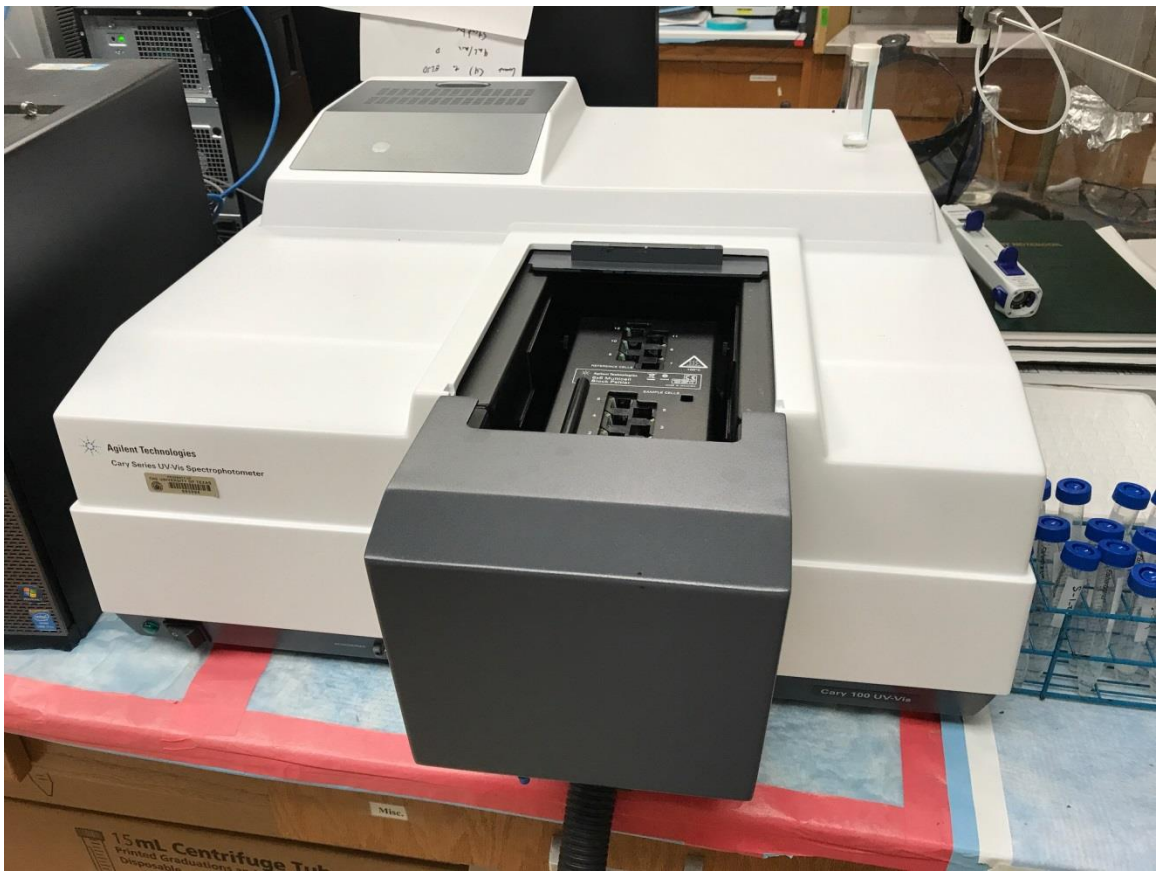

Figure 3-7: UV-Vis instrument

3.2 Rheological Measurements

3.2.1 Ares LS-1 Rheometer

The LS-1 Rheometer (TA Instruments) contains a motor-driven sample holder and a transducer-equipped spindle with modular interfaces to a wide range of rheological measurement devices/geometries (Figure 3-8). All of the rheological measurements presented in this thesis were performed with a double-wall couette (TA Instruments). The device is basically a hollow, bottomless cylinder suspended from the LS-1 spindle that fits into the annular space of a complementary sample holder (Figure 3-9). The thickness of the cylinder wall is less than that of the annular area, such that space remains for the fluid to be measured. The rheometer motor spins the sample holder, which transmits torque to the spindle attachment through the fluid. The torque is measured by a transducer and reported in software. A temperature-controlled water circulation apparatus maintains the sample temperature as specified by the user.

Figure 3-8: TA Instruments ARES LS-1 rheometer

Figure 3-9: Double-walled couette

The most basic requirements for accurate and precise measurements are careful measurement of sample volume, careful zeroing, and temperature stability. Temperature stability and zeroing are intertwined, as the metal instrument will expand or contract in concert with rises and falls in temperature, affecting the relative vertical positioning of the

mating parts. If steady state measurements are undertaken (e.g. constant shear rate measurements), it is very important to set measurement delay and integration time so that true steady state behavior is captured, rather than transient responses (see following sections).

Measurements from the LS-1 rheometer must be manually vetted. While the instrument has internal settings that specify a minimum torque threshold for accuracy, measurements that meet this threshold frequently diverge qualitatively from known trends, and are not reproduced upon adjusting measurement protocols. A trusted rheological model of the fluid being measured is therefore immensely helpful. As a rule of thumb, polymer solutions need to be around 5 cP or more in the Newtonian plateau (low shear) region for accurate viscosity measurements at low shear rate.

3.2.2 Temporal Response to Step Change in Shear

For steady state shear experiments, the timescale of convergence of the torque to a time-invariant plateau must be characterized beforehand. Since polymer solutions have elastic character, step changes in shearing forces are initially partially stored within the solution rather than dissipated, while purely viscous behavior is observed at longer times. The exact timescale of convergence is a property of the particular polymer solution at the measurement temperature. The LS-1 rheometer allows the user to visualize the timeseries torque data for step changes in shear rate for arbitrary shear rates of arbitrary duration (Figure 3-10).

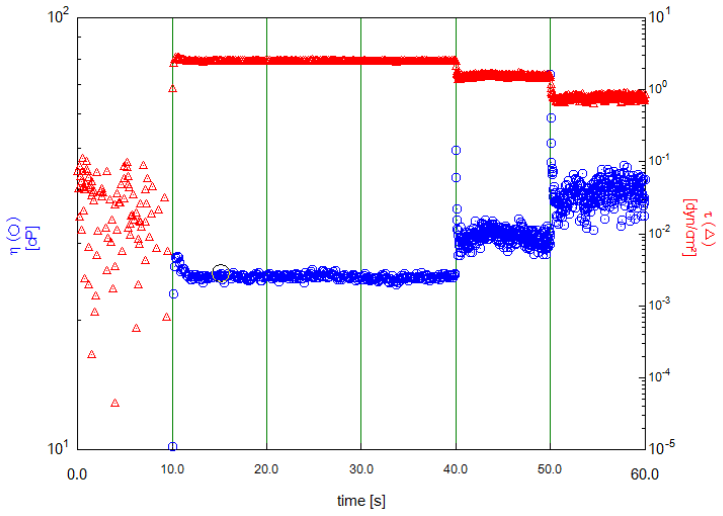

Figure 3-10: Temporal response to shearing (TA Orchestrator)

For steady shear rate sweep experiments, one should investigate the response of the polymer solution to step changes of a size similar to that which will be used in the sweep experiment. As one looks at the timeseries data, a judgement call should be made as to how long (in seconds) it takes for the torque to reach steady state, and then how much time should be averaged over to accurately measure the torque plateau. This can be validated in the steady shear sweep experiment by adjusting the measurement delay and integration time and assessing its impact on the final result.

3.2.3 Steady Shear Rate Sweep

Steady shear rate sweep experiments are the most common rheological measurements reported in this thesis. Polymer solutions are subjected to a sequential series of discrete shear rates of equal duration and equal rate spacing on a log scale (Figure 3-11).

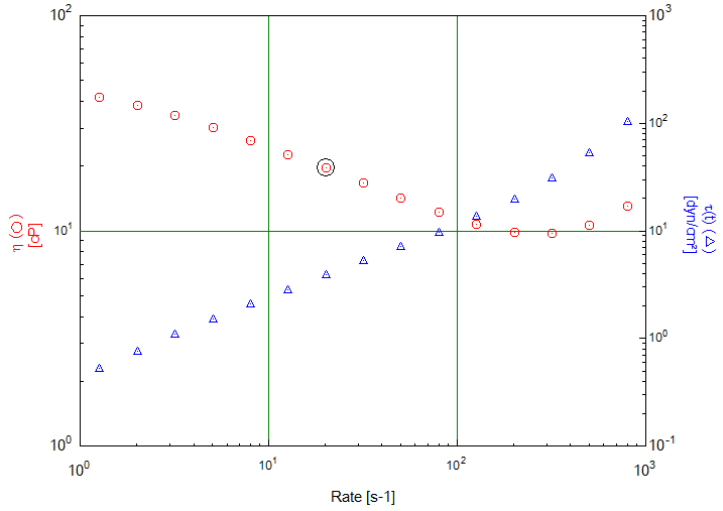

Figure 3-11: Shear rate sweep (TA Orchestrator)

Temporal characterization done beforehand should be used to set the measurement delay and integration time applied to each shear rate. In some cases, duplicate measurements are helpful, particularly when the ordering of measured rates is reversed. The data, including time, shear rate, torque, viscosity, and recorded temperature are reported by the rheometer software at each shear rate step in the sweep. These data are imported into Excel, triaged, and fitted to the Carreau model for analysis (Figure 3-12). The rate sweep is useful for finding the Newtonian plateau viscosity of a fluid, as the plateau range must be determined from the data trends. The rate sweep is also particularly useful for polymer flood analysis, as the apparent viscosity versus effective shear rate trend maps well onto rate sweep measurements.

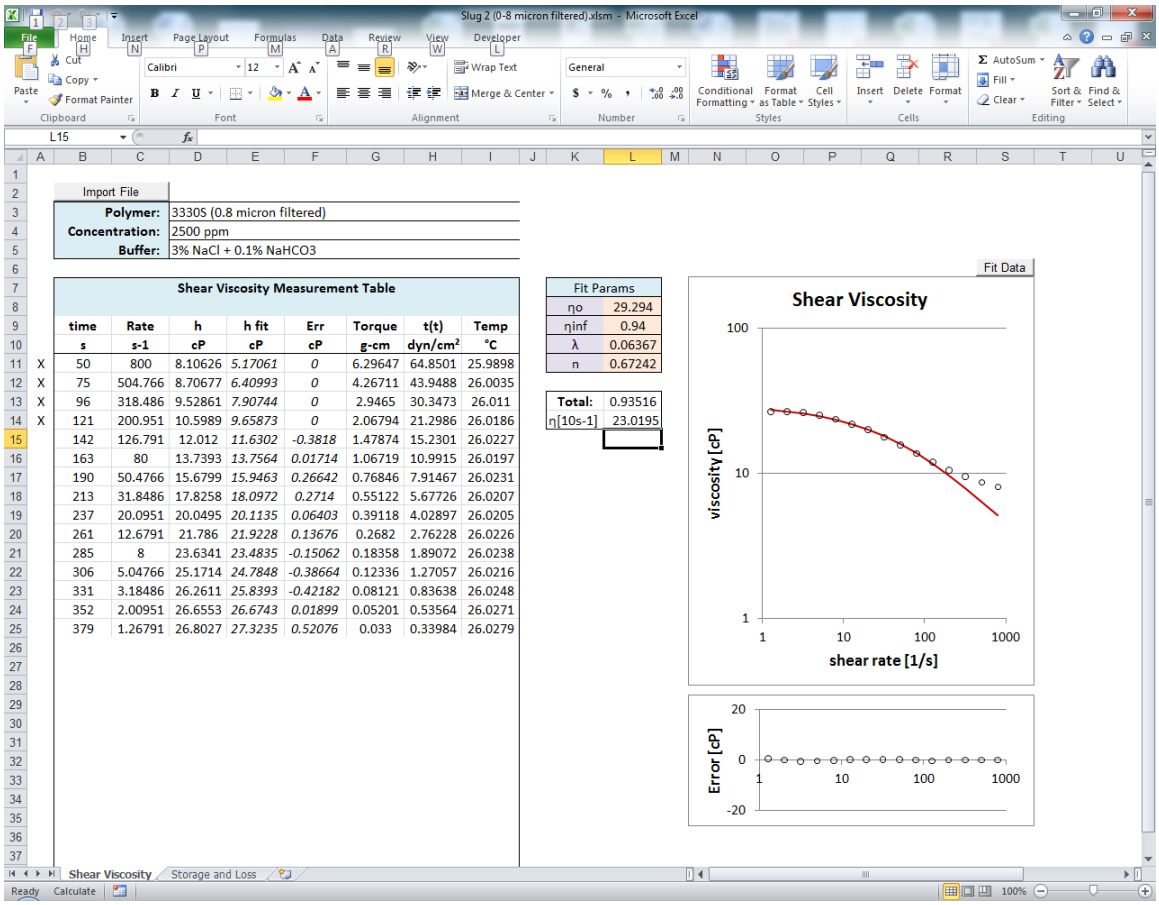

Figure 3-12: Shear rate sweep analysis spreadsheet

Rate sweeps produce accurate data only over a finite range of shear rates. As shear rates decrease, the torque applied to the spindle decreases, eventually falling below the threshold for accurate measurement. At very high shear rates, aberrantly high viscosities are typically measured (instead of falling to the Newtonian viscosity of the solvent), and this artifact must be identified and removed by modeling.

3.2.4 Strain Sweep

For dynamic (oscillating) measurements, the stress-strain response of the fluid should be characterized. The rheometer allows the user to specify a frequency of interrogation and a range of strains (in %) to apply to the fluid (Figure 3-13). By doing this at two frequencies, the user should be able to identify a region in strain space where the stress response is strain-invariant. A strain should be selected in the middle of this region for subsequent frequency sweep experiments.

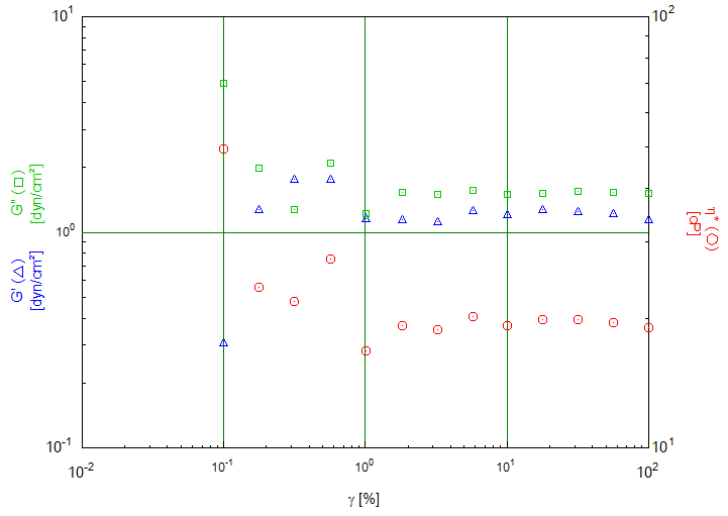

Figure 3-13: Strain sweep (TA Orchestrator)

3.2.5 Frequency Sweep for Dynamic Moduli

The viscous and elastic characters of a polymer solution can be deconvolved through the phase delay in its strain response to a sinusoidally varying strain applied to it. The magnitude and relative contribution of the elastic response generally increases at higher frequency, so it is useful to measure the respective moduli over a range of frequencies. The

LS-1 frequency sweep function is used for this purpose, and scans constant-amplitude strain at discrete frequencies with equal spacing on a log scale (Figure 3-14). The data are reported and can be plotted and analyzed in Excel. As in the case of the shear rate sweep, frequency sweep data are only valid over a finite range of strain frequencies, with frequencies on the low end generating too little torque for accurate quantitation and frequencies on the high end generating phase delays too large relative to the frequency itself.

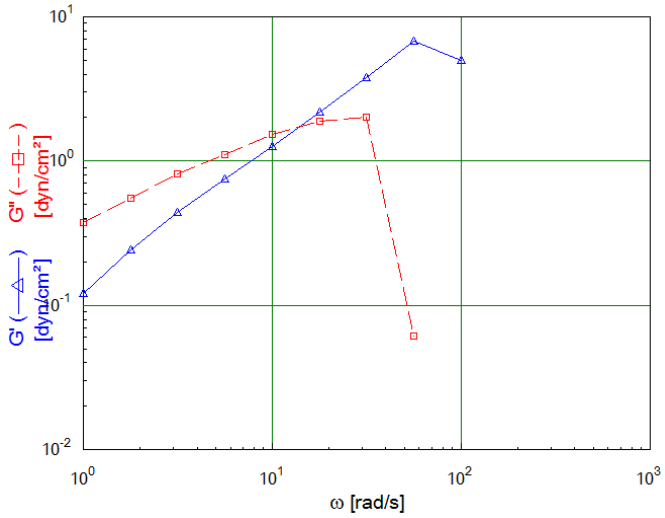

Figure 3-14: Frequency sweep (TA Orchestrator)

3.3 Core Flooding

3.3.1 Core Preparation

Cylindrical core samples are cut from outcrop or reservoir blocks using a specialized cutting machine. Cores are weighed using a scale with a nominal precision of ±0.01 g.

Their lengths are measured with a metal ruler with a precision of ±1.0 mm, and their widths are measured in three places with micrometers (nominal precision of ±0.1 mm), with the median value used in subsequent calculations. These measurements are used to determine bulk density and to estimate porosity from the grain density of the dominant lithology of the core (sandstone = 2.65 g/cc, limestone = 2.71 g/cc, dolomite = 2.87 g/cc).

$$\phi = 1 - \frac{\rho_b}{\rho_m} \qquad [3\text{-}2]$$

This porosity is also measured by imbibition volume and later by tracer tests. These three independent measurements are usually within experimental error estimates.

After the initial measurements are taken, a heat shrink sleeve is cut to just over the length of the core, and the core is loaded in the sleeve and placed in a ~90ºC oven for ~1 hour, or as long as is needed to shrink the sleeve securely around the core. The core is removed from the oven and allowed to cool before loading into the core holder so that the temperature of the core holder and confining oil is stable after loading. Stable temperature is a requirement for the detection of leaks in confining pressure. Before loading into a core holder, the core ends are labeled with a sharpie marker as "In" and "Out" for inlet and outlet (bottom and top of the core holder, respectively), so that physical inspection of the core can be conducted after the flood in correct context with sectional pressure drop data and oil recovery (if multiphase).

3.3.2 Core Holder

For transport testing, cores were loaded into a 1.5" diameter steel core holder (Figure 3-15). The core holder accommodates a tapped rubber sleeve around the core that provides

pressure communication between the outside and the core itself while creating a sealed space between the sleeve and the steel core holder that can be pressurized with mineral oil. The space is sealed at the ends by o-rings and metal endcaps and is accessible through inlet and outlet taps fitted with valves and a pressure gauge.

Figure 3-15: Core holder (center) and column (left)

Pressure around the sleeve must be maintained over 500 psi (1000 psi was used in these experiments) to compress the sleeve and provide a good seal between the sleeve and core. For reservoir applications using reservoir cores, it is also important for the effective stress on the rock to be the same as the reservoir rock. Due to the thermal expansion of mineral oil and remaining trapped air in the confining space, internal pressure fluctuates with changes in temperature unless it is actively maintained by a pump. A stable temperature environment is therefore required to check the core holder for leaks, which is done by leaving the core holder under active pressure maintenance overnight and monitoring the net input of mineral oil from the pump. After vacuum saturation of the core with brine, the sleeve and heat shrink wrap must be drilled through to establish pressure communication between the core and the pressure transducers. There is a dead volume (volume not occupied by core material) in the flow path through the core holder between the inlet and outlet valves of approximately 2 mL, and this must be accounted for in certain measurements, e.g. tracer tests.

3.3.3 Air permeameter

An air permeameter (TEMCO #GPM-10-2) equipped with pressure and flow gauges was used to measure the permeability of cores before saturation with brine. Pressure and flow rate data were analyzed in an Excel spreadsheet to extrapolate to the Klinkenberg-corrected permeability (infinite pressure). This permeability was used to vet cores by permeability, and to track and evaluate the influence of clay swelling on permeability.

3.3.4 ISCO Pump

Flow in core flood experiments is provided by a Teledyne ISCO 500D pump filled with mineral oil (500 mL capacity; Figure 3-16). The pump is controlled with a controller (200 mL/min max flow rate, ±0.001 mL/min precision) capable of constant flow or constant pressure operation.

Figure 3-16: Teledyne ISCO pump with controller

Mineral oil is pumped into the top of sealed columns loaded with denser, aqueous injection solutions, so that the mineral oil floats on top of and displaces the solutions. The ISCO pump is separately used in constant pressure mode to set and/or maintain confining pressure in the core holder.

3.3.5 Pressure Transducer Calibration and Operation

Differential and absolute pressure transducers (Rosemount) are used to measure fluid pressures during core flood experiments (Figure 3-17). These transducers measure the deflection of an internal membrane that has a finite physical pressure tolerance. Within that tolerance, the current response of the transducer can be set to an arbitrary sensitivity for optimal detection. The transducer leads are connected to an external DAQ in a circuit with resistors to generate voltages that are measurable by a PC. Each differential transducer is equipped with a flow bypass that allows pressure equilibration across the membrane, as well as a three-way valve with a waste line attached for flushing of the transducer. Each differential transducer is connected in series with the next (low side to high side), sharing lines with either an absolute transducer or a neighboring differential transducer.

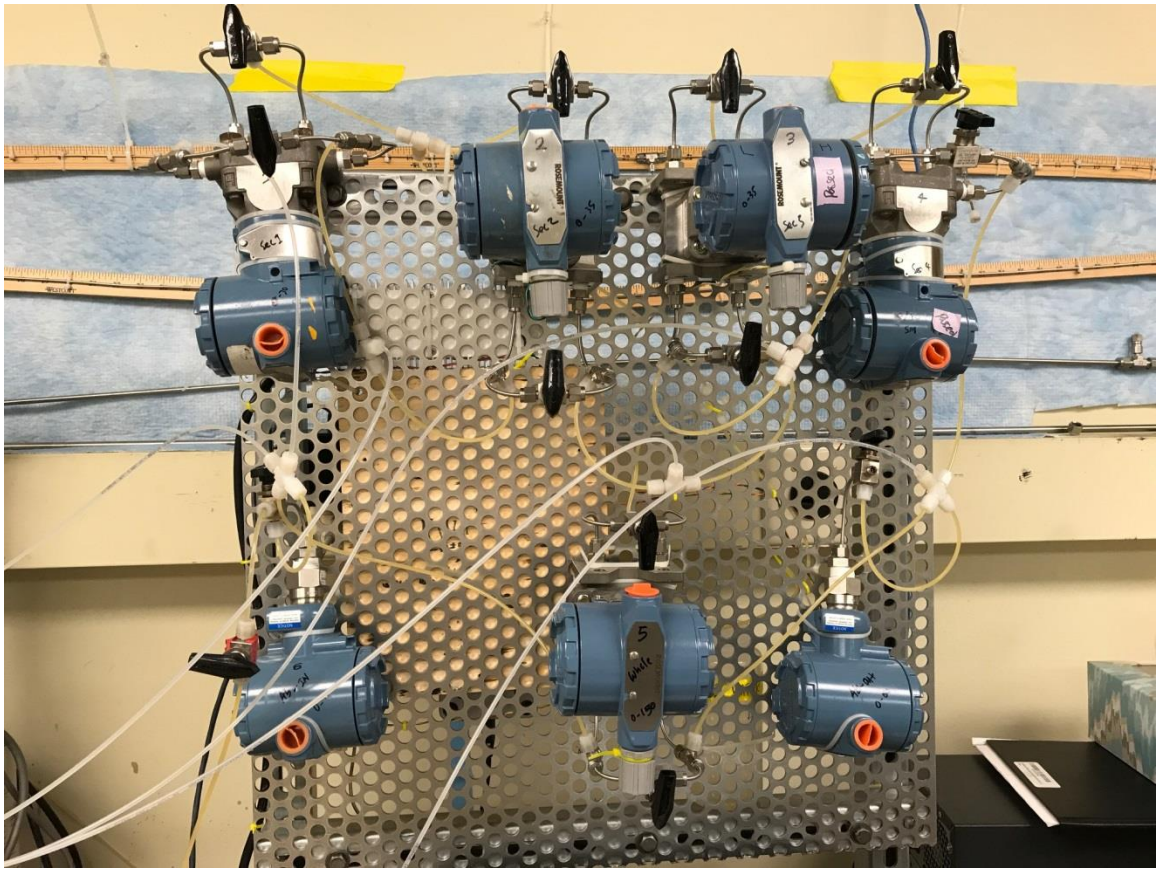

Figure 3-17: Pressure transducer manifold

Pressure transducers are prepared for calibration by draining and drying them overnight with constant air flow. Once dry, precise pressures (measured to within ±0.001 psi) can be applied using a specialized air pressure machine (General Electric, Druck PACE6000). The voltages are read by the DAQ card on the PC and reported in LabView software. Pressure and voltage readings are recorded over the desired detection range and a linear regression is built to map voltage to pressure. After calibration, the pressure transducers are vacuumed and refilled with distilled water. Remaining air is removed by driving pressurized flow of distilled water through the transducer manifold, one piece at a time,

until no bubbles are observed in the waste lines and pressure readings are stable. The manifold is flushed before each use (flood stage). The pressure transducer lines are connected to the core holder pressure taps through three-way valves that provide for flushing of each line individually.

3.3.6 Back Pressure Regulation

Back pressure is used in some floods to improve communication between the transducer and the core, and to prevent the boiling of fluids at high temperature. Relatively low pressures (15-30 psi) can be used to compress air bubbles that frequently leak into plastic lines and disrupt pressure transmittance. For this purpose, a mechanical back pressure regulator (BPR, Swagelok #LQ1166001) is installed on the effluent line, and flow is only transmitted through the BPR once the pressure inside the BPR rises above the value set at the knob (pressure inside the BPR at any given time is reported on an attached mechanical gauge; Figure 3-18).

Figure 3-18: Swagelok back pressure regulator

The device is a form of passive regulation, and there is some low frequency, low amplitude noise visible in pressure data associated with floods where a BPR was used. Generally, this noise does not interfere with the interpretation of the pressure data. The BPR has a volume that must be accounted for as part of the effluent dead volume in polymer flood data for adsorption calculations, and tends to retain oil that enters it during oil recovery experiments and must be added *ex post facto* to recovery data.

3.3.7 Core Cleaning

Core material can be cleaned for reuse in subsequent flood experiments, or for post flood analysis, e.g. scanning electron microscopy (SEM) analysis or mercury injection capillary pressure (MICP) measurements. The cleaning procedure required is dictated by the fluids to which the core was exposed. Cores that have been brine flooded only may be flooded with 100% methanol for 5 to 10 pore volumes with 15 psi backpressure and then flooded with air overnight to dry. Cores accidentally exposed to mineral oil may be cleaned with toluene for as many pore volumes as are required to recover permeability, then flooded with methanol and air as for brine-flooded cores. Cores flooded with HPAM polymer require bleach solution; methanol and toluene help to remove surfactant and oil, respectively. The procedure for cleaning a core sample from a tertiary oil recovery experiment is as follows, with all head pressure supplied by house air at ~100 psi (e.g. SAMA-13R):

(1) Flood the core with 5-10 PV 2% KCl (0 psi BPR).

(2) Flood the core with 5-10 PV 2% KCl + 0.1% NaOCl (0 psi BPR).

(3) Flood the core with 3-5 PV 2% KCl (0 psi BPR).

(4) Flood the core with 5 PV methanol (15-20 psi BPR).

(5) Flood the core with 10-20 PV toluene (15-20 psi BPR).

(6) Flood the core with 3-5 PV methanol (15-20 psi BPR).

(7) Flood the core with air overnight to dry (0 psi BPR).

3.3.8 SEM and MICP analysis

Scanning electron microscopy (SEM) and mercury injection capillary pressure (MICP) analyses were performed by Core Laboratories in Houston, TX. MICP data were converted into inferred pore size data by Core Laboratories using standard physical modeling. Core samples sent to Core Laboratories were cleaned before shipping. Pore sizes and contributions to permeability were inferred by Core Laboratories (Purcell, 1949; Burdine, Gournay, & Reichertz, 1950).

4 Shearing and Filtration

A quantitative characterization of shear degradation of polymer solutions and their plugging behavior on various filter papers is a prerequisite for preparation of polymer solutions for injection into porous media. Polymers can be sheared in valves and blenders, both of which are examined in this chapter. Information about the average size and size distribution of polymers in solution can be found in viscosity and filtration plugging data, thus these methods are used to quantify the effects of mechanical shear degradation, salinity, and hydrolysis. These experiments culminate in the development of a procedure for the optimization of polymer shearing for filtration through small pore size filters for maximum viscosity.

4.1 Shearing of HPAM Solutions

4.1.1 Shearing through valves

Flopaam 3630S supplied by SNF is an 18 MDa HPAM polymer with very high shear sensitivity. Per existing literature, this sensitivity is enhanced in the presence of calcium. To investigate this sensitivity quantitatively, 150 g 3630S dilutions (0.2% polymer, 2.49% NaCl + 0.02% $NaHCO_3$) with and without 0.12% Ca^{++} were made from a 0.5% polymer stock (0.1% NaCl + 0.04% $NaHCO_3$). These dilutions were split into 40 mL portions for shearing through a 3-way valve (Swagelok, $C_v = 0.15$). The 3-way valve was fitted to the bottom of a 500-mL steel oil bomb, which had a valve at the top for the application of air pressure. One portion of each solution was left unsheared, while the other two were passed

through the valve with 50 and 100 psi head pressure (measured under static conditions). The results are depicted in Figure 4-1.

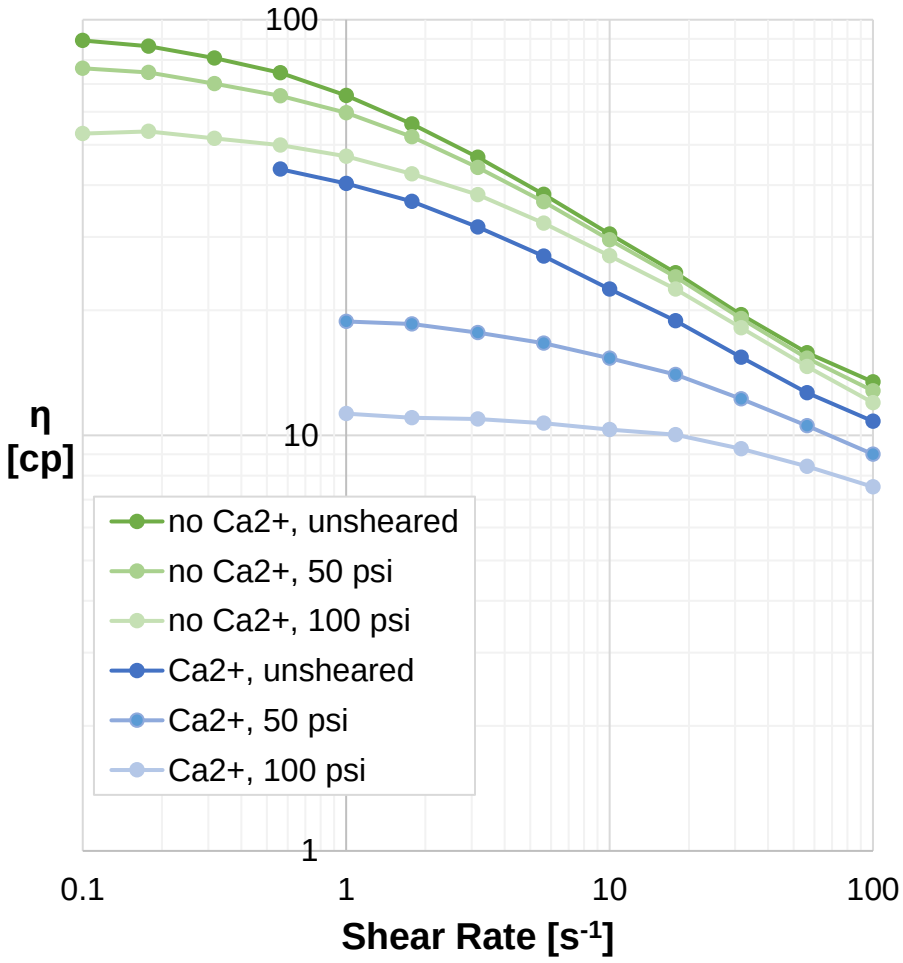

Figure 4-1: 3630S shear viscosity comparison, valve pressure and calcium

It is apparent that the percentage loss of original viscosity is much higher when calcium is present. At 10 s^{-1}, the viscosity reduction without calcium is 3.2% at 50 psi and 11.5% at 100 psi, while it is 31.8% and 54.1% when calcium is added. Because the viscosities of

the unsheared solutions differ, the flow rates (and therefore the shear rates) are naturally different. The viscosity of the calcium-free solution is ~20-60% higher over the measured range, decreasing as shear rate increases, and the effective shear rate through the valve is likely to be quite high. The flow rate difference (not measured) is therefore most likely proportionally small.

In an effort to gain measurement control over the shear rate applied to a polymer solution, an accumulator (piston) apparatus was constructed to drive polymer solution through a Swagelok needle valve at a steady, controlled rate using an ISCO pump. The needle valve was chosen because it could be set at a restrictive setting to ensure that it served as the point of constriction (as opposed to the Swagelok metal tubing, ID = 0.175 cm) based on pressure readings. Polymer (0.2% FP3330S + 1% NaCl + 0.16% $NaHCO_3$) was loaded into the accumulator (~90 mL) and flowed through the Swagelok valve at 125 mL/min. A sample of the product was reserved for rheological measurement, and the remainder was reloaded into the accumulator and passed through the valve again. This process was repeated for a total of eight passes. The pressure drops across the valve assembly as a function of extruded volume are plotted in Figure 4-2 (left), along with the extracted pressure plateau values (right).

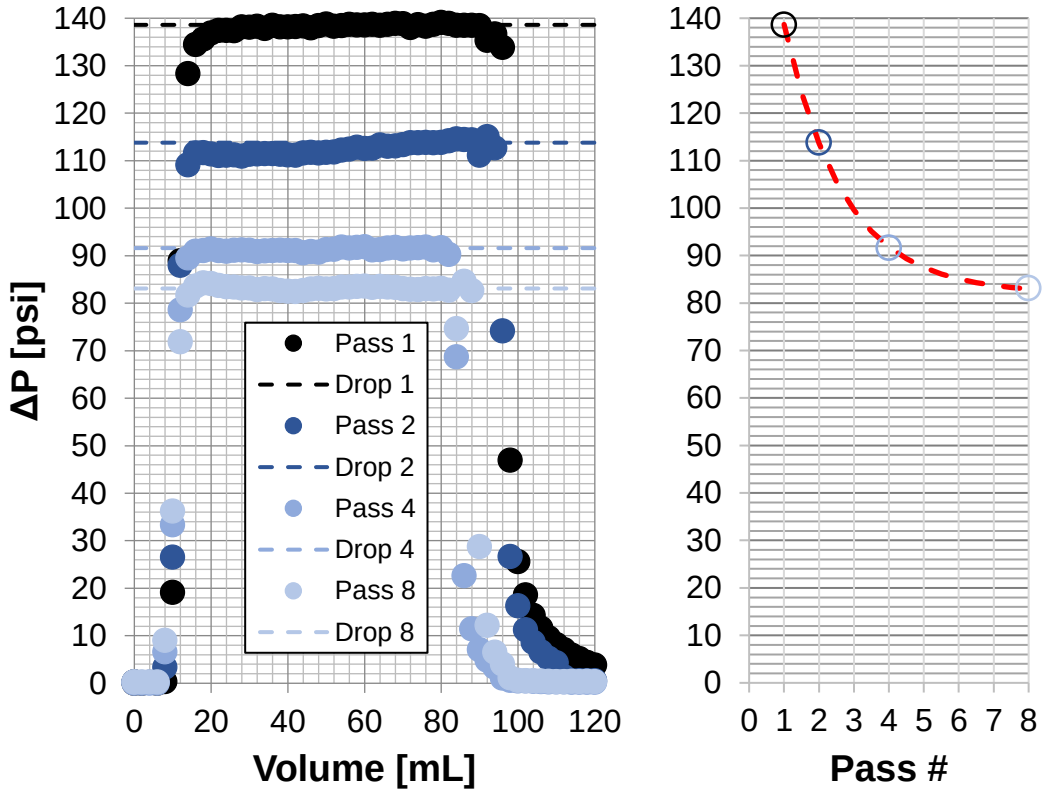

Figure 4-2: Pressure drops during needle valve shearing (left) with extracted plateau values (right)

The pressure rises rather quickly in each case to a stable value characterized by the median value in the latter part of the plateau, marked by dashed lines. These values are also plotted as a function of pass # in the righthand graph, which displays an exponential decay (see [4-1]). The viscosity of the polymer solution at the Newtonian plateau is plotted in Figure 4-3 as a function of pass #.

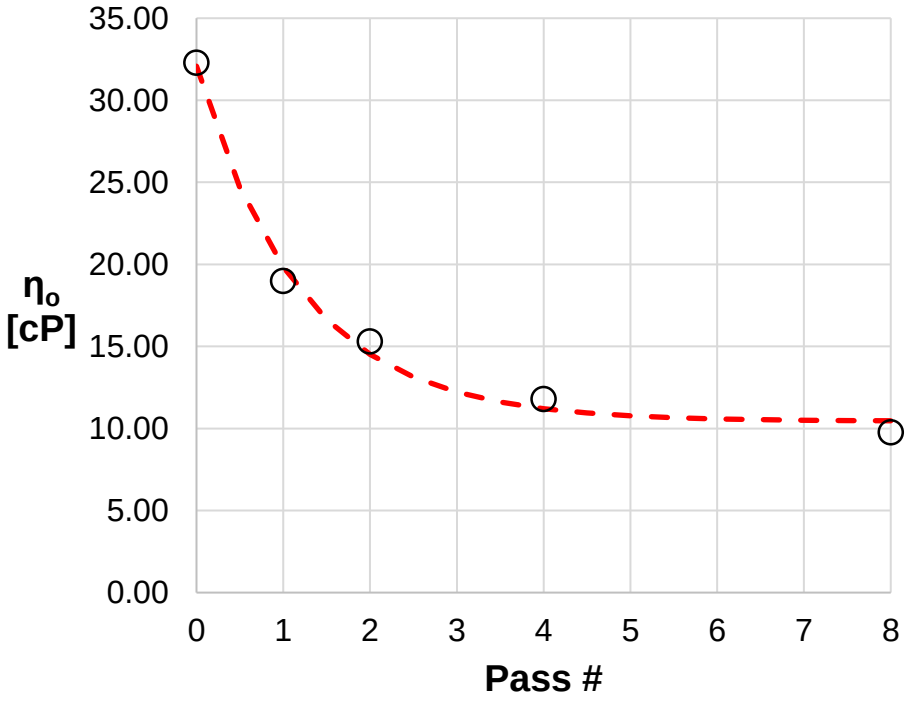

Figure 4-3: Shearing through Swagelok needle valve

The viscosity data show an apparent exponential decline, with a model fit to a simple decaying exponential giving close agreement with the data.

$$[\,4\text{-}1\,] \qquad \eta_o = \eta_o[\infty] + (\eta_o[0] - \eta_o[\infty])e^{-n/\tau}$$

The best fit comes with a time constant of 1.2 passes and an infinite pass floor viscosity of 10.4 cP. While calculating the shear rates within the needle valve would require sophisticated computational modeling, if one approximates the valve as an orifice constriction, an effective orifice area and maximum shear rate can be estimated using pressure data from water flow through the valve (Bird, Stewart, & Lightfoot, 1960).

$$A_{ori} = \frac{Q}{C}\sqrt{\frac{\rho}{2\Delta P}} \qquad [4\text{-}2]$$

The pressure drop across the valve was 1.19 psi and 1.79 psi for water flowing at 75 mL/min and 100 mL/min, respectively. With $C = 0.7$ (a typical value), the effective orifice areas are 0.0044 cm^2 and 0.0048 cm^2, an average of 0.0046 cm^2, corresponding to an effective orifice radius of 0.038 cm. If the shear rate is approximated using the pipe wall shear rate equation, this equates to an effective shear rate of ~40,000 s^{-1}.

4.1.2 Blender shearing

Blenders apply modulable, consistent shear rates to polymer solutions, and are thus ideal to calibrate for preparation procedures. Time course viscosity data can be fit to exponential models to allow for an arbitrary viscosity target to be set, though interpolation is often more accurate.

A 12-speed Osterizer blender was calibrated at its lowest speed setting for easy reproducibility with 250 g samples of FP3330S (0.2% in 1% NaCl + 0.16% $NaHCO_3$). Time points in a power series progression were selected from 0 to 16 minutes of shearing time. For each sheared solution, the viscosity at the Newtonian plateau was estimated from shear rate sweep data collected from the LS-1 rheometer. The data are plotted in open circles in Figure 4-4, and fit to an exponential with a long-time limit of 9.1 cP and a time constant of 1.4 minutes (red dashed line). The time rate of viscosity loss certainly decreases with blending, but these data do not conclusively show that there is a limit above solvent viscosity below which the device cannot degrade (note the undershoot at the end). Data from an equivalent test with the highest speed setting (#12) are plotted with x's.

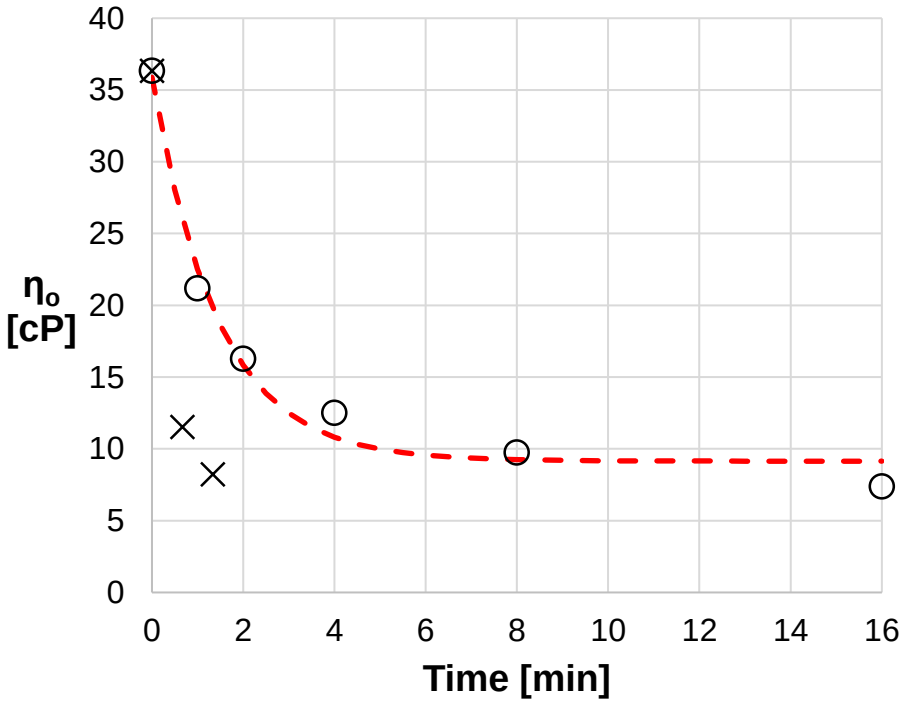

Figure 4-4: FP3330S (0.2% in 1% NaCl + 0.16% $NaHCO_3$) in Osterizer blender

The time constant of degradation is helpful because it is strongly dependent on blade speed and the speed at which polymer solution turns over within the blender to contact the blades. The time constant for the highest speed setting is 0.33 minutes, roughly 4x faster than the lowest speed setting. One might predict that an equal mass of a different molecular weight of HPAM would degrade with an equal or similar time constant. This appears to be the case, as an identical slug of FP3630 loses viscosity with a time constant of 1.1 minutes (Figure 4-5). The long-time limit of viscosity from the exponential fit (13.6 cP) is quite similar to that for 3330S (9.1 cP) despite the ~5.5x difference in initial viscosity, as one might expect for different starting molecular weights of the same material.

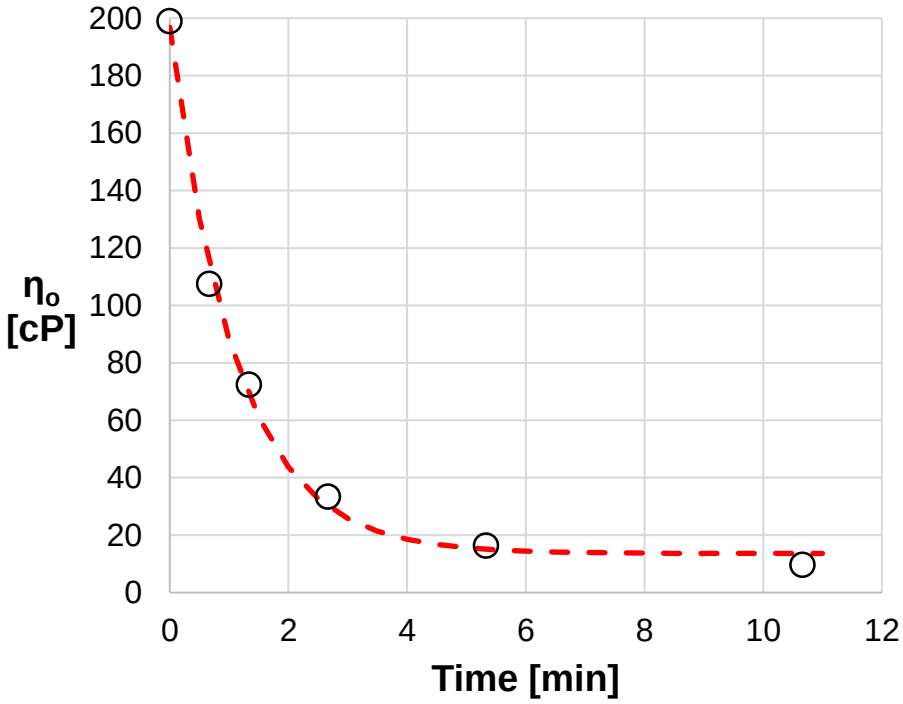

Figure 4-5: FP3630S (0.2% in 1% NaCl + 0.16% $NaHCO_3$) in blender

4.2 Filtration of 3330S Solutions

The filtration behavior of FP3330S solutions were investigated on a range of filter papers at varying concentrations, salinities, and degrees of shearing. Plugging was evaluated using the β coefficient defined in Chapter 2 (Filtration of Polymers), extracted from each filtration time course plot (Figure 4-6).

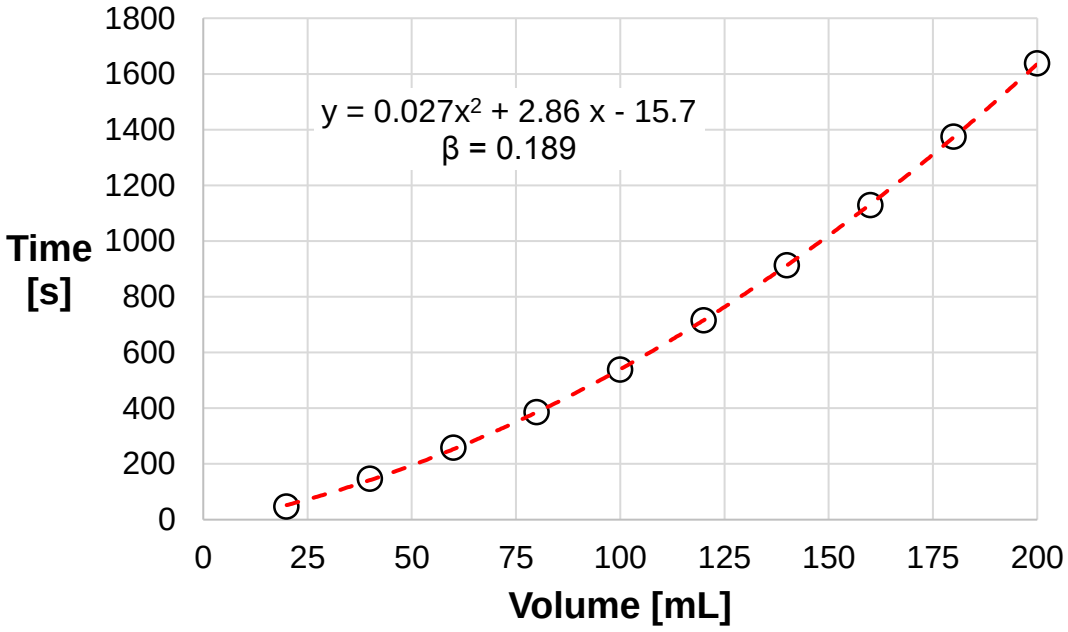

Figure 4-6: Filtration test example, FP3330S on 0.45 µm cellulose filter paper

4.2.1 Filter pore size

Plugging rates have been shown to vary with filter pore size (Lee, 2015). For submicron pore sizes, this is presumably the result of filtering out high molecular weight species in the molecular weight distribution that have hydrodynamic diameters similar to the filter pores. By quantitating plugging on a range of filter pore sizes, one can obtain a measure of the shape of the leading edge of the molecular weight distribution.

A solution of FP3330S (0.2% polymer, 1% NaCl, 0.016% $NaHCO_3$) was split into equal portions and filtered on 1.2 µm, 0.80 µm, and 0.45 µm cellulose filter papers (Millipore). Pressure was maintained at 15.0 ± 0.5 psig, and time points were recorded as shown in Figure 4-6. The plugging coefficients extracted are plotted in Figure 4-7. As

expected, plugging increases as the filter pore size is reduced. The increase is very sharp, and is slightly upward sloping even with the y-axis on a log scale.

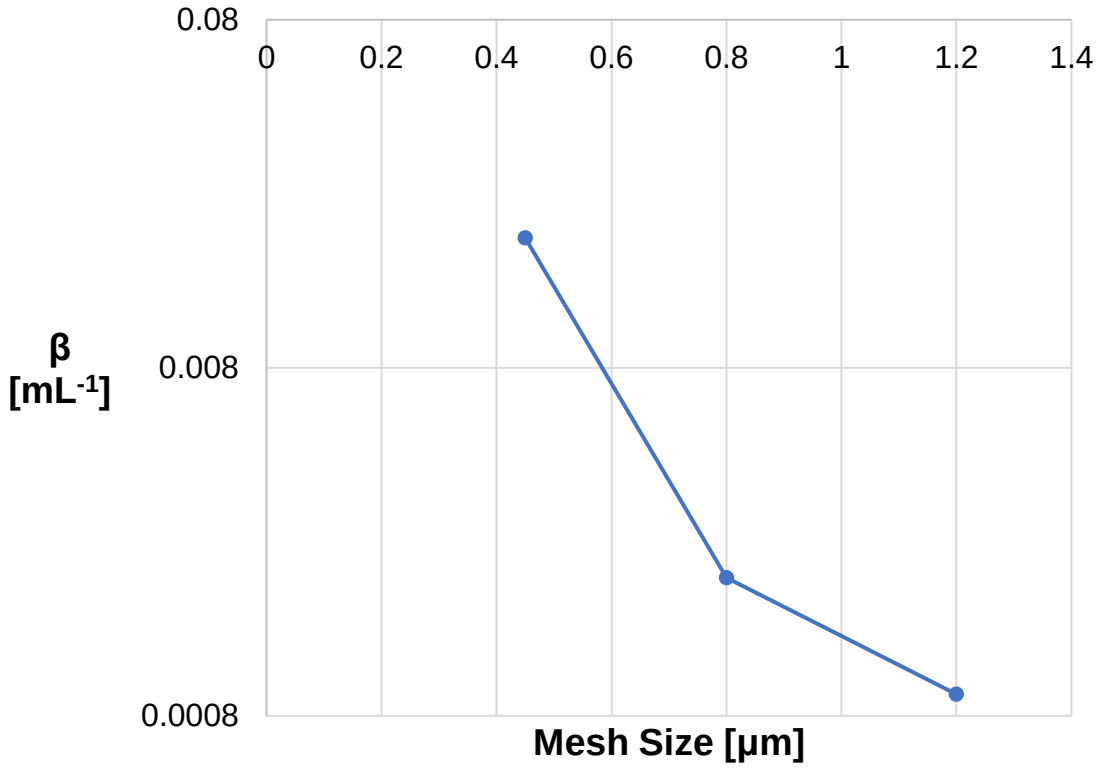

Figure 4-7: Plugging trends with filter pore size

4.2.2 Blending time

Mechanical degradation is believed to reduce the molecular weight of polymer molecules by chain scission. To measure this change using the filter polymer size assay from the previous subsection, two samples of the same polymer solution were sheared in the Osterizer blender on its lowest speed setting, one for 20 seconds and the other for 120 seconds. The polymer solutions were filtered using 0.80 µm, 0.45 µm, and 0.22 µm filters

because this was the range over which plugging was easily measurable. The data (Figure 4-8) indicate that the filter assay is able to measure a decrease in molecular size with increased shearing (the "unsheared" data is the same data as in Figure 4-7).

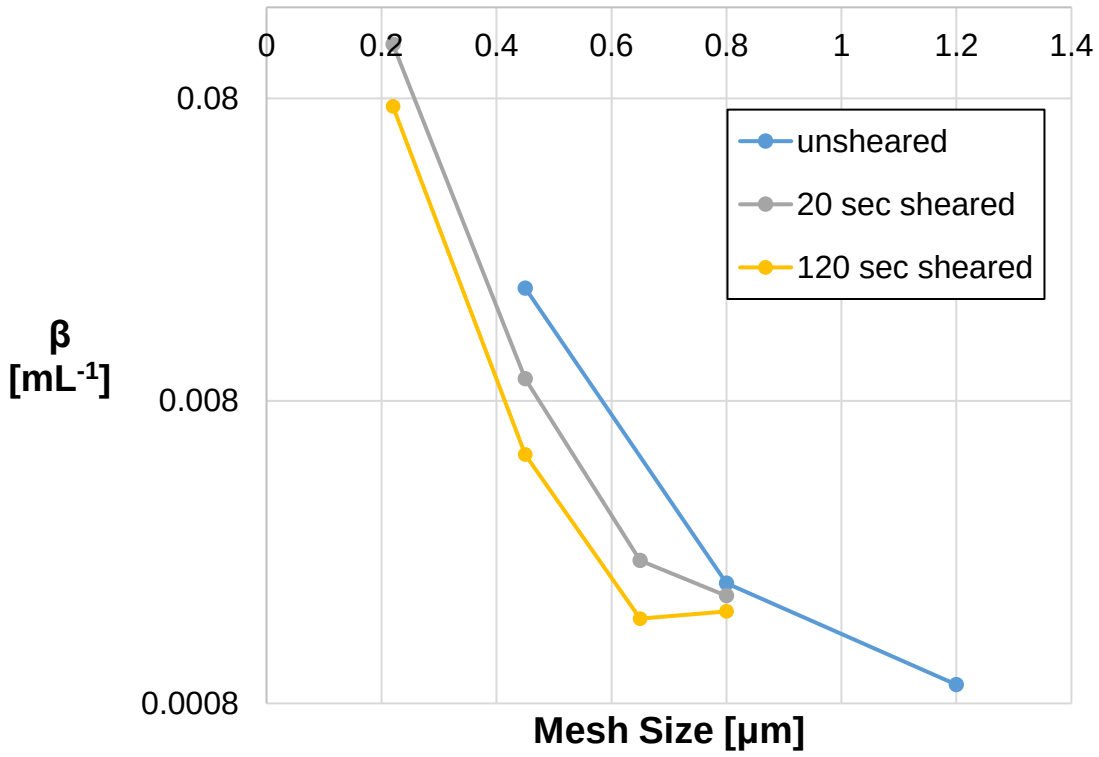

Figure 4-8: Shearing effects on filterability

The shape of the molecular weight distribution of each looks very similar, indicating that perhaps the polymer in the measured size range is shifted to lower molecular weight without a substantial change in the shape of the molecular weight distribution. The absolute magnitude of the shift on the pore size axis is, if anything, greater for the first 20

seconds of blending than for the ensuing 100 seconds, though the reverse is true if we measure the loss of viscosity (Figure 4-9).

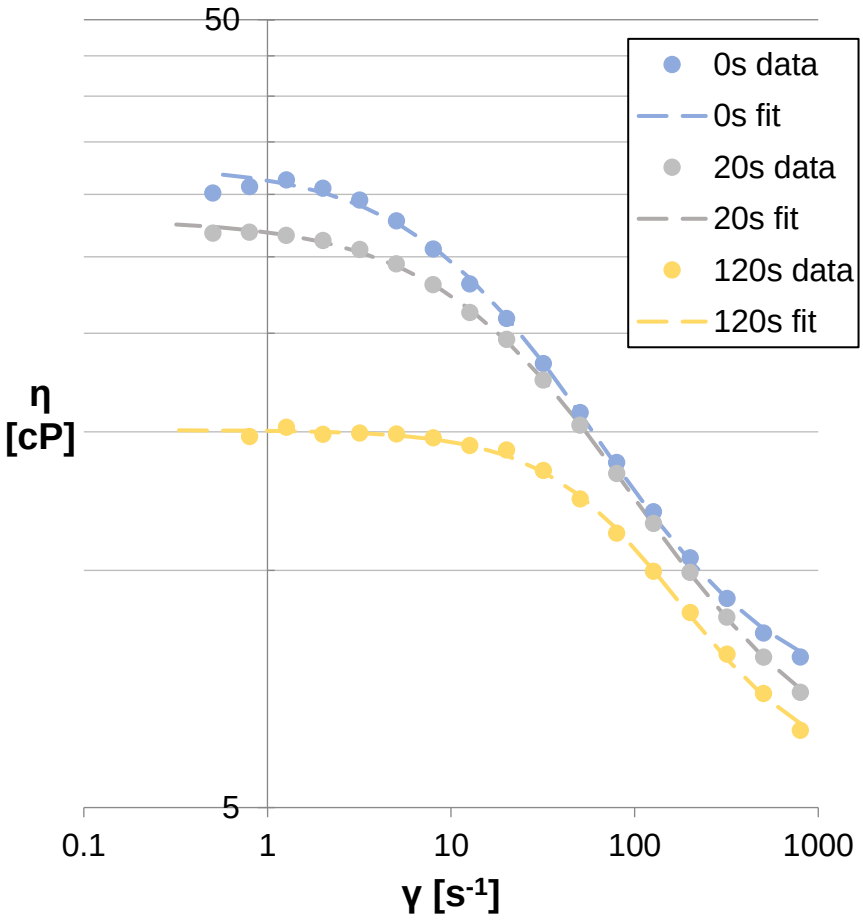

Figure 4-9: Viscosity of sheared 3330S

By contrast to the absolute shift, the *proportional* shift in polymer size measured by filtration is similar, with each step reducing the diameter by around 15-20%. The intrinsic viscosity of HPAM is proportional to the cube of the hydrodynamic diameter, so we would expect this to translate to a ~40% reduction in intrinsic viscosity at each step, translating

to ~35% remaining. Because viscosity is described well by a cubic equation in intrinsic viscosity / polymer concentration, the reduction in viscosity at the Newtonian plateau would be expected to be even more significant. The data show that 50% of the original viscosity remains after 120 seconds of shearing. The simplest way to reconcile this result is to assert that shear degradation in the blender disproportionally degrades the high molecular weight polymer within the molecular weight distribution, and that this subpopulation of polymer is what is being measured in the plugging assay.

4.2.3 Salinity

Increases in salinity decrease viscosity very precipitously at low effective salinity. These changes in viscosity reflect changes in polymer swelling that, in principle, should be reflected in the filtration assay. To test this hypothesis, a batch of FP3330S polymer was prepared identically to the previous batch, except that the salinity was reduced to 0.1% NaCl, creating a much more viscous solution (η_o = 874 cP). Filters with pore sizes of 1.2 μm, 0.80 μm, 0.65 μm, and 0.45 μm were used; on all but the smallest pore size, the 0.1% NaCl polymer solution was indistinguishable from the previous 1% NaCl polymer solution (Figure 4-10). At the 0.45 μm pore size, plugging became very aggressive and required quantitation over a reduced volume. This result would indicate that the vast majority of the polymer is less than 0.65 μm in diameter, and may suggest that plugging at larger pore sizes than 0.45 μm comes from polymer that is not monodisperse. It also confirms that swelling the polymer increases plugging on filter papers with pore sizes similar to the hydrated size of the polymer.

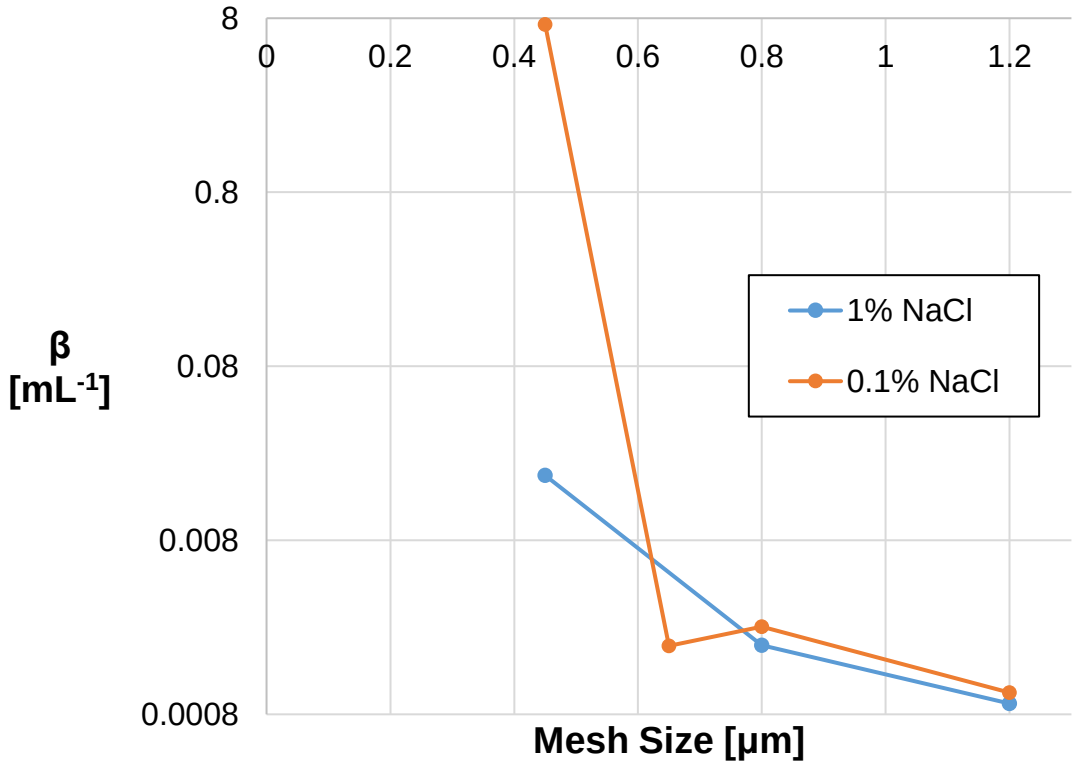

Figure 4-10: Salinity effects on filterability

4.2.4 Polymer concentration

One would naturally expect, *a priori*, that plugging should be proportional to the mass of solvated polymer since plugging is caused by polymer getting trapped in the filter. To test this hypothesis, an FP3330S polymer solution was created, identical to the original but for a reduction in polymer concentration to 0.1% from 0.2%. This new solution was filtered using the same four filters as in the salinity study. The results are surprising, and demonstrate the need for caution in making predictions and in interpreting results when all

variables are not controlled. The plugging parameter for the low-concentration solution is actually *higher* across the full range of filters tested, rather than being lower (Figure 4-11).

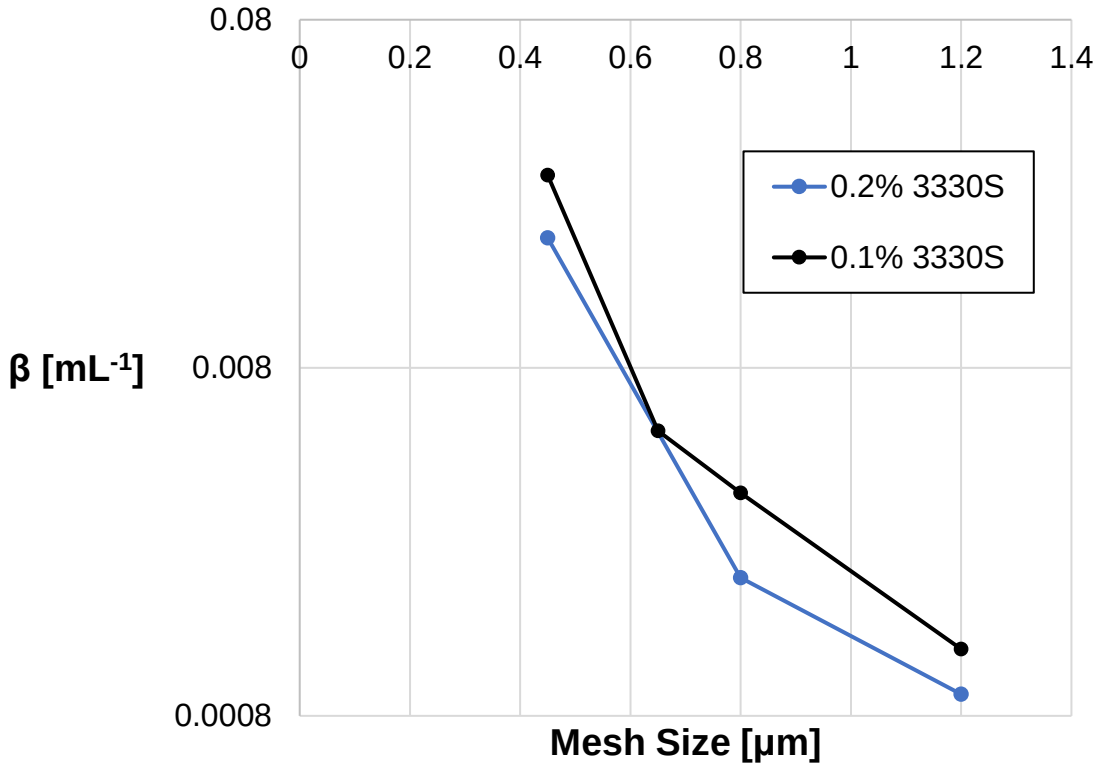

Figure 4-11: Concentration effects

There are a couple of possible explanations for this observation. First of all, pressure is controlled rather than flow rate, meaning that the low concentration polymer solution flows through the filter faster (~50%) than the high concentration polymer solution. This could account for the difference. Another important point to consider is that polymer in this concentration regime is above the interaction / entanglement threshold, wherein the shape and motion of individual polymer molecules is affected by the presence of other molecules.

4.2.5 Hydrolysis

Hydrolysis affects the swelling of HPAM polymers, and therefore potentially their filtration and plugging characteristics. Just as with a reduction in salinity (see 4.2.3: Salinity), an increase in the degree of hydrolysis causes HPAM to increase in hydrated volume to screen out charged moieties, and one would therefore predict that hydrolysis would increase plugging in a manner similar to that shown in Figure 4-10.

Mimicking the shearing and filtration procedure from a core flood discussed later, FP3330S (0.483% polymer in 2% Na_2CO_3 + 0.3% NaCl + 0.75% Na_2SO_4) was analyzed by serial filtration through 0.80 μm, 0.65 μm, 0.45 μm, and 0.22 μm cellulose filter papers. In all, 1000 g of material was made and split into four equal 250 g batches. The first was filtered with no shearing or hydrolysis. The remaining three were argon bubbled for 2 hours and hydrolyzed overnight (24 hours) at 95ºC. One was filtered without shearing, while another was sheared in the Osterizer blender at the intermediate speed setting (#6 of 12) to a Newtonian plateau viscosity of 157 cP, similar to the viscosity of the polymer used for the core flood (146 cP). The last batch was sheared to match the Newtonian viscosity of the unsheared polymer (66 cP actual, 65 cP target). The filtration results are shown in Figure 4-12.

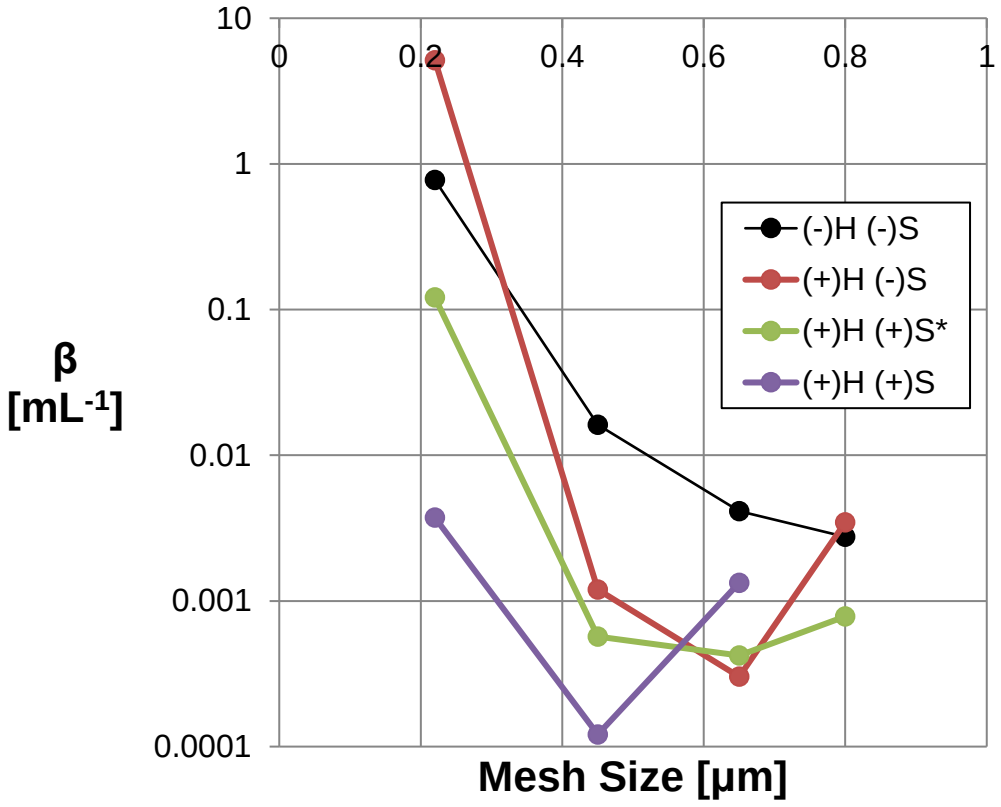

Figure 4-12: Filtration analysis of hydrolysis and shearing

The comparison between the hydrolyzed and unhydrolyzed polymer (black and red lines, respectively) is striking. Filtration at the larger pore sizes generates less plugging (by a full order of magnitude) with hydrolyzed polymer than with unhydrolyzed polymer, despite the swelling induced by hydrolysis. By contrast, at the smallest filter pore size tested (0.22 µm), the hydrolyzed polymer plugs the paper at 6.6x the rate of the unhydrolyzed polymer. Shearing generally reduces plugging with a couple of exceptions where the absolute difference in the plugging factor is small (green and purple lines for 157 cP and 66 cP solutions). The largest plugging reduction from shearing occurs at 0.22 µm. For the special

case of the viscosity-matched polymer solution, plugging is significantly reduced for all pore sizes relative to the unhydrolyzed, unsheared control (purple line compared to black). Since polymer mass concentration and brine conditions are the same between these two samples, this demonstrates that HPAM polymers of equal intrinsic viscosity (volume in solution) but different degrees of hydrolysis and swelling (and therefore likely different shapes) filter measurably differently: the hydrolyzed polymer plugs the paper less.

4.2.6 Serial filtration

It is commonly observed that after filtering a polymer solution, one may re-filter the same solution and obtain a different (lower) filtration ratio. In other words, filtration sometimes removes enough polymer that the change in the polymer molecular weight distribution can be measured, even if little-to-no shear viscosity is lost. A systematic study of filtration effects requires one to do filtration assays similar to the original in Figure 4-7 on the product solutions from a filtration assay.

A new polymer solution (0.25% FP3330S, 3% NaCl, 0.1% $NaHCO_3$) was prepared in bulk, split into ~250 mL samples, and filtered using 0.80 μm, 0.65 μm, and 0.45 μm pore size filter papers (Figure 4-13, black line). Each of the product solutions of these filtrations were filtered by three filters in series: the next larger pore size, the same pore size, and the next smaller (Figure 4-13, colored lines). The 0.45 μm pre-filtered solution plugged the 0.22 μm paper too aggressively for quantitation. The data are plotted in terms of β-estimated filtration ratio.

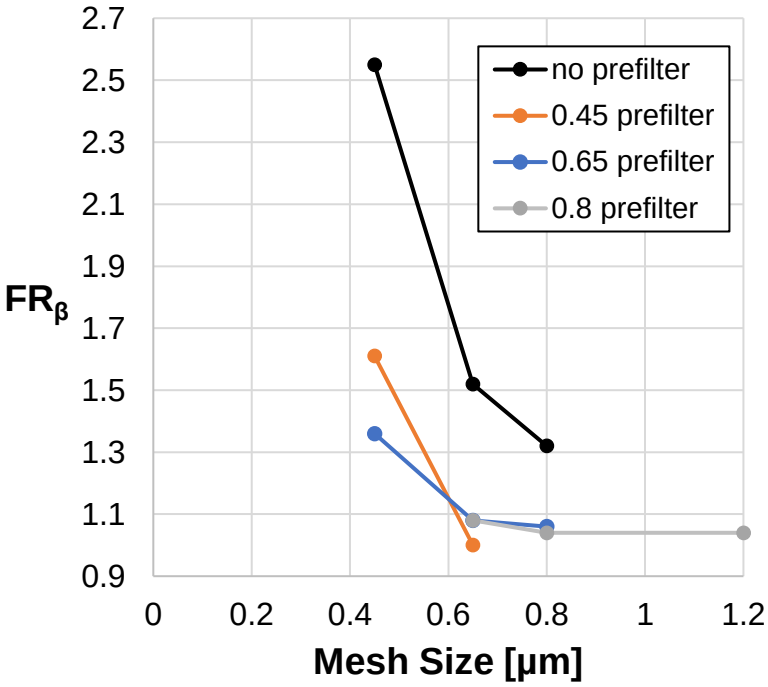

Figure 4-13: Filtration of filtered polymers

It is clear that pre-filtration has a substantial impact on subsequent filtrations, as all filtration ratios are markedly reduced. The serial filtrations largely overlap, with the possible exception of the 0.45 µm pre-filtered solution, which seems to plug a bit more on a second filtration at 0.45 µm than does the 0.65 µm pre-filtered solution. This seems consistent with the results of the earlier polymer concentration test (Figure 4-11), wherein lower concentration polymer solutions can actually give a higher plugging metric. As is shown later, the initial filtration at 0.45 µm removes a substantial amount of polymer.

4.2.7 Polycarbonate filters

Defined pore size polycarbonate filters are often used for the filtration of polymer solutions as an alternative to cellulose filters. Plugging rates on these filters may differ in principle from those observed on cellulose because of the defined pore size, but also because the material properties of the filters may differ, including lateral stretching (based on Young's modulus) of the filter and its pores, vertical compression, and pore structure.

To elucidate the filtration behavior of HPAM polymer on polycarbonate filters, serial filtrations were performed with FP3330S (0.25% polymer, 0.1% KCl + 0.15% $CaCl_2$ + 0.468% $MgCl_2$) using the 1.0 µm, 0.60 µm, 0.40 µm, and 0.20 µm filters (Figure 4-14).

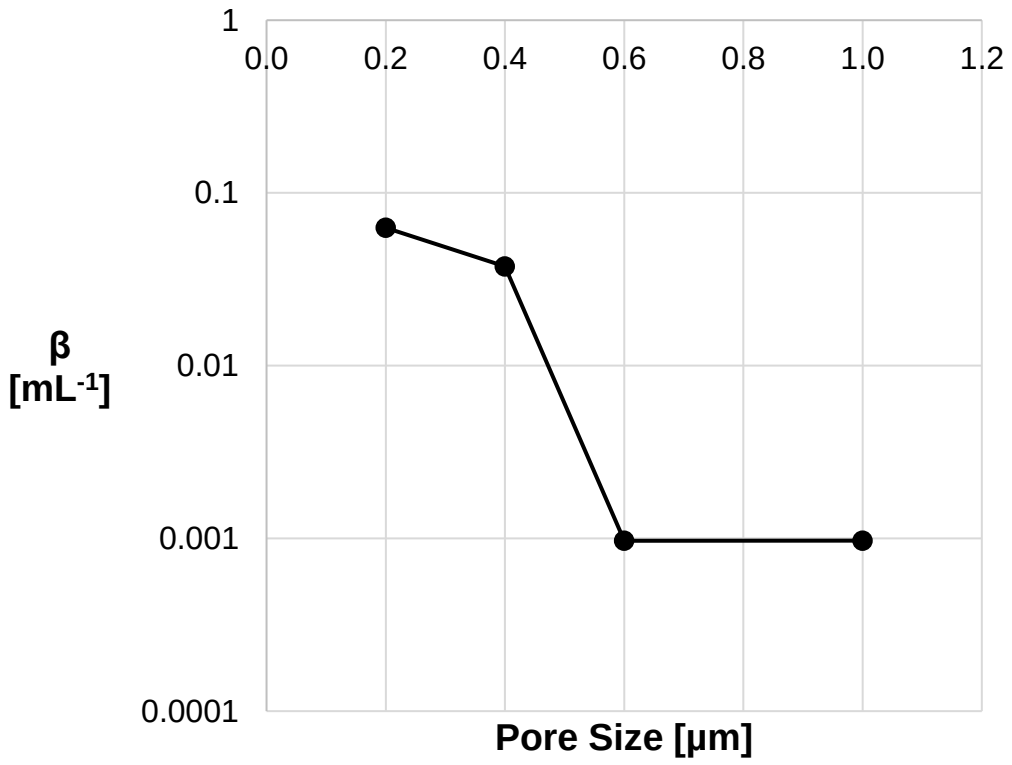

Figure 4-14: Serial filtration of FP3330S in hard brine on polycarbonate filters

Plugging rates for this polymer solution on polycarbonate filters follow a similar trend as those tested on cellulose filters (Figure 4-8). Plugging remains low for pore sizes of 0.60 μm and larger, but becomes high starting at 0.40 μm. Furthermore, solution viscosity remains high through the serial filtrations through 0.40 μm (Figure 4-15), also similar to the behavior seen on cellulose filters (see Figure 4-21, orange line, later in text).

Qualitative differences between the plugging behaviors on these different filter papers can be seen at the smallest pore sizes (0.20 μm and 0.10 μm for polycarbonate, 0.22 μm and 0.10 μm for cellulose). Plugging rates increase far more slowly on polycarbonate filters compared to cellulose filters as serial filtration proceeds from 0.40 μm to 0.20 μm to 0.10 μm (versus 0.45 μm to 0.22 μm to 0.10 μm). Unsheared FP3330S solutions were not observed to filter through 0.22 μm cellulose filters for more than ~20 mL at 15 psig, while filtrations with 0.20 μm and 0.10 μm polycarbonate filters could proceed for ~200 mL.

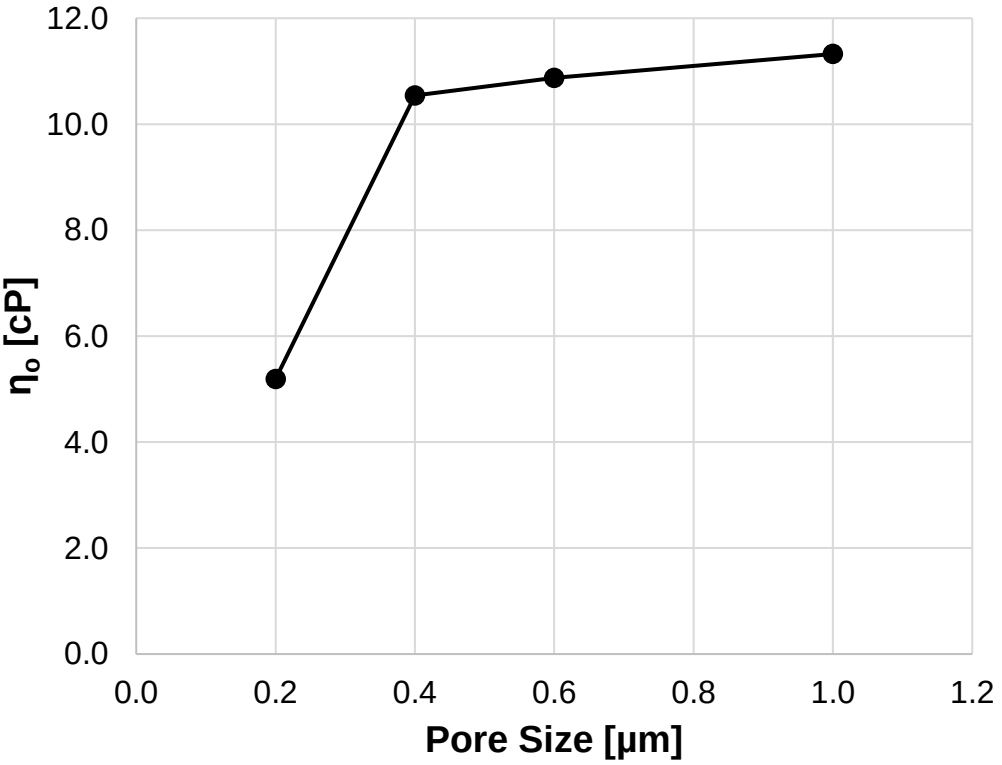

Figure 4-15: Filtrate viscosity of serially-filtered FP3330S in hard brine on polycarbonate filters

On polycarbonate filters, the FP3330S solution loses around 50% of its filtrate viscosity from the 0.40 µm to 0.20 µm filtrations (Figure 4-15), versus. 80% moving from the 0.45 µm to 0.22 µm filtrations. Perhaps more revealing is the plugging behavior through filtrations to 0.10 µm, as summarized in Table 4-1.

Table 4-1: Filtrations with FP3330S in hard brine on polycarbonate filters

Filtration	Pore Size	Previous	FR_β
1	1	0	1.16
2	0.8	0	1.1
3	0.6	2	2.1
4	0.6	3	2.51
5	0.4	4	1.75
6	0.4	5	1.58
7	0.4	6	1.61
8	0.4	7	1.5
9	0.4	8	1.43
10	0.4	9	1.45
11	0.4	10	1.43
12	0.4	11	1.54
13	0.2	12	2.13
14	0.1	13	1.69
15	0.2	14	1.94
16	0.4	15	1.32
17	0.1	16	1.75
18	0.4	0	1.94
19	0.1	17	1.84
20	0.2	19	1.95

Note that the β-estimated filtration ratio (FR_β) actually decreases moving from 0.20 µm to 0.10 µm (13^{th} and 14^{th} filtrations), and appears reliably lower at 0.10 µm than 0.20 µm across the three tests. While it is possible that these differences stem from the difference in brine composition compared to the tests with cellulose filters, the qualitative decrease in plugging on 0.10 µm polycarbonate filter paper compared to 0.20 µm does not make sense and was not observed in any case with the tight cellulose filters.

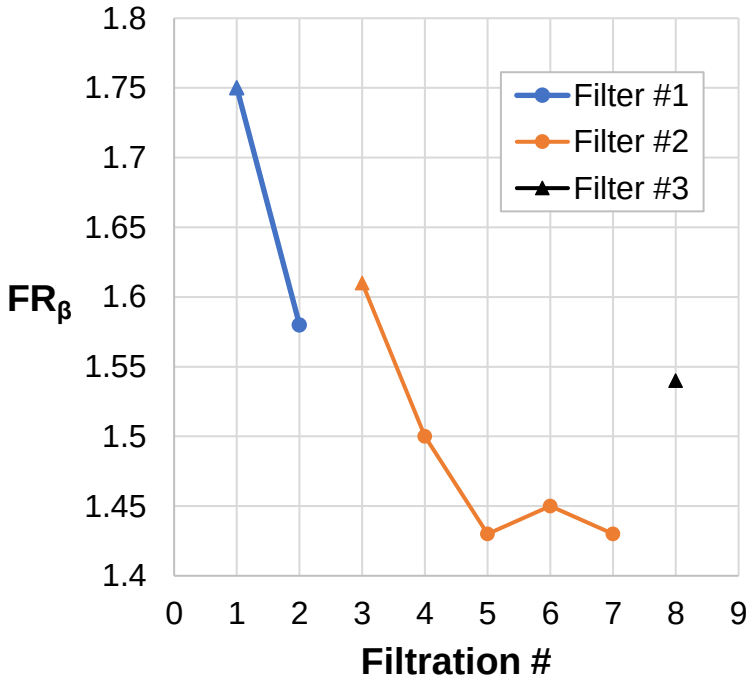

Figure 4-16: Serial filtrations of FP3330S in hard brine on 0.40 µm filters

The filtration efficiency of the 0.40 µm polycarbonate filters is probed in Table 4-1 and plotted in Figure 4-16 with colored lines to indicate filter changes. The data indicate that approximately four filtrations are required (probed by the 5th plugging measurement) to reach a residual level of plugging. There also appears to be a measurable, intrinsic difference between filter permeabilities.

4.3 Filtration of Scleroglucan Solutions

Scleroglucan is a glucose-derived biopolymer that is a rod-like triple helix (total molecular weight = 3 MDa) in solution. Due to its shear thinning rheology (in turn due to its rod-like structure), scleroglucan solutions typically filter exceedingly quickly through 1.2 µm

cellulose filters at 15 psi and give filtration ratios much less than 1.2, though this has never equated to good transport in sub-darcy sandstones (Lee, 2015).

Despite its low molecular weight, the intrinsic viscosity of scleroglucan is high. A solution of scleroglucan (0.1% polymer in synthetic seawater: 2.38% NaCl + 0.393% Na_2SO_4 + 0.028% $NaHCO_3$ + 0.08% KCl + 0.116% $CaCl_2$ + 0.517% $MgCl_2$) was prepared from 0.35% active paste by double homogenization through an IKA Magic Lab mixer at 20,000 rpm (see Materials and Methods: Hydration). Serial dilutions were prepared in SSW at 500 ppm, 250 ppm, 187.5 ppm, 125 ppm, 62.5 ppm, and 31.25 ppm for steady shear sweep measurement on the LS-1 rheometer. The Newtonian plateau viscosities were extracted for each solution, converted to reduced viscosities, and plotted as a function of polymer concentration (Figure 4-17). A linear fit over the range of 62.5-250 ppm yields an intrinsic viscosity of 84.6 dL/g.

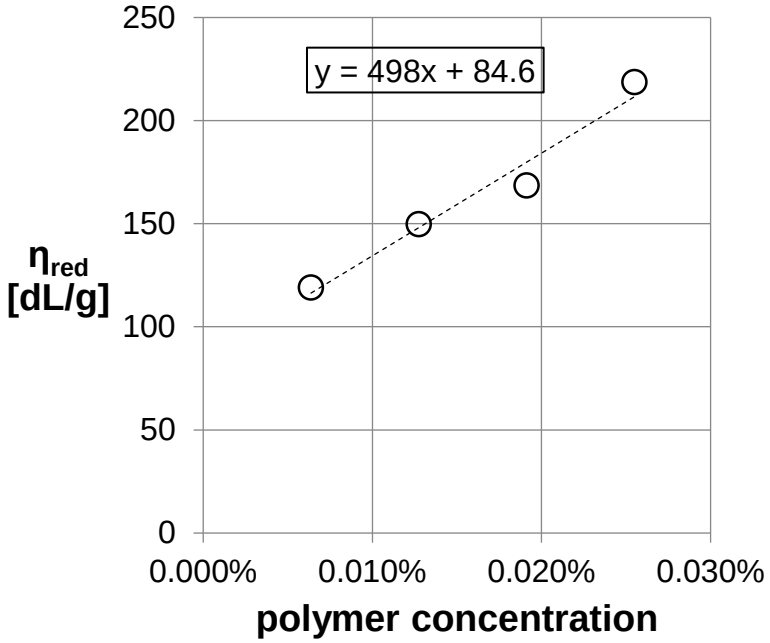

Figure 4-17: Intrinsic viscosity of scleroglucan in SSW

By contrast, FP3630S (~18 MDa) has an intrinsic viscosity of 56.7 dL/g in the same brine, and FP3230S (~5 MDa) has an intrinsic viscosity of 25.0 dL/g (Figure 4-18). In single molecule terms, these correspond to $[\eta]M = \sim 1000$ dL/mol and ~125 dL/mol, respectively, in contrast to ~250 dL/mol for scleroglucan.

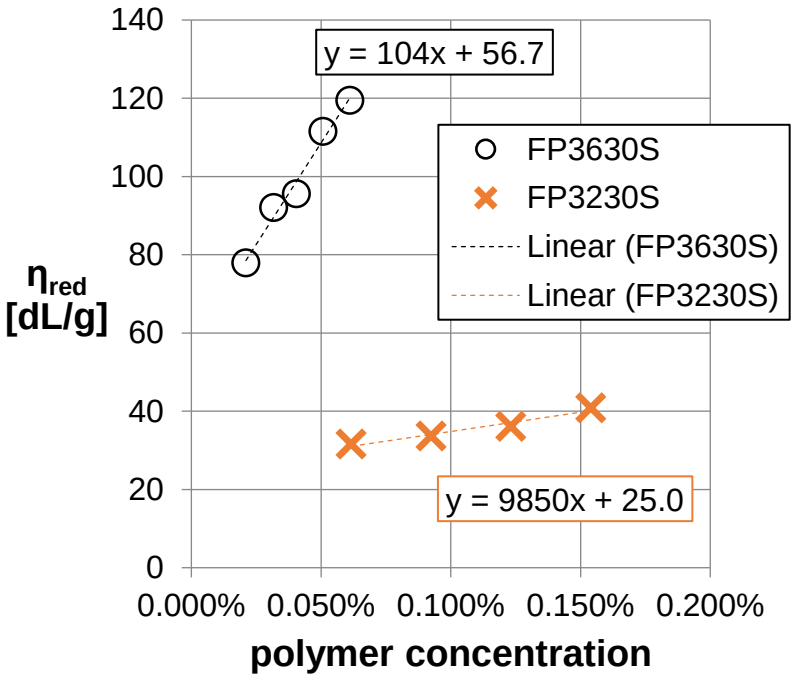

Figure 4-18: HPAM polymer intrinsic viscosity in SSW

In the Mark-Houwink model with a typical value of α=0.6 for HPAM in a high salinity, hard brine, a 250 dL/mol HPAM polymer would be expected to have a molecular weight of ~7.7 MDa. This is very similar to the 8 MDa reported molecular weight for FP3330S by SNF. Therefore, the volume of a scleroglucan triple helix is very similar to that of FP3330S in synthetic seawater (SSW), even though it is a very different shape. This informs how one interprets filtration and transport data.

To combat the high flow rate of scleroglucan filtrations at 15 psig head pressure, the head pressure was lowered to 2.5 psig. Serial filtrations of scleroglucan in SSW were

conducted on cellulose filter papers, with observed plugging behaviors reported below in Figure 4-19.

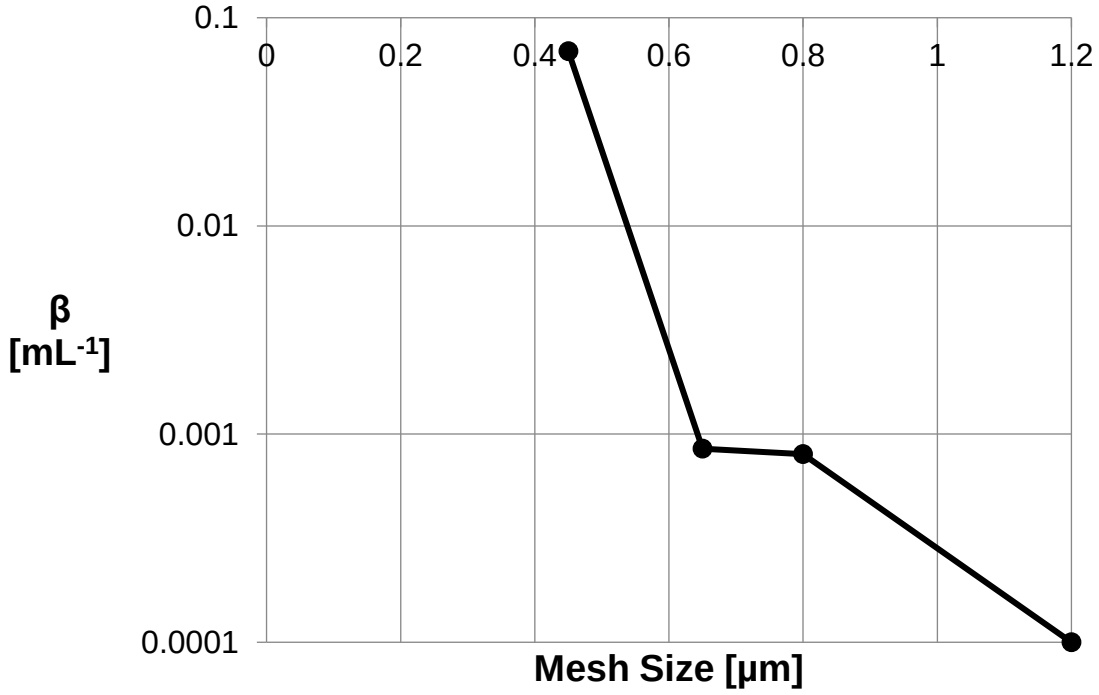

Figure 4-19: Scleroglucan serial filtration on cellulose filter paper

The inflection from low to high plugging occurs between the 0.65 µm and 0.45 µm filters as it does for FP3330S, consistent with its similar single molecule size. Overall, the inflection is sharper (~2 orders of magnitude between the 0.65 µm and 0.45 µm filters) than observed with most FP3330S solutions, however the increase over the same span for the very low salinity FP3330S solution was greater (Figure 4-10), both proportionally and in the absolute sense. This points to a possible explanation: the shape of the scleroglucan molecule causes it to filter with lower plugging at pore sizes larger than its inflection and

greater plugging at smaller pore sizes as compared to a more globular polymer of the same volume (e.g. HPAM at moderate or high salinity). Mechanistically, this may be due to a transition between travelling through the filter with the long axis oriented along the pore axis to a disoriented configuration.

4.4 Shearing Optimization for Filtration through Small Pore Size Filters

4.4.1 Viscosity and concentration versus filtered volume

One practical consideration with small pore size laboratory filters is the volume of polymer solution that they can filter with consistent quality. They are often changed on the basis that the filtration is taking more time than the experimentalist would like, but a greater concern is whether the plugging of the filter causes it to remove an ever-increasing amount of polymer from solution.

A solution of FP3330S (0.25% FP3330S, 3% NaCl, 0.1% $NaHCO_3$, identical to that from the Serial filtration subsection) was pre-filtered at 0.65 μm and then filtered at 0.45 μm and 40 mL fractions were collected (Figure 4-20, black line). Some of this 0.45 μm pre-filtered solution was then filtered at 0.22 μm, and 11 mL fractions were collected (Figure 4-20, orange line). The data indicate that while the effluent viscosity from the 0.45 μm filter is consistent, while the effluent viscosity from the 0.22 μm filter falls off sharply. The lesson is that volume must be controlled for any filter that produces a filtrate of lower viscosity than the starting solution, unless it can be affirmatively established that filtrate viscosity is invariant to filtered volume.

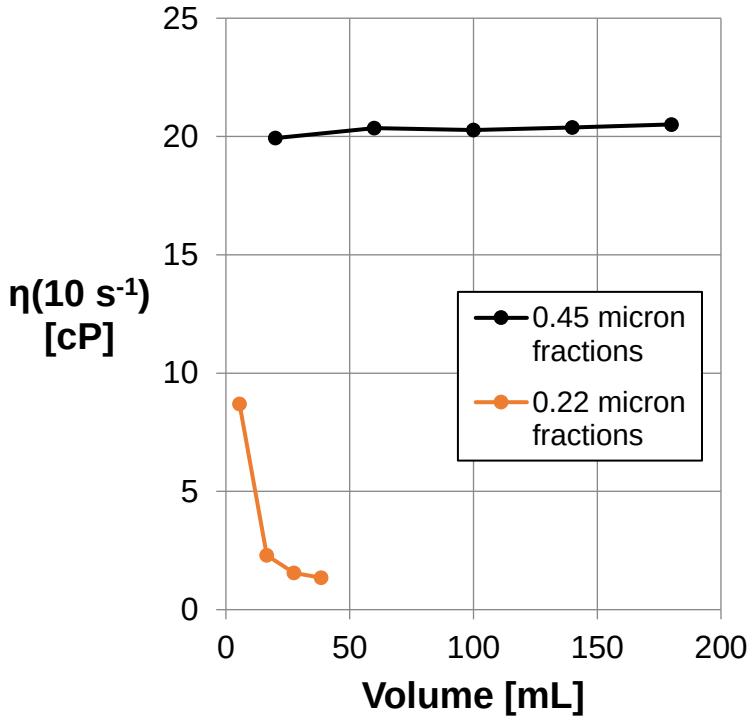

Figure 4-20: FP3330S filtrate viscosity with filtered volume

For this FP3330S solution, consistent viscosity can be obtained through a filter of 0.65 µm pore size or larger without shearing or pre-filtration. With pre-filtration at 0.65 µm, a subsequent filtration at 0.45 µm results in no loss of viscosity (Figure 4-21, top panel, orange line). By shearing briefly in a low power blender (Osterizer) to mimic the loss of viscosity from pre-filtration at 0.65 µm, all filtrations at 0.45 µm pore sizes and larger are lossless as measured by shear viscosity (Figure 4-21, top panel, grey line). Interestingly, the pre-filtered, sheared solution measurably outperforms the unsheared, pre-filtered solution when filtered at 0.22 µm, despite having a similar shear viscosity (Figure 4-21, top panel, orange and blue lines). However, the elastic modulus of the sheared, pre-filtered

solution is lower than that of the unsheared, pre-filtered solution (Figure 4-21, bottom panel, orange and blue lines). These data are consistent with the notion that shearing is more efficient at removing large polymer species from solution than filtration, at least in this size regime. It is also possible that there is a subtle difference in shear viscosity that is simply amplified in the elastic modulus measurement.

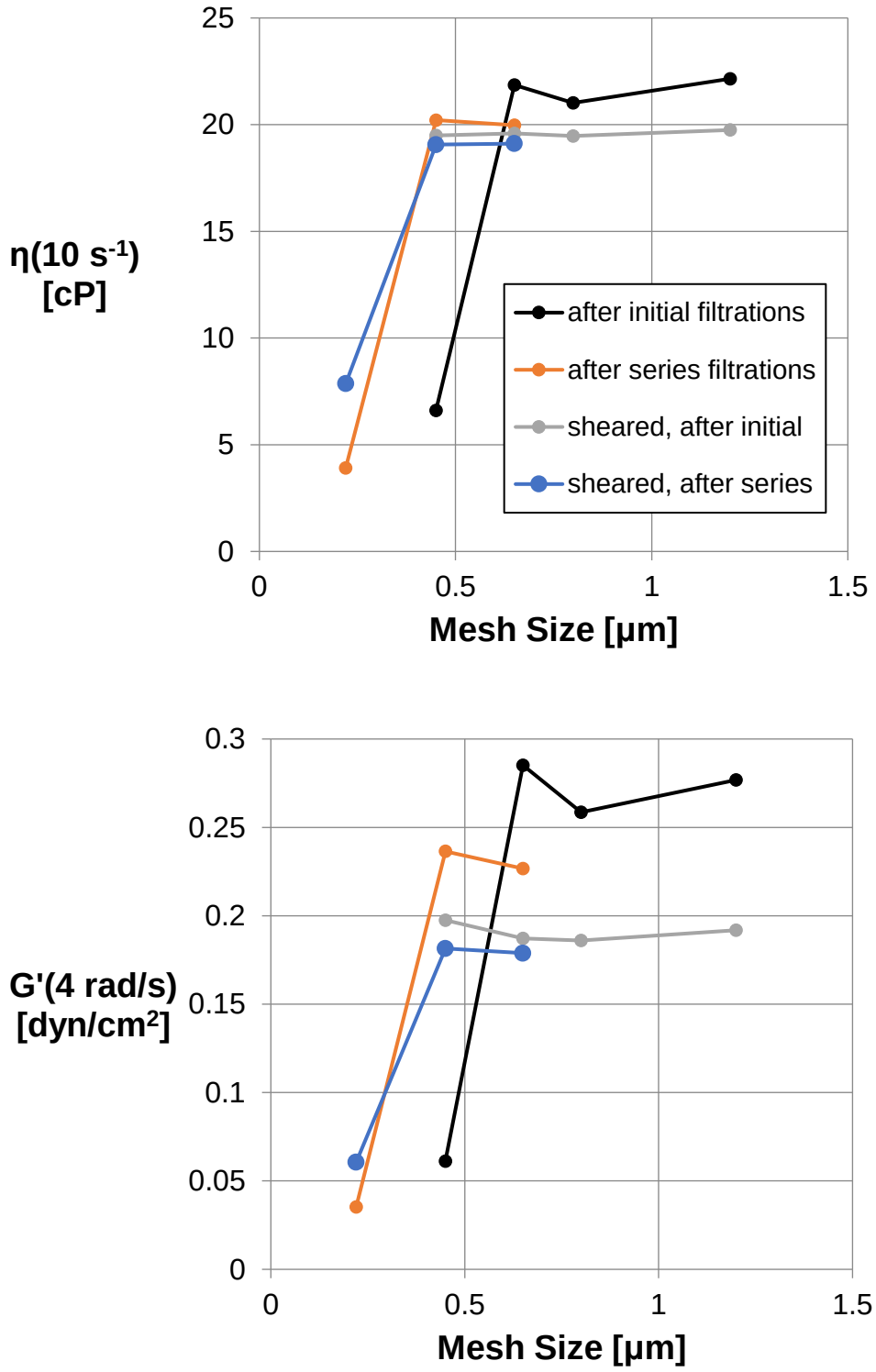

Figure 4-21: Shearing and filtration improve filtrate viscosity (top) and elastic modulus (bottom)

HPAM polymer concentration was measured using a bleach assay. The polymer viscosity samples used to generate the data in Figure 4-21 were prepared as described in Chapter 3 (UV-Vis Assay for Polymer Concentration), which was calibrated from dilutions of the starting polymer solution as a standard. The resultant polymer concentrations are reported in Figure 4-22. They mirror the viscosity data, but, as expected, polymer concentration falls off less sharply than viscosity. Still, the majority of the filterable mass was removed by the 0.22 μm filter after 0.45 μm filtration (Figure 4-22, orange line). While one may naively interpret this to mean that ~67% of the polymer mass falls between 0.22 μm and 0.45 μm in filtration size, the results of the fractionation test obfuscate the interpretation (Figure 4-20, orange line). Nevertheless, it is clear that shearing reduces the size of the polymer enough to allow far more to pass the tight, 0.22 μm filter (Figure 4-22, blue line).

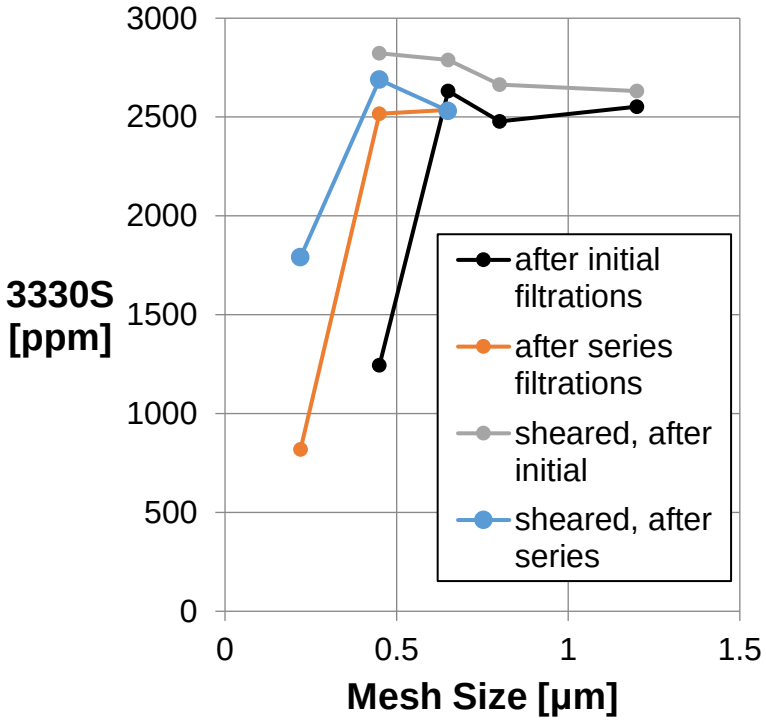

Figure 4-22: Shearing and filtration improve filtrate concentration

4.4.2 Effluent viscosity versus shearing time

To demonstrate the optimization of HPAM polymer shearing for a tight filter (0.22 µm), the FP3330S solution from the previous section was sheared in three separate 260 g batches in the Osterizer blender for three blending times: 20, 40, and 80 seconds. A sample of the unsheared polymer was reserved as well. Each large polymer sample was serially filtered through the 0.65 µm and 0.45 µm filters. For the 0.22 µm filtrations that followed, the filtration volume was standardized to 20 mL as a minimal laboratory volume. All filtrations were done at room temperature and 15 psig. The viscosity summary results are shown in Figure 4-23, below.

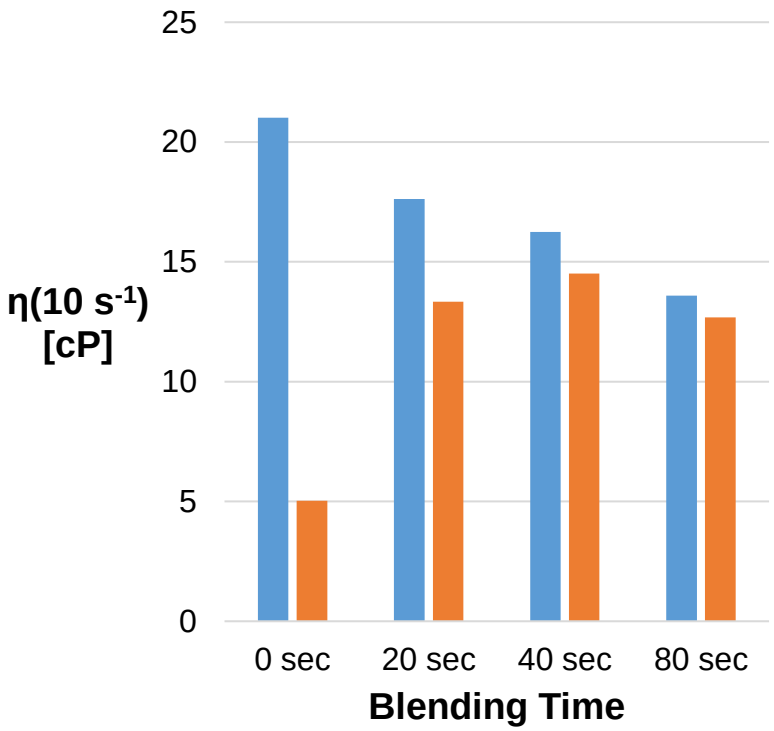

Figure 4-23: Viscosity of sheared polymer before (blue) and after (red) 0.22-micron filtration

The original solution viscosity is 21 cP at a shear rate of 10 s^{-1}. The 20, 40, and 80 second time points are 84%, 77%, and 65% of this original viscosity, a predictable monotonic decline. The filtrate viscosities were 24%, 76%, 89%, and 93% of these sheared, pre-filtered viscosities, a monotonic but diminishing increase. The result of these countervailing effects is an optimum (in terms of filtrate viscosity) around 40 seconds of shearing time, with an overall viscosity of 69% of the original, unsheared solution viscosity. Because of the power series relationship between solution viscosity and intrinsic viscosity, the change in intrinsic viscosity underlying this viscosity change is even less than

this moderate (31%) decline, meaning that the mean square hydrodynamic radius changes by 10% or less to fit through the filter.

The plugging data are illustrated in Figure 4-24. Plugging of the less stringent filters is barely differentiable (0.65 μm) or indifferentiable (0.45 μm). Plugging of the 0.22 μm filter is very high for all solutions (for reference, $\beta = 0.02$ corresponds to $FR_\beta = 2$), but shows a clear trend of decreasing plugging with increasing shearing time. Relative to the unsheared solution, plugging is attenuated 28%, 55%, and 81% for the 20, 40, and 80 second sheared solutions, respectively, a trend that mirrors their steady loss of viscosity. Percentage-wise, plugging decreases more quickly than viscosity falls, likely because plugging is produced by a subset of the molecular weight distribution at the high end that is also disproportionally affected by shearing.

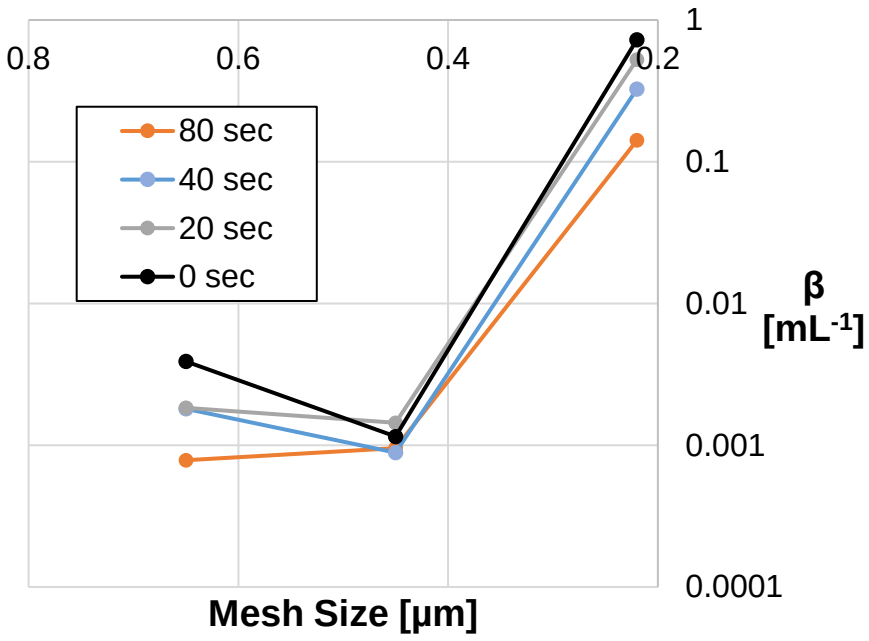

Figure 4-24: Serial filtrations on sheared 3330S

4.5 Chapter Conclusions

1. Consistent with previous reports, valves and blenders irreversibly degrade high molecular weight HPAM, and this degradation is enhanced by the presence of calcium ions. The extent of degradation observed decreases with time or pass number in an apparent exponential fashion, indicative of the reduced susceptibility of lower molecular weight HPAM to shear degradation. The exponential model suggests a simple way to quantitate the speed and strength of degradation in any given device, as illustrated by the blender speed comparison.
2. Filtration can be used to quantitatively assay the overlap between the filtration size of polymer molecules within the molecular weight distribution and a narrowing pore aperture. This assay can be used to analyze the effects of changes in polymer solutions like mechanical shear degradation, hydrolysis, brine salinity, and polymer concentration. The effects of mechanical shear degradation are qualitatively in line with *a priori* expectations. In conjunction with viscosity data, filtration assays on sheared solutions illustrate that it is the high end of the molecular weight distribution that causes plugging, and that the shape of this high molecular weight tail is barely affected. The effects of hydrolysis and brine salinity are, not surprisingly, qualitatively alike: plugging increases at small pore sizes relative to the unhydrolyzed HPAM polymer filtration size. Plugging can remain the same or even decrease at pore sizes above the inflection in unhydrolyzed polymer plugging, which is surprising because hydrolysis causes an increase in HPAM's

hydrodynamic volume. With the increase in volume comes a change in shape towards a more rod-like structure, which may account for the effect.

3. Filtrates that are re-filtered can give reduced plugging at the originally filtered pore size, as well as on filter papers with pore sizes that are a step away. Filtration at a pore size one step above a target pore size (e.g. filtration at 0.65 μm before filtration at 0.45 μm) can reduce plugging on the target filter and significantly improve filtrate viscosity. This is perhaps the simplest tool for viscosity preservation available.
4. Shearing optimization for any given filter can be done to preserve filtrate viscosity. Pre-filtration with the next larger pore size is advised (as in conclusion #3). Filtrate volume per filter must be standardized. Surprisingly high viscosities can be obtained in filtrates from tight filters, e.g. 69% of an FP3330S solution viscosity through 0.22 μm pore size.
5. Scleroglucan is a rod-like biopolymer that filters very quickly at pressures around 15 psig. A pressure of 2.5 psig gives interpretable results, and reveals that rod-like character may influence the steepness of the plugging curve in the pore size assay, in a similar but more dramatic fashion than for hydrolyzed HPAM.

5 Core Floods

A series of core floods were undertaken to evaluate polymer transport in porous media. Both HPAM and scleroglucan were studied. With two exceptions (CQ-1 and SCL-06), all cores are pressure tapped, foot-long, 1 ½ inch diameter cores (see Table 5-1). In the case of HPAM, both single-phase and multiphase flow experiments were conducted. Scleroglucan was studied only in single-phase flow experiments, but important progress was nonetheless achieved.

Table 5-1: Core Floods

Flood	Lithology	Length [cm], Dia. [cm]	Perm. [mD] Porosity	Polymer	Test Type
CQ-1	Sandstone (Outcrop)	7.205; 2.524	40; 18.4%	FP3330S	Single phase injectivity
CT-01	Sandstone (Outcrop)	30.4; 3.79	28; 15.0%	FP3330S, FP3630S	Single phase injectivity
SAMA-13R	Carbonate (Reservoir)	29.97; 3.81	18; 24.0%	FP3330S	ASP
SAMA-16R	Carbonate (Reservoir)	27.23; 3.80	35; 23.8%	FP3330S	ASP
SCL-06	Sandstone (Outcrop)	30.24; 5.06	414; 23.0%	Scleroglucan	Single phase injectivity
SCL-08	Sandstone (Outcrop)	29.31; 3.78	105; 20.9%	Scleroglucan	Single phase injectivity
SCL-09	Sandstone (Outcrop)	30.38; 3.83	218; 23.7%	Scleroglucan	Single phase injectivity

5.1 Single-Phase HPAM Floods

The limits of HPAM transport in sandstone are not well established despite many years of laboratory experiments and numerous field projects. Herein, an efficient experimental

design is delineated to determine the maximum filterable size of HPAM polymer that will transport in a given laboratory core. Serial flooding is used to incrementally probe the transport behavior of HPAM of increasing hydrodynamic size in each rock sample. Hydrodynamic size is set using shearing and filtration. Polymer solutions are injected in order of ascending viscosity to prevent unstable displacement and fingering.

5.1.1 CQ-1 Sandstone

The CQ-1 block is a Berea sandstone outcrop rock. A 2.8-inch-long, 1-inch diameter core plug was drilled from this block and vacuum saturated with hard brine (3% NaCl + 0.1% KCl + 1% $MgCl_2$ + 0.2% $CaCl_2$; see Chapter 4: Polycarbonate filters). From pre- and post-saturation weight measurements, the core's porosity was determined to be 14.3% (ρ_{brine} = 1.026 g/cm^3). However, this figure would imply a matrix density of 2.52 g/cm^3, below that of sandstone (2.65 g/cm^3), the least dense of lithologies. The error likely stems from the estimation of dead volume for the core holder. It is therefore considered more accurate to assume a sandstone lithology to derive the porosity, which gives 18.4%.

Brine and polymer injection were accomplished through the use of the piston apparatus previously employed for needle valve shearing (see Chapter 4: Shearing through valves). A schematic is presented below in Figure 5-1. Rate control is still achieved through the ISCO pump.

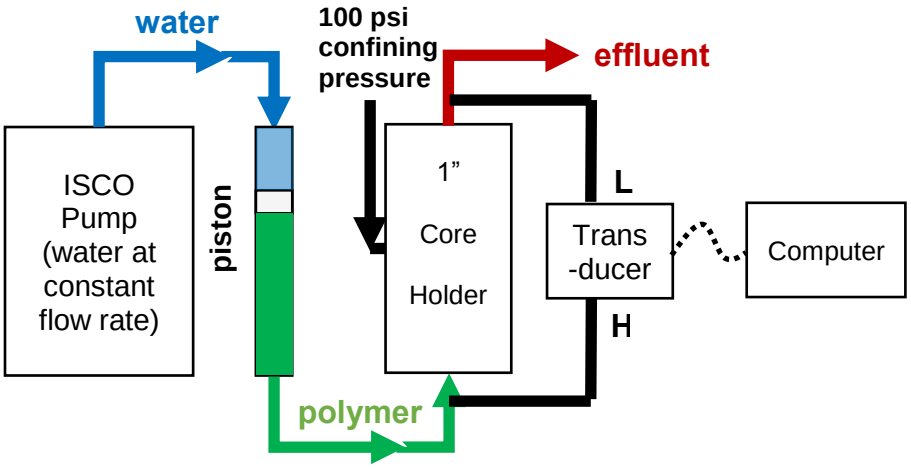

Figure 5-1: Schematic of piston-driven polymer injection

The pressure drop across the core plug was measured for brine flow rates of 0.1, 0.2, 0.4, 0.6, 0.8, and 1.0 mL/min. The data were fit to a regression line with a slope of 8.22 psi-min/mL (Figure 5-2), translating to a permeability of approximately 40.3 millidarcys ($\mu_{brine} \approx 0.94$ cP).

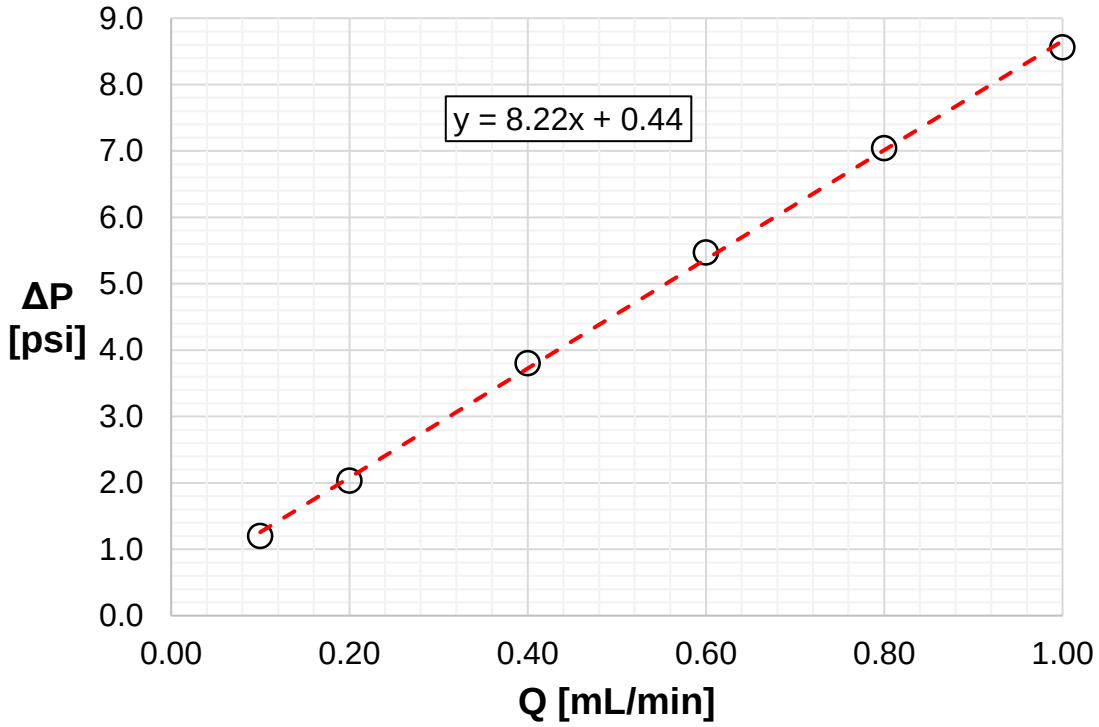

Figure 5-2: Permeability testing of CQ-1

Polymer was prepared by hydrating FP3330S in a brine of moderate salinity (1% polymer, 3% NaCl). A 180 g mass of the stock was loaded into the Osterizer blender and sheared on its lowest setting for 0.5, 1, 2, 4, and 8 minutes, with a 20 g sample removed at each time point and diluted to the final solution conditions (0.25% polymer, 3% NaCl + 0.1% KCl + 1% $MgCl_2$ + 0.2% $CaCl_2$). The 8-minute and 4-minute samples were chosen for injection into the core, in addition to the unsheared polymer. The sheared samples were filtered at 0.40 µm using polycarbonate filters; the unsheared sample was filtered at 0.60 µm. The shear-dependent viscosities of the blended, filtered samples are shown in Figure 5-3. The differences in viscosity are modest between the injection solutions.

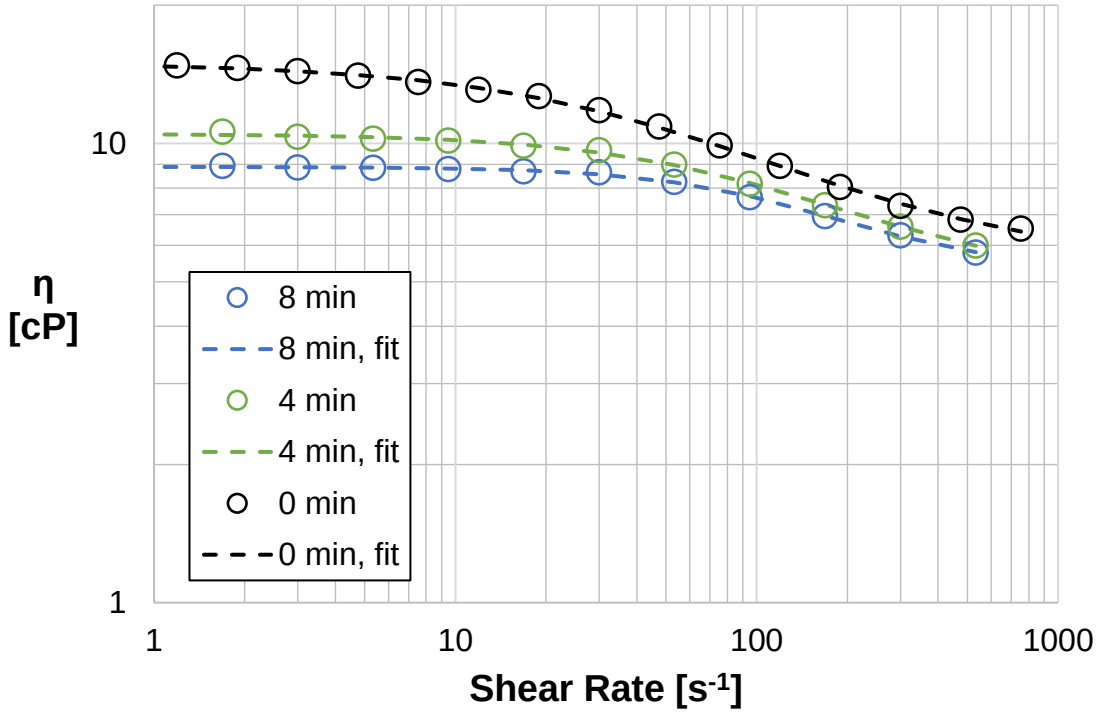

Figure 5-3: Viscosity of CQ-1 injected polymer solutions

The lowest viscosity injection solution was injected primarily at 0.030 mL/min (1.98 ft/d) for 4.4 pore volumes. The pressure plateau is unstable due to residual air in the piston (Figure 5-4, black data), however the baseline pressure reading at that flow rate appears to be 3.1 psi, which corresponds to an apparent viscosity of 9.4 cP, which is greater than the viscosity of 9 cP registered in the Newtonian plateau region of the shear rate sweep curve for this polymer solution, but well within experimental error. For this solution, the Newtonian plateau extends to approximately 30 s^{-1}. Grey data in Figure 5-4 were collected after removal of excess air in the piston.

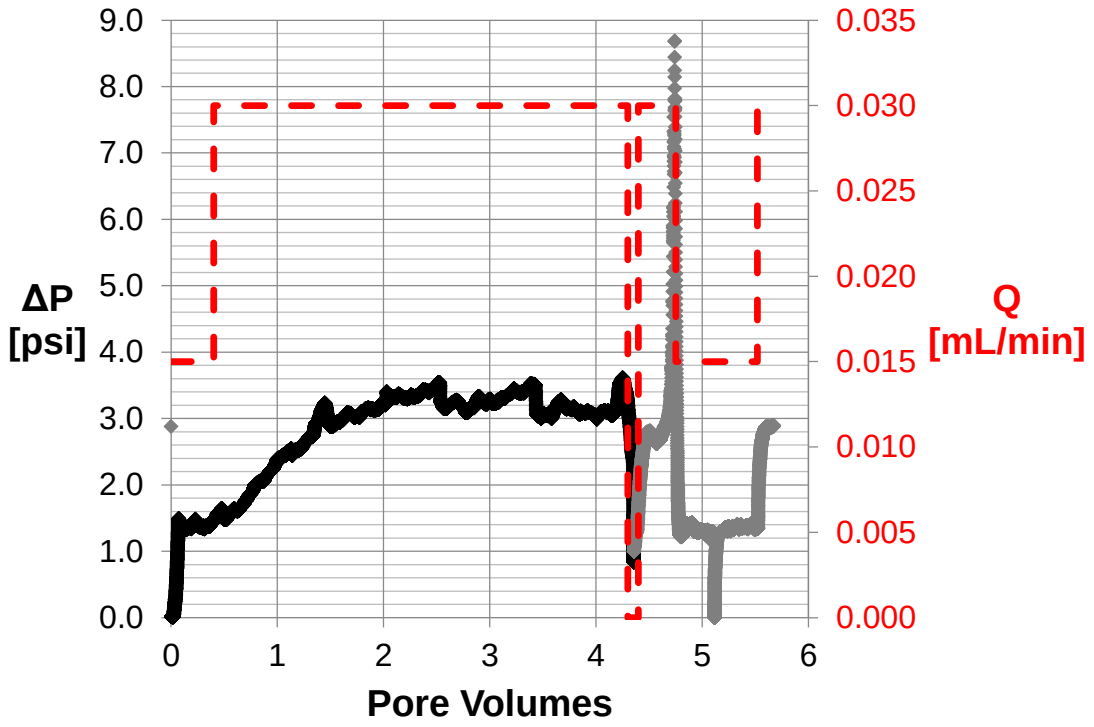

Figure 5-4: Pressure drop during injection of 8-min blended polymer into CQ-1

The 4-minute sheared solution was injected behind the 8-minute solution. Focusing again on the pressure plateau region from 4 to 4.6 pore volumes injected, the average pressure drop is 3.73 psi, and the effective viscosity is 11.3 cP, slightly above the Newtonian plateau viscosity of 10.3 cP measured in the LS-1, but again, within experimental error (Figure 5-5). The Newtonian plateau for this solution extends to approximately 16 s^{-1}.

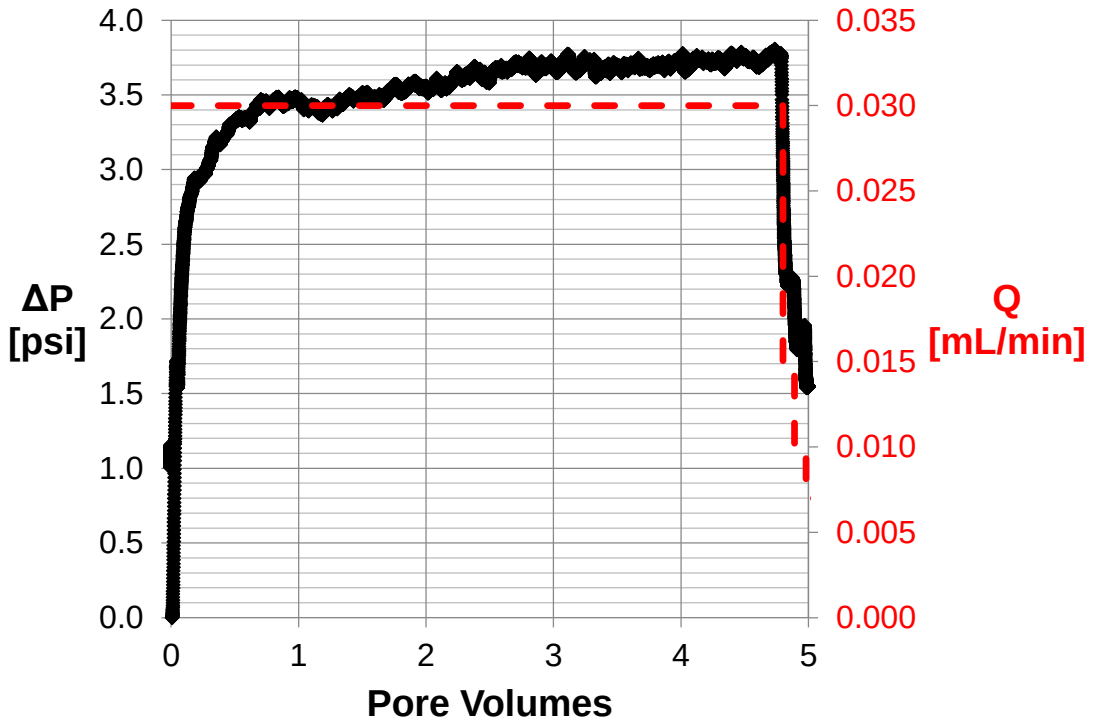

Figure 5-5: Pressure drop during injection of 4-min blended solution into CQ-1

The third and final solution, the unsheared, 0.60 µm filtered solution, was injected at 0.030 mL/min for 3.7 pore volumes before rate modulation (Figure 5-6). The pressure drops at 0.030, 0.020, and 0.010 mL/min were 4.13, 2.75, and 1.38 psi, respectively, giving apparent viscosities of 12.7, 13.6, and 14.2 cP.

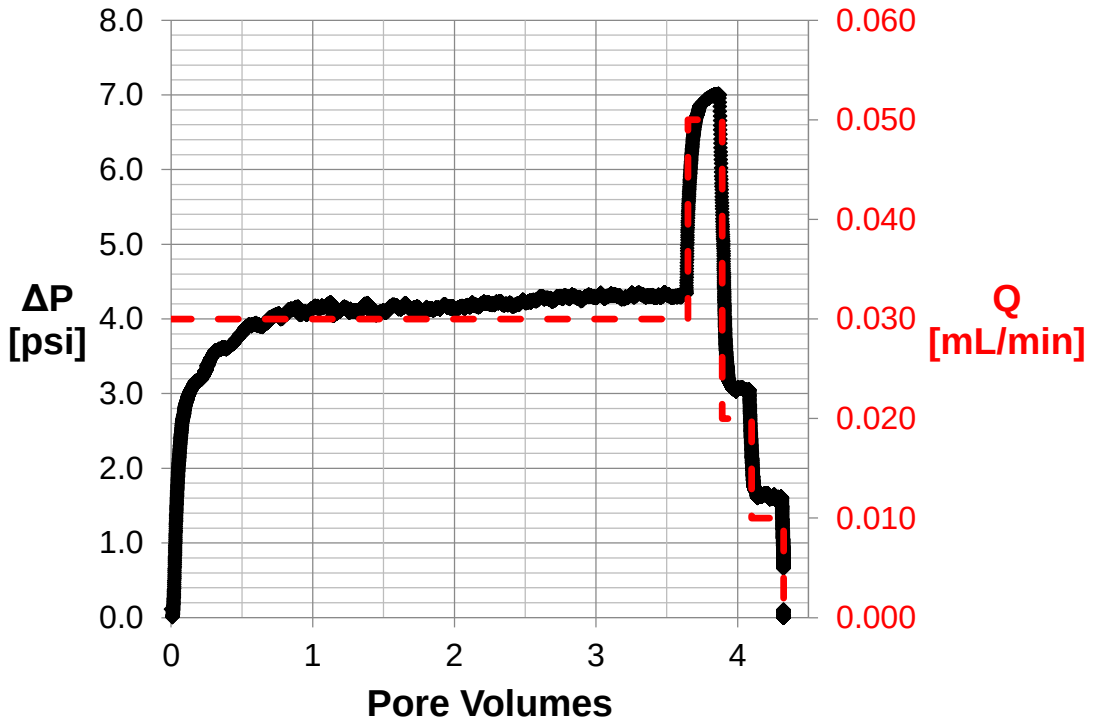

Figure 5-6: Pressure drop during injection of unsheared solution into CQ-1

This last solution was just shear thinning enough in this shear rate regime to begin to measure the effect of shear rate on apparent viscosity. Plotted on top of the rheometer data for this solution, the apparent value of the shear correction factor, *C*, is 4 (Figure 5-7). The permeability reduction factor, $R_k = \frac{\mu_{\text{brine}}/\Delta P_{\text{brine}}}{\eta_{\text{polymer}}/\Delta P_{\text{polymer}}}$, is presumed to be 1. The measurement technique in subsequent floods needed to be improved, as the volume of the piston was insufficient to ensure that multiple pressure plateaus could be achieved. Note that with the shear correction factor at its highest level, the highest shear rate assayed is still within the Newtonian plateau region of the previous two solutions (the highest is 14.6 s^{-1}).

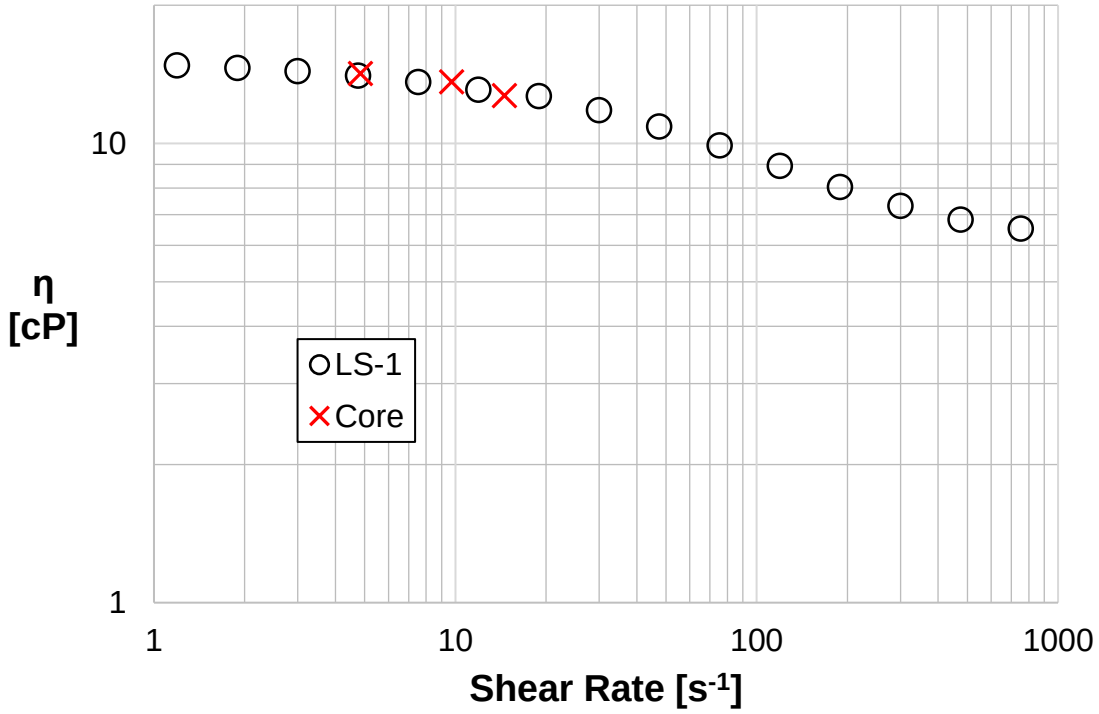

Figure 5-7: CQ-1 apparent viscosity versus LS-1 shear viscosity for final injected solution

Only slight plugging was observed in the CQ-1 core flood, as judged by the pressure plateauing behavior of the unsheared polymer solution (Figure 5-6) and the consistency of the apparent viscosity measurements with the rheological data with an undamaged core.

5.1.2 CT-01 Sandstone

Learning from the CQ-1 flood, it was apparent that some combination of a tighter sandstone and polymer of larger filtration size would be required to instigate plugging. Air and brine (6% KCl) permeability testing with a 1-inch diameter, 2-inch long plug from a block of the Carbon Tan outcrop sandstone (Kocurek) gave permeabilities of 69.6 millidarcys and 30.6

millidarcys, respectively. The rock's porosity was estimated to be 16.5% based on its bulk density and assuming a sandstone lithology for the grain density.

After brine testing, the plug was purged with 3 pore volumes of methanol and then dried overnight by air injection at 40 psi to prepare it for mercury injection capillary pressure measurement (MICP) at Core Laboratories. The MICP results are shown in Figure 5-8, courtesy of Core Laboratories. They measured a porosity of 17.8%, and pore sizes that are somewhat larger than one would expect: median pore size is 3.32 μm in radius, and 99% of the predicted permeability is realized at a radius of 1.95 μm. The matrix lithology implied by the porosity measurement is ~2.70 g/cm^3, similar to that of limestone (2.71 g/cm^3). The porosity value thus seems less reliable than the values measured here.

Company:	University of Texas at Austin
Well:	Unknown_University Sample
File:	HOU-1701173

Sample:	**2m**	un-	Host Plug	
Depth, feet:	NA	stressed	n/a	n/a
Klinkenberg Permeability, md:		N/A	-	-
Permeability to Air, md:		N/A	-	-
Swanson Permeability, md:		56.5	-	-
Porosity, fraction:		0.178	-	-
maximum Sb/Pc, fraction:		0.315		
R35, microns:		5.41		
R50 (median pore throat radius):		3.32		

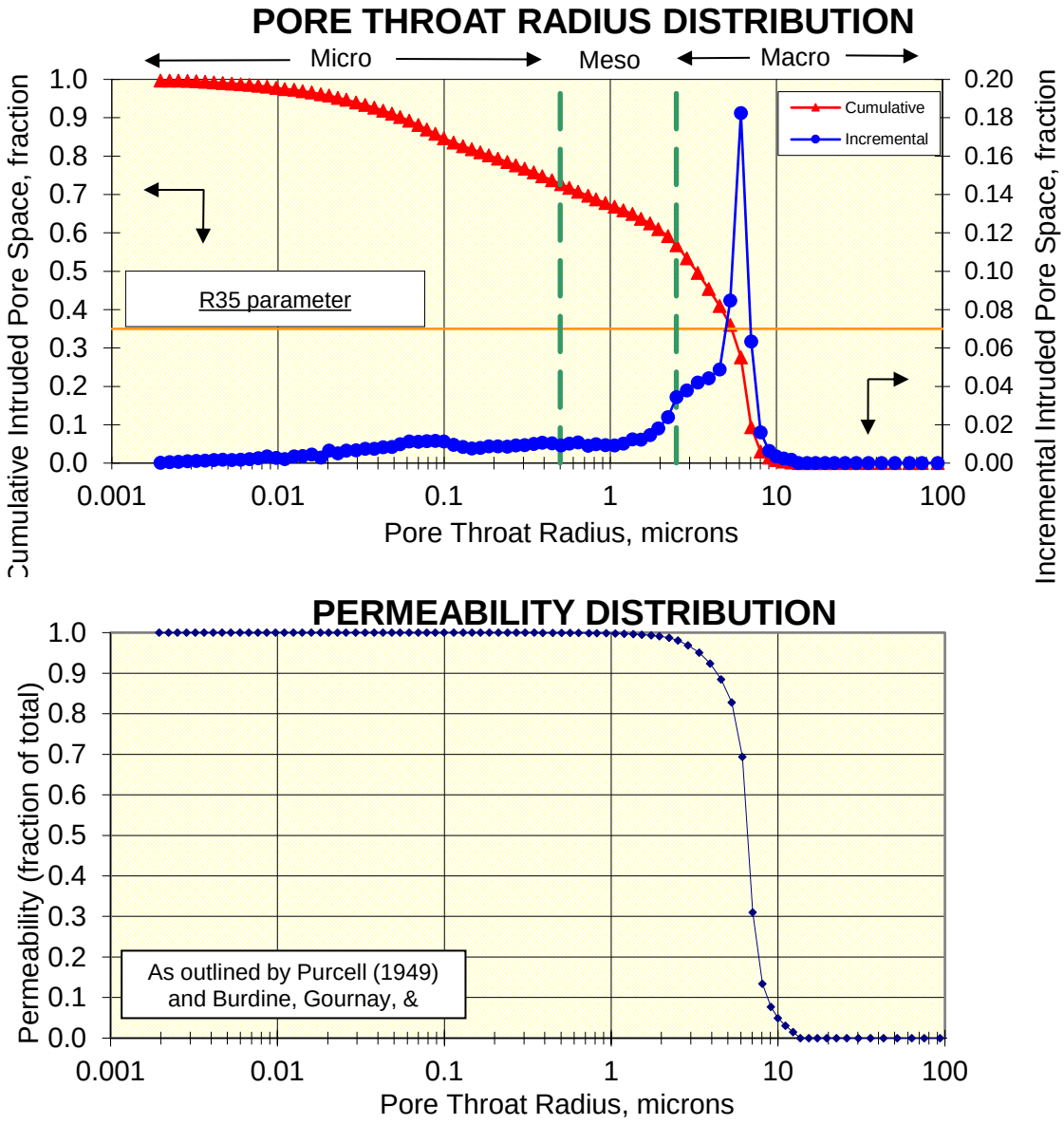

Figure 5-8: Carbon Tan Core Labs MICP data

As these MICP measurements were underway, a 1.5-inch diameter, 1-foot long core was prepared for HPAM polymer injectivity testing. With a mass of 773.25 g and bulk volume of 342.96 cm^3, a sandstone lithology implies a porosity of 14.9%. The core was loaded into the core holder, placed under 1000 psi of confining pressure from mineral oil, and vacuum saturated with 55.01 g (52.9 mL) of 6% KCl. After a 2-mL dead volume correction, this implies a porosity of 14.8%, perfectly consistent with that predicted by the bulk density measurement.

Initial permeability testing revealed very low permeability in section 4 of the core, requiring treatment with 11 pore volumes of 4% $CaCl_2$ as an antidote to suspected clay swelling. The permeability of section 4 and of the overall core recovered to its anticipated level under subsequent re-injection of 6% KCl (29 millidarcys).

A salinity tracer test with 2% KCl generated an estimated pore volume of 51.5 cm^3 after dead volume correction (porosity = 15.0%). The core was then flooded with 17 pore volumes of EDTA treatment solution to remove amorphous iron and reduce the core (4% $NaHCO_3$ + 1% EDTA-4Na + 1% dithionite), during which time the iron concentration peaked at 1500 ppm and then fell to 500 ppm (Rajapkesha, et al., 2014). Injection was then switched to EDTA-free reduction solution for an additional 3 pore volumes, and the iron concentration in the effluent fell to undetectable levels (0.95 g total removed), while the ORP fell to below -700 mV. The core was subsequently flooded with 2.8 pore volumes of 3% NaCl in preparation for the polymer flood, during which it was determined that BPR would be necessary to ensure pressure communication. A final flood with 3% NaCl + 0.1% $NaHCO_3$ was used to establish core permeability before polymer injection (Table 5-2).

Table 5-2: CT-01 permeability

Pre-polymer Permeability @ 25°C	
Section 1	30 md
Section 2	28 md
Section 3	27 md
Section 4	26 md
Whole	28 md

After a holistic consideration of available data, including past laboratory experience, the CQ-1 flood results, the MICP data from the Carbon Tan core plug, and the permeability of CT-01, a slug series to be injected was chosen as follows: (1) a sheared FP3330S slug (0.25% polymer, 3% NaCl + 0.1% $NaHCO_3$) filtered at 0.22 μm after pre-filtration at 0.45 μm, (2) an unsheared slug of the same composition filtered at 0.80 μm, and (3) an unsheared slug of FP3630S (0.175% polymer, 3% NaCl + 0.1% $NaHCO_3$) filtered at 1.2 μm. All filtrations were done on cellulose filter papers at 15 psig. The concentration of FP3630S in the final slug was chosen to closely match the viscosity of the preceding FP3330S slug. Per previous experiments, the first FP3330S slug was sheared in 250 g batches for 40 seconds in the 12-speed Osterizer blender on its lowest setting (see Chapter 4: Effluent viscosity versus shearing time). The rheology of each injected solution is plotted in Figure 5-9. The filtration results are plotted in Figure 5-10, Figure 5-11, and Figure 5-12.

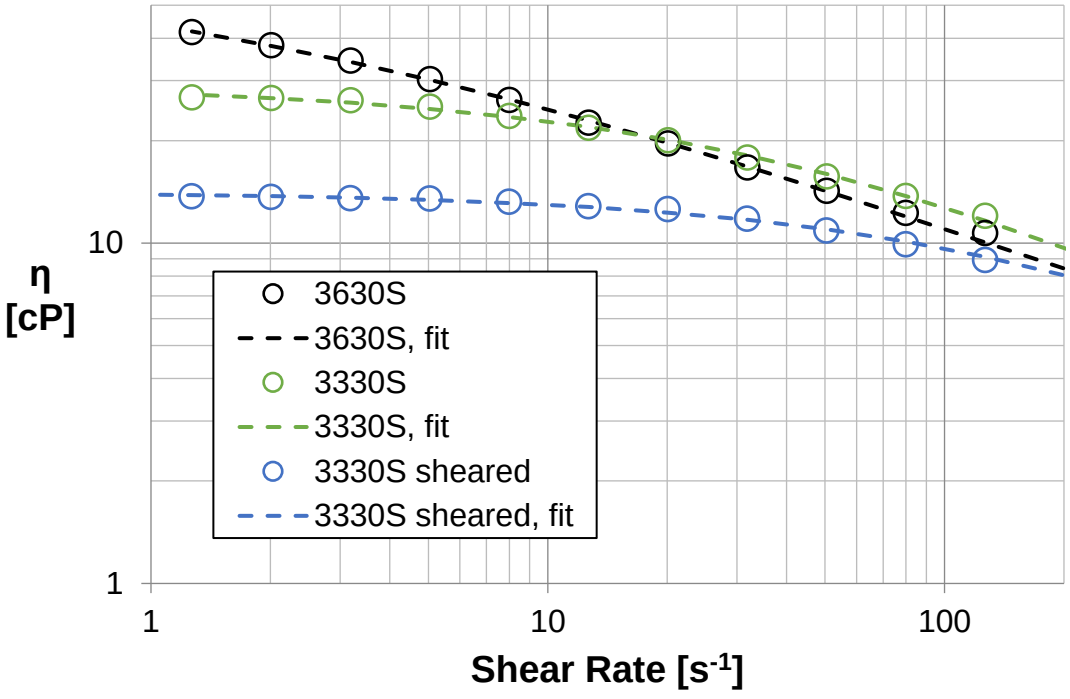

Figure 5-9: CT-01 injected polymer solution viscosity

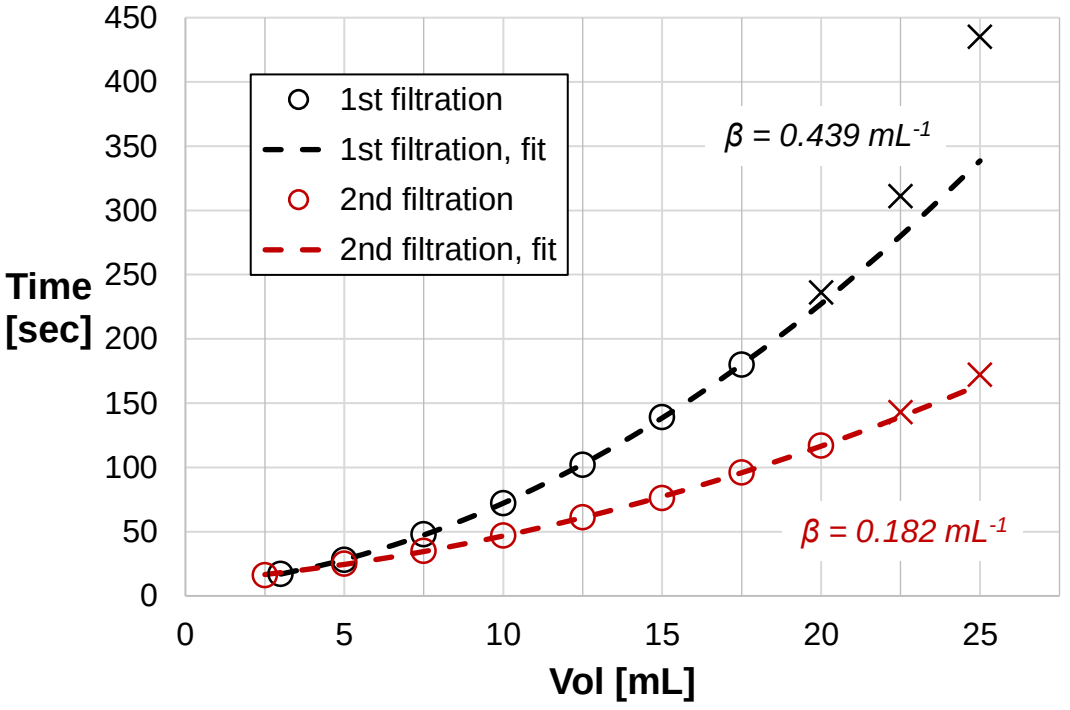

Figure 5-10: 0.22 micron filtration of sheared FP3330S

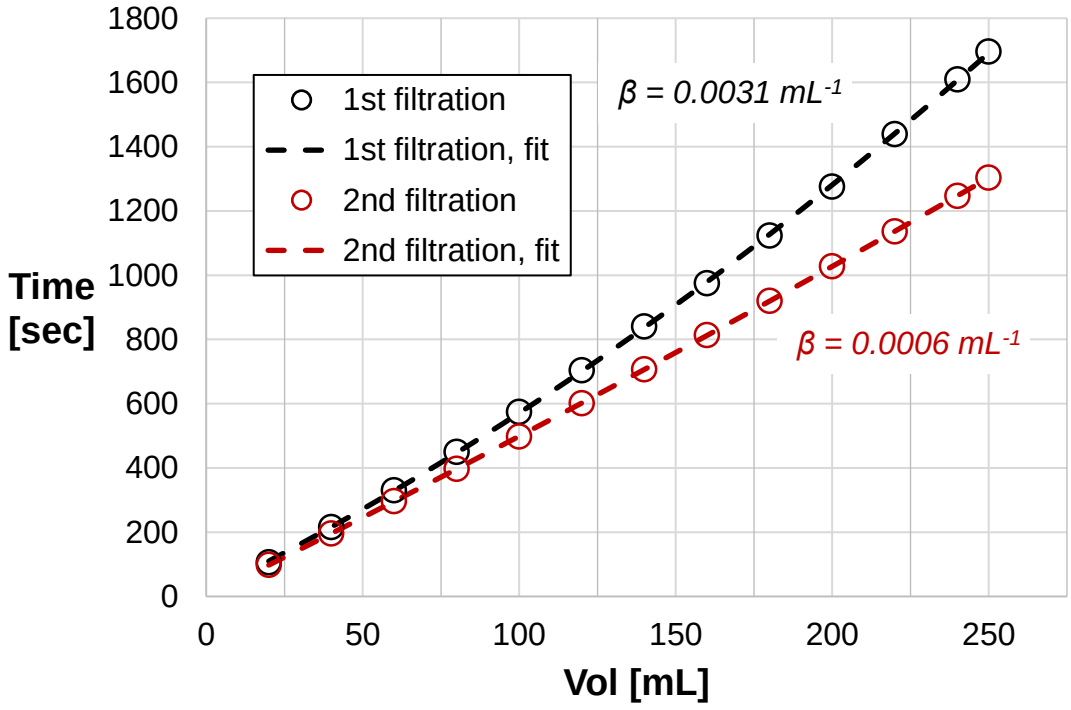

Figure 5-11: 0.80 micron filtration of unsheared FP3330S

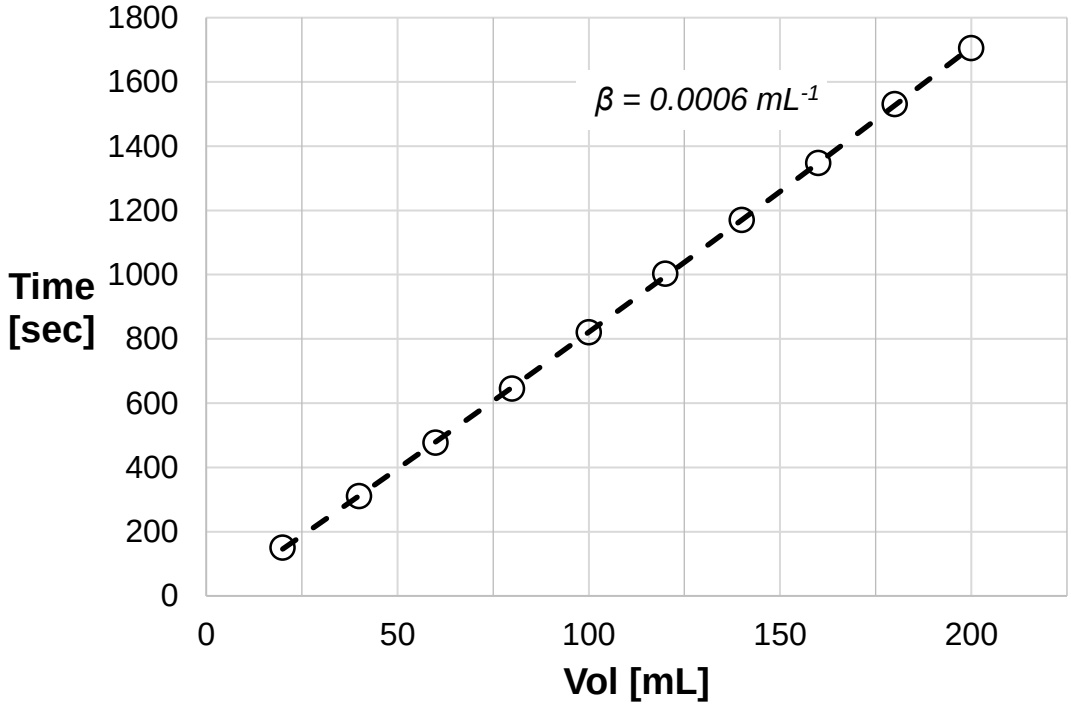

Figure 5-12: 1.2 micron filtration of FP3630S

The filtration results for the sheared, 0.22 µm filtered FP3330S demonstrate significant plugging of the filter, which is not uncommon. A second filtration demonstrates a measureable (2.4x) improvement, though the filter still plugs nonlinearly above ~20 mL. Predictably, the unsheared FP3330S solution filters better at 0.80 µm (FR_β = 1.30), and shows marked improvement on the second filtration (FR_β = 1.07). The FP3630S slug filters well at the outset on the 1.2 µm filter paper (FR_β = 1.07), and is thus not tested thereafter.

Injection of the sheared, 0.22 µm filtered FP3330S solution commenced for approximately 10 pore volumes (Figure 5-13). It is quite clear that no plugging occurred, as expected, judging from the plateauing of the pressure readings after 2 pore volumes.

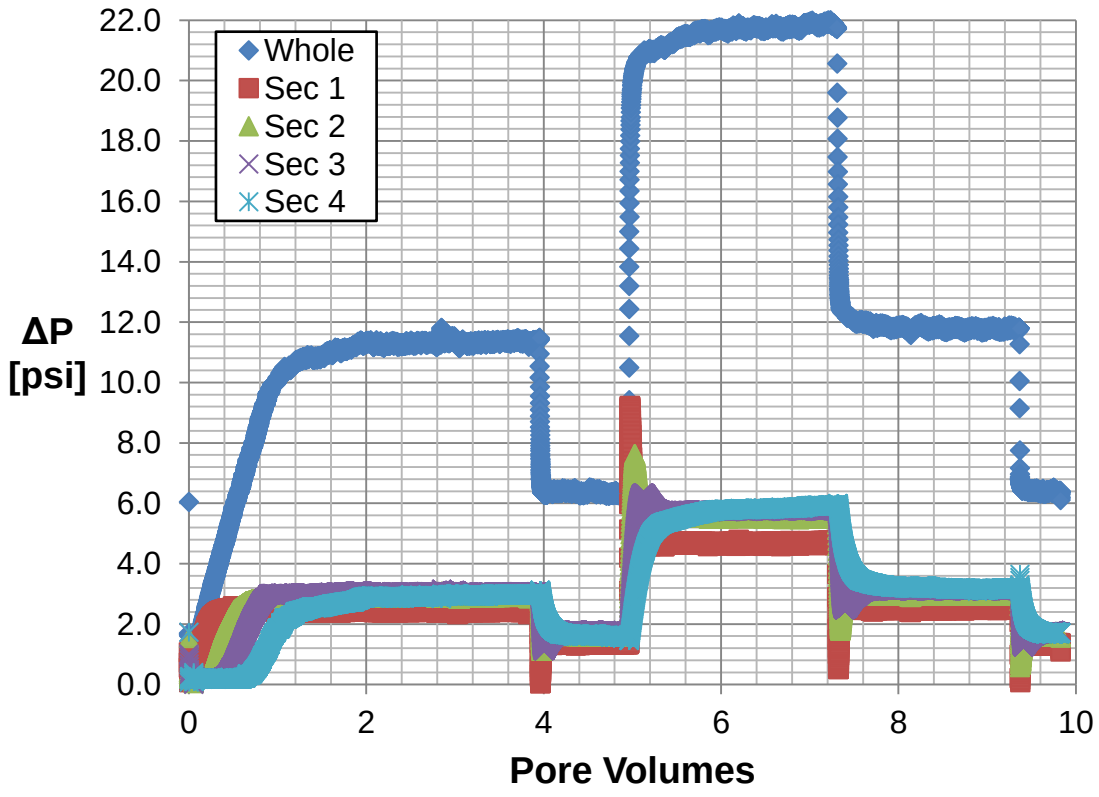

Figure 5-13: CT-01 pressure drops during injection of 0.22 micron filtered slug

After the first 4 pore volumes, the velocity was modulated from 2 ft/d to 1 ft/d to 4 ft/d, then back to 2 ft/d and finally to 1 ft/d. Effective viscosities were calculated from the plateau pressures and plotted against those from the rheometer measurements of the first polymer slug (Figure 5-14).

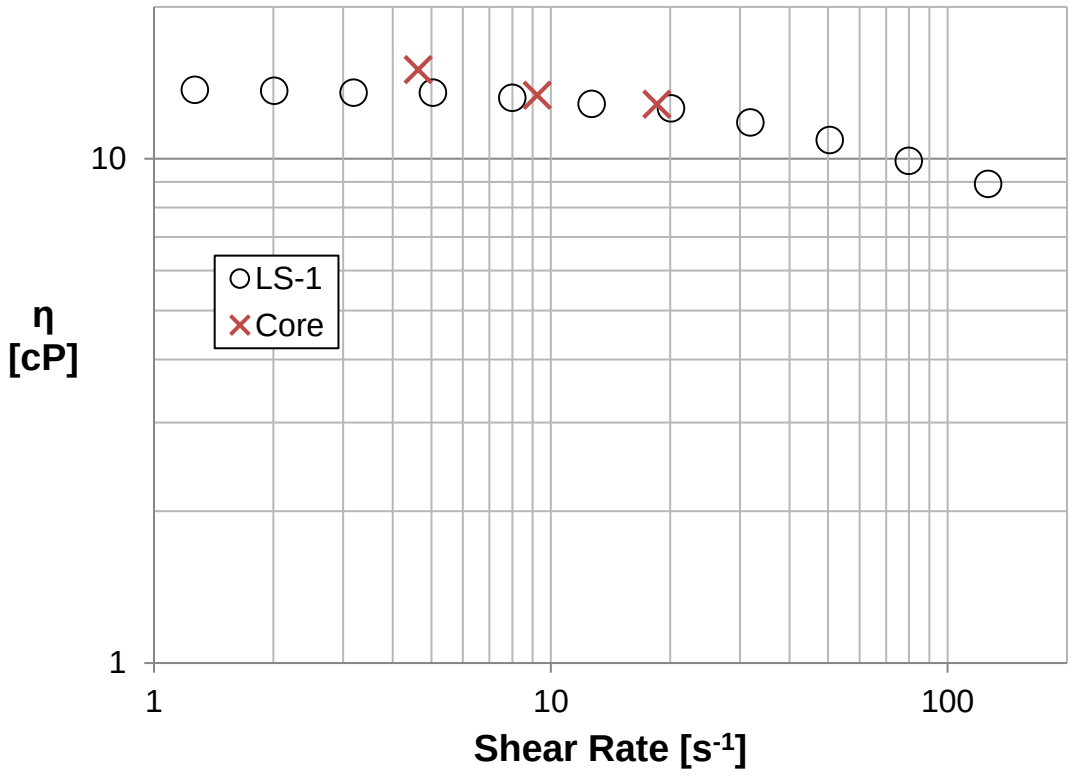

Figure 5-14: CT-01 apparent viscosity versus LS-1 shear viscosity for 0.22 micron filtered slug

Intriguingly, both the permeability reduction factor and the shear correction factor are set to one in this comparison, though the insensitivity of the polymer solution to shear rate in this regime should temper the interpretation of the shear correction factor.

The viscosity of effluent fractions can be used to estimate the polymer retention. Polymer concentration is inferred from a quadratic fit of dilution viscosities of the later effluent samples and the 2500 ppm injected solution. The results of this analysis are plotted in Figure 5-15. Integration of the recovered polymer yields an estimated retention of 66.9 µg/g of rock, a relatively high level.

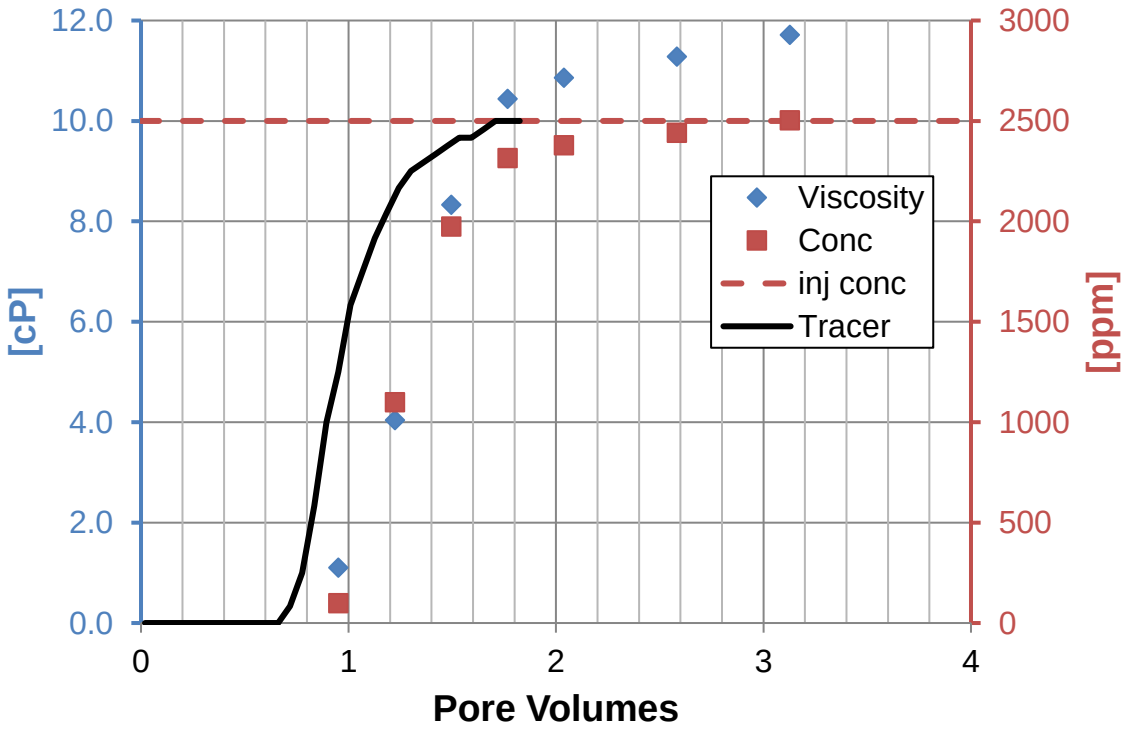

Figure 5-15: CT-01 retention measurement

After stopping the injection of the first polymer slug, injection of the second polymer slug (unsheared, 0.80 µm filtered FP3330S) began and continued for 9 pore volumes at 2 ft/d. The pressure drops (Figure 5-16) gradually increased until the injection was stopped at 9 pore volumes.

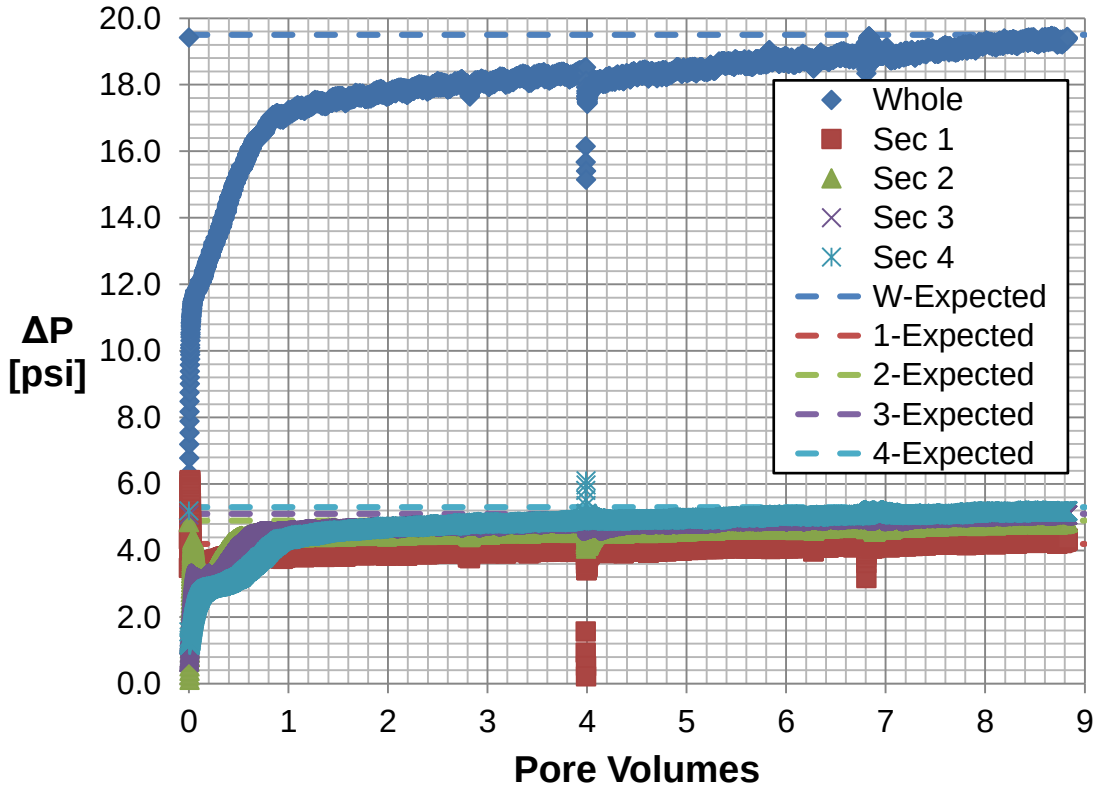

Figure 5-16: CT-01 pressure drops during injection of 0.80 micron filtered slug

Unfortunately, there was not enough polymer slug available to continue the injection past 9 pore volumes to determine if the pressure drop would plateau. Note, however, that the whole pressure drop never exceeded the expected value based on the measured viscosity at the shear rate corresponding to the shear correction factor of 1 based on the first injection.

The last slug (FP3630S, unsheared, 1.2 µm filtered) was injected for 9 pore volumes. In contrast to the previous case, the core substantially over-pressured relative to the expectation (Figure 5-17). This, in combination with the lack of a pressure plateau, was interpreted as evidence of plugging.

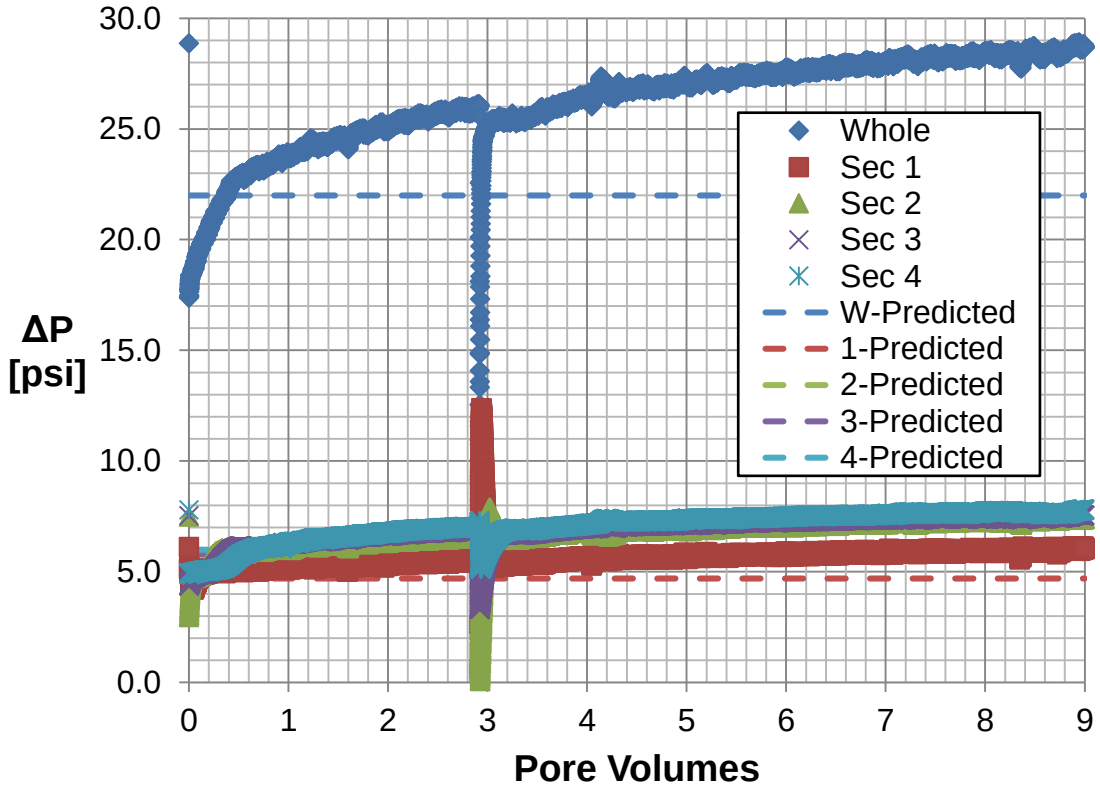

Figure 5-17: CT-01 pressure drops during injection of 1.2 micron filtered slug

5.2 Tertiary Oil Recovery

Tertiary oil recovery experiments using alkali-surfactant-polymer (ASP) flooding is able to reduce oil saturation to very low values approaching zero; the polymer included in these floods primarily navigates a pore space that is close to single-phase, meaning that the results of single-phase injectivity testing is likely to be applicable to an ASP flood. A successful flood conceptually requires that a polymer solution both transports well and provides adequate viscosity for mobility control at a concentration low enough to be

economical and to avoid interfering with a surfactant/chemical formulation. The polymer must, of course, be stable under the conditions of the flood.

In low permeability rocks, this can be especially challenging. In this section, viscosity-optimized, filtered polymer solutions are developed for two ASP core floods performed jointly with co-workers in the same lab. The floods are done in cores from a low-permeability carbonate reservoir requiring high pH (>12) to combat surfactant adsorption. As a consequence, polymer (FP3330S) needed to be pre-hydrolyzed to avoid *in situ* hydrolyzation during the floods and misleading pressurization of the core due to changes in rheology. In turn, the pre-hydrolysis of polymer needed to be included in the shearing optimization procedure.

5.2.1 Shearing optimization for SAMA

In order to flood low-permeability carbonate reservoir cores, a shearing optimization was performed for 0.10 μm cellulose filters, which were deemed necessary to avoid plugging. The optimization procedure varied blender speed rather than time, as it was unclear at the outset whether lower speeds would produce sufficient shearing after any shearing time to permit low-loss filtration through the tight filter.

The FP3330S polymer was hydrated as a 1% solution and subsequently diluted to working conditions (0.483% polymer, 2% $CaCO_3$ + 0.215% NaCl + 0.75% Na_2SO_4; 83.0 cP @ 10 s^{-1}, 26ºC). Each 250-g slug was blended for one minute at either speed setting #1, #6, or #12 in the 12-speed Osterizer blender (higher is faster). These slugs respectively had viscosities of 63.4 cP, 44.5 cP, and 35.0 cP @ 10 s^{-1}, 26ºC. After argon bubbling for

one hour, the polymer solutions were hydrolyzed for 6 hours and reached viscosities of 84.0 cP, 59.4 cP, and 48.0 cP. These hydrolyzed polymer solutions were filtered in series at 0.45 μm, 0.22 μm, and 0.10 μm. In each case, approximately 200 mL of solution was filtered through the large pore size filter, while 40 mL was filtered through the intermediate pore size filter. The filtered amount in the 0.10 μm filter depended on the degree of plugging.

All solutions preserved their viscosities through the first two filters. Plugging through the 0.45 μm filter was very low in all cases (Figure 5-18). Plugging through the 0.22 μm filter was moderate for the solutions blended on speed settings #6 and #12, but 10x higher for the low speed (#1) slug (Figure 5-19). At 0.10 μm, plugging became impermissibly high for all slugs except the high-speed blended slug, which was the only sample that fully filtered (Figure 5-20). The viscosities of the filtrates were 9.0 cP, 34.1 cP and 46.1 cP at the previously quoted measurement conditions (Figure 5-21), representing 10.7%, 57.4%, and 96.0% of the post-hydrolysis viscosity of each slug.

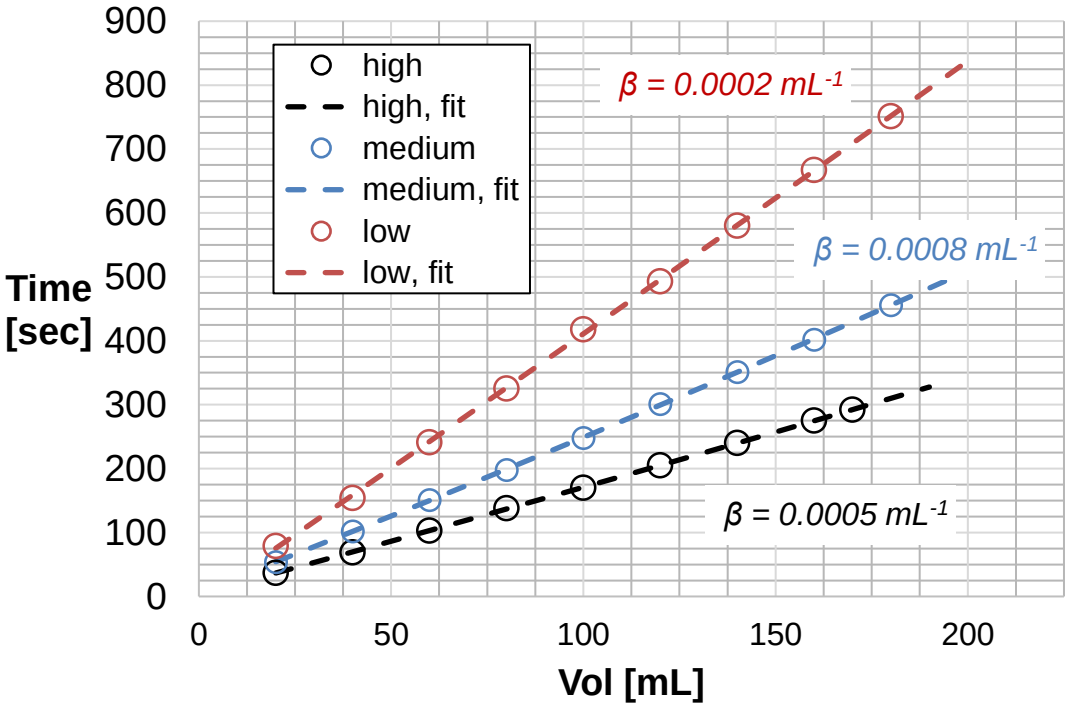

Figure 5-18: 0.45 micron filtration of 1-min sheared FP3330S solutions

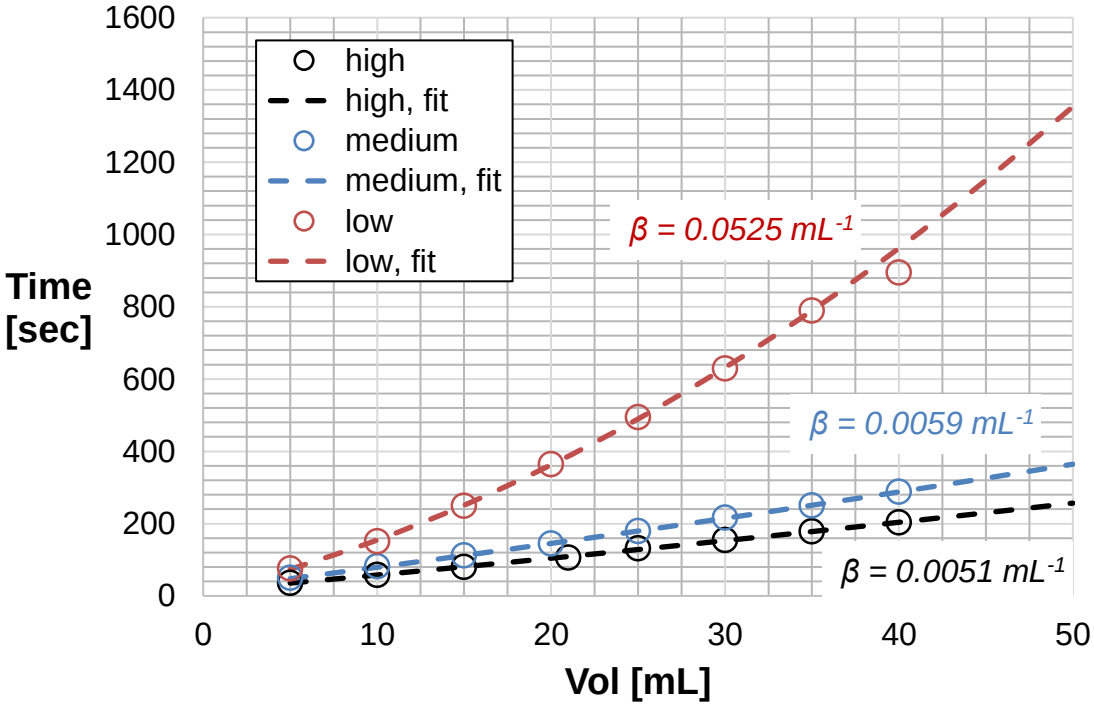

Figure 5-19: 0.22 micron filtration of 1-min sheared FP3330S solutions

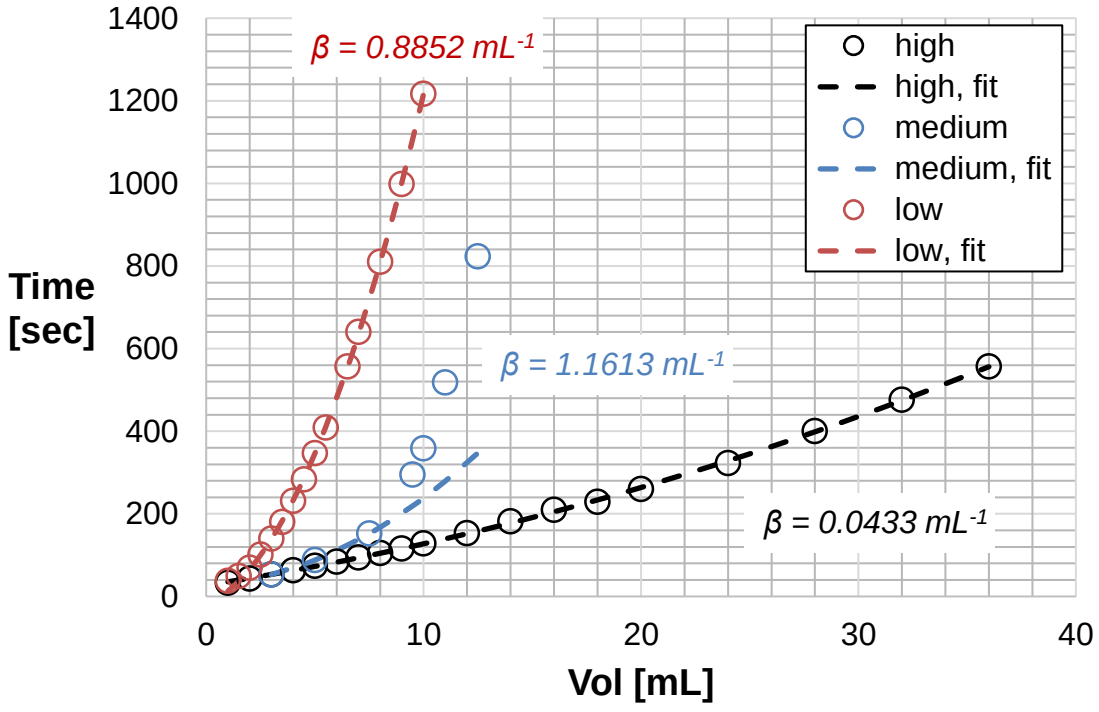

Figure 5-20: 0.10 micron filtration of 1-min sheared FP3330S solutions

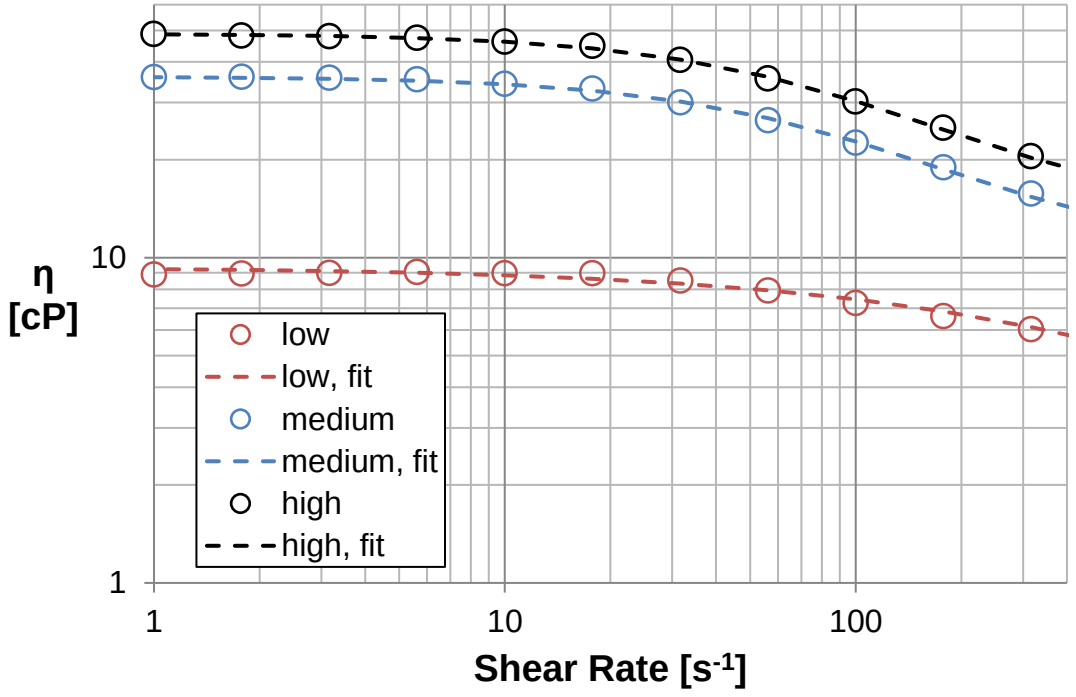

Figure 5-21: Viscosity of 1-min sheared, 0.10 micron filtered FP3330S solutions

Given the trend in viscosity and retained viscosity percentage, the conclusion was that one minute of blending at the blender's highest speed setting was near optimal for serial filtration of the candidate polymer solution down to 0.10 μm on cellulose filter papers.

5.2.2 SAMA-13R

The SAMA-13R reservoir core flood is one of two core floods targeted for optimized polymer filtration due to its low permeability (17.5 mD overall, see Table 5-3). Sodium hydroxide was used to increase the pH of both the ASP slug and the polymer drive to neutralize the surface charge in the pore space to reduce the adsorption of the surfactant. The core flood itself was led by Pathma Liyanage, who adopted the procedure delineated in the previous section for the preparation of the ASP slug and polymer drives. The brine is the same as listed in the previous section.

Table 5-3: SAMA-13R brine permeabilities before oil flood

Section	Permeability (mD)
Section 1	35.3
Section 2	20.0
Section 3	13.7
Section 4	12.6
Whole	**17.5**

The ASP slug and polymer drive filtration measurements are tabulated below in Table 5-4. Due to an increase in polymer solution mass (300 g) and an increase in the time of hydrolysis, the polymer drives needed to be sheared for a total of 1.5 minutes instead of 1 minute as shown in the previous section. The ASP slug with cosolvent was able to pass

the filter well with 1 minute of shearing, which points to an interesting variable in polymer filtration. The abbreviation "F.R." refers to the standard filtration ratio measurement requiring > 200 mL of polymer material to be filtered, not a beta-estimated filtration ratio. Final viscosities at the core flood conditions are listed in the far-right column. The required viscosity for a stable displacement of an oil bank based on the estimated relative permeability of oil and water was predicted to be around 7.2 cP (Corey exponents n, m = 2.5).

Table 5-4: SAMA-13R filration measurements and resultant viscosities

Solution	0.22 µm filter		0.10 µm filter	Viscosity [cP] @ 78°C, 31 s^{-1}
	F.R.	β [mL^{-1}]	β [mL^{-1}]	
ASP Slug	1.15	0.0015	0.0566	8.65
PD1 before inject	1.14	0.0015	0.0943, 0.0224	10.71
PD1 after inject	N/A	N/A	N/A	8.81
PD2 before inject	1.07	0.0014	0.0194	11.75
PD 2 after inject	NA	0.0049	0.0291	10.39

As shown in Table 5-4, all injected solutions had a $\beta < 0.0019$ mL^{-1} at 0.22 µm (equivalent to $FR_\beta < 1.2$) before injection. The exact significance of the plugging metrics at 0.10 µm is difficult to predict as it relates to transport in a core; it is only clear that by the previous standards of a "good" polymer solution (FR < 1.2), these solutions would meet that criterion at a filter size between 0.10 µm and 0.22 µm. It should also be noted that filtration at 0.10 µm removes high molecular weight polymer from solution and that subsequent filtration reveals improvement, as is the case with polymer drive 1 (4.2x improvement, see Table 5-4, 2nd row).

The pressure data from the chemical flood demonstrate good transport of the ASP slug and first polymer drive (0.0 to 1.9 pore volumes, see Figure 5-22). The sectional pressure drops were unreliable during the flood, but the whole core pressure drop flattens from 1.5 to 1.9 pore volumes right around the expected value of 19.4 psi. The final oil saturation S_{orc} following the ASP flood was 0.066.

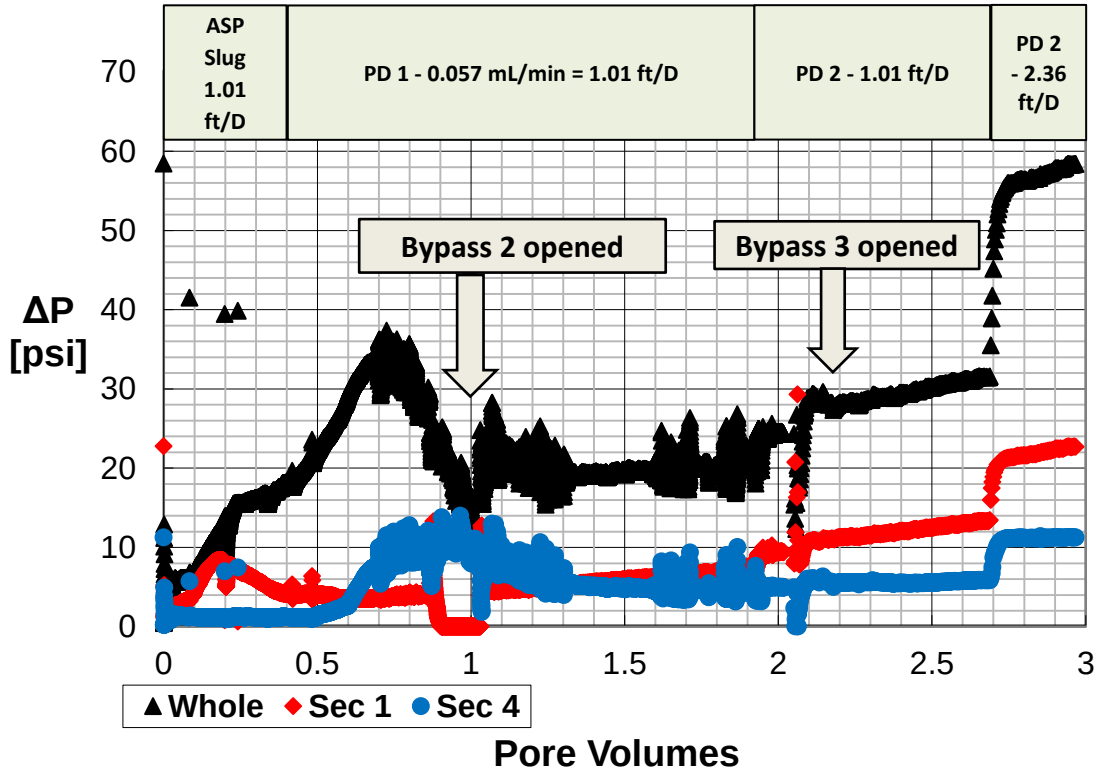

Figure 5-22: SAMA-13R pressure drops during chemical flood

Injection of the second polymer drive caused plugging that continued for a full pore volume at two different flow rates. At the conclusion of the injection, the polymer remaining in the column was filtered at 0.22 µm and 0.10 µm. Interestingly, the plugging metrics had increased, 3.5-fold in the case of the 0.22 µm paper. As plugging was not a problem with

the first polymer drive, corresponding filterability measurements after injection were not made. It nonetheless remains plausible that the second polymer drive deteriorated in some way during its time at 78°C that made it less injectable. Both polymer drives displayed a slightly reduced viscosity, consistent with oxidative degradation.

After the core flood was completed, the core sections were cleaned (see Chapter 3: Core Cleaning), and section 4 (the lowest permeability section) was sent to Core Laboratories for MICP analysis. The data appear in Figure 5-23, courtesy of Core Laboratories. The pore sizes measured are clearly smaller than for the 30 mD sample of Carbon Tan. Ninety-nine percent of the section's permeability is predicted to come from pores of 0.70 μm in diameter and larger, as opposed to 3.9 μm for Carbon Tan, a 5.6x size difference. The Carbon Tan sandstone began plugging with a polymer (FP3630S) filtered at 1.2 μm with $\beta = 0.0006$ mL^{-1}. A proportional decrease in pore size would be almost exactly 0.22 μm; while $\beta = 0.0015$ mL^{-1} appeared to transport well, $\beta = 0.0049$ mL^{-1} did not. The guidance these metrics give from one experiment to the next is not perfect, but it does appear to be useful.

Company:	University of Texas at Austin
Well:	Unknown_University Sample
File:	HOU-1701173

Sample:	**1m**	un-	Host Plug	
Depth, feet:	NA	stressed	n/a	n/a
Klinkenberg Permeability, md:		N/A	-	-
Permeability to Air, md:		N/A	-	-
Swanson Permeability, md:		7.71	-	-
Porosity, fraction:		0.247	-	-
maximum Sb/Pc, fraction:		0.0969		
R35, microns:		1.20		
R50 (median pore throat radius):		0.718		

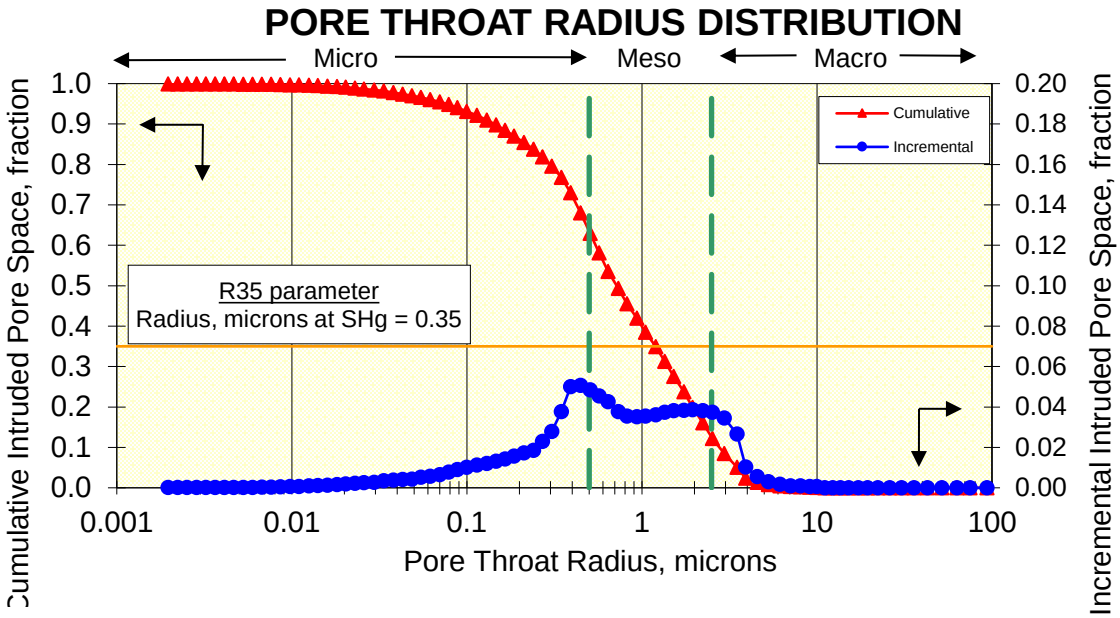

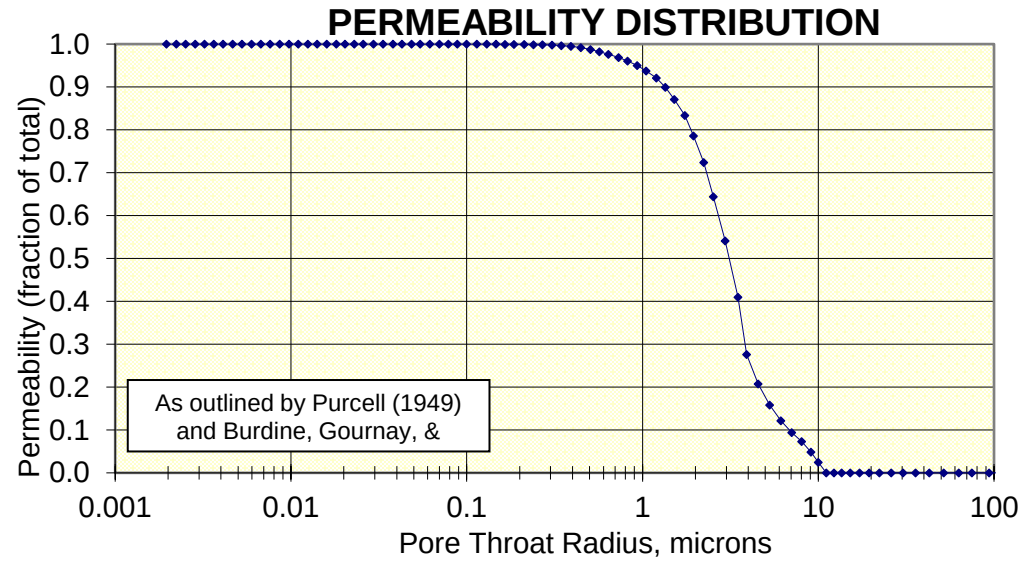

Figure 5-23: Core Labs MICP data for SAMA-13R section 4

5.3 Single-Phase Scleroglucan Floods

Previously, acceptable scleroglucan transport appeared to be limited to high-permeability sandstones (Lee, 2015). In an effort to improve upon this limitation, three changes were made: (1) scleroglucan was homogenized using an IKA Magic Lab mixer and a procedure optimized by the manufacturer (Cargill), (2) scleroglucan was filtered at reduced pressure and pore size to remove high-molecular weight components more efficiently and (3) the core floods were carried out at 95ºC and higher temperature since its transport is expected to be improved at high temperature and also the primary target EOR applications of this polymer are in high-salinity, high-temperature reservoirs. The scleroglucan provided by Cargill was manufactured by a new process that allows it to be produced as a solid rather than a broth, with improved performance.

Three cores are successfully tested (see Table 5-1). Each core is reduced with a bicarbonate-buffered EDTA/dithionite solution to prevent *in situ* degradation of the biopolymer. After reduction, each core is flooded with synthetic seawater (SSW; 2.38% NaCl + 0.393% Na_2SO_4 + 0.028% $NaHCO_3$ + 0.08% KCl + 0.116% $CaCl_2$ + 0.517% $MgCl_2$) with a trace amount (500 ppm) of dithionite to maintain a low oxidation-reduction potential (< -700 mV) and consume any oxygen that might invade the core. Also, all brines and polymer solutions during and after reduction were argon bubbled to remove oxygen that might degrade the polymer.

5.3.1 SCL-06

The core for SCL-06 was cut from PD block (Berea Upper Grey, Kocurek Resources) and initially saturated with 2% KCl brine. A salinity tracer test with Cargill synthetic seawater revealed a pore volume of 140 mL in a core of bulk volume 608.1 mL and mass 1281 g, translating to a porosity of 0.23 and a matrix density of 2.74 g/cm^3 (2.65 g/cm^3 for sandstone). The core was then re-flooded with 2% KCl before flooding with 13 pore volumes of treatment solution (4% $NaHCO_3$, 1% EDTA-4Na, 1% $Na_2S_2O_4$). EDTA-free reduction solution was injected for 2 pore volumes to flush out the EDTA and stabilize the ORP below the standard target of -700 mV before heating to 95ºC. After heating, 2% KC1 with 500 ppm dithionite was injected for 1.5 pore volumes to remove the bicarbonate prior to seawater injection. Seawater with 500 ppm dithionite was then injected at 2 mL/min initially and 4 mL/min transiently to saturate the core and determine its permeability prior to polymer injection (Table 5-5).

Table 5-5: SCL-06 brine permeabilities before polymer injection

Section	Brine Permeability (mD) at 95 ºC
Section 1	401
Section 2	449
Section 3	473
Section 4	423
Whole	**414**

The scleroglucan polymer solution was prepared as described in the methods section. The polymer was filtered at 2.5 psig using 0.80 μm cellulose filter paper (Figure 5-24).

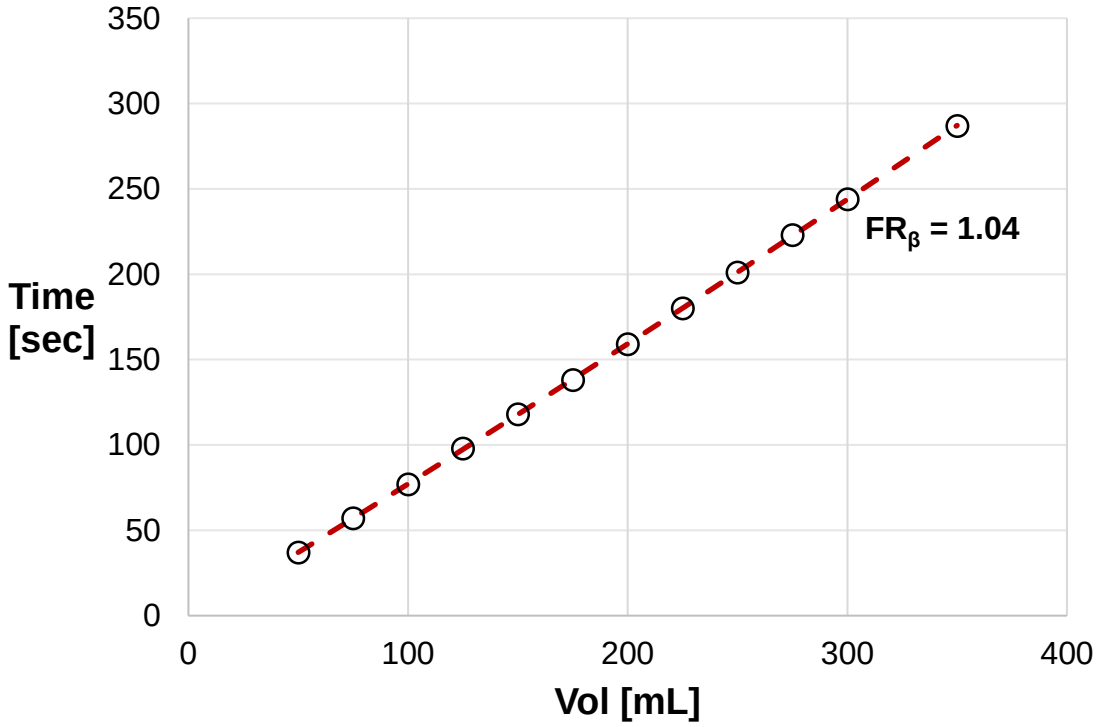

Figure 5-24: Filtration (0.80 microns) of scleroglucan for SCL-06

The beta-estimated filtration ratio of 1.04 is in the expected range for scleroglucan on this filter paper at this pressure. This filtration does not adversely affect solution viscosity whatsoever, as steady shear rate sweep measurements on the LS-1 rheometer confirm (Figure 5-25). It stands to reason that only a tiny amount of polymer is removed by this process.

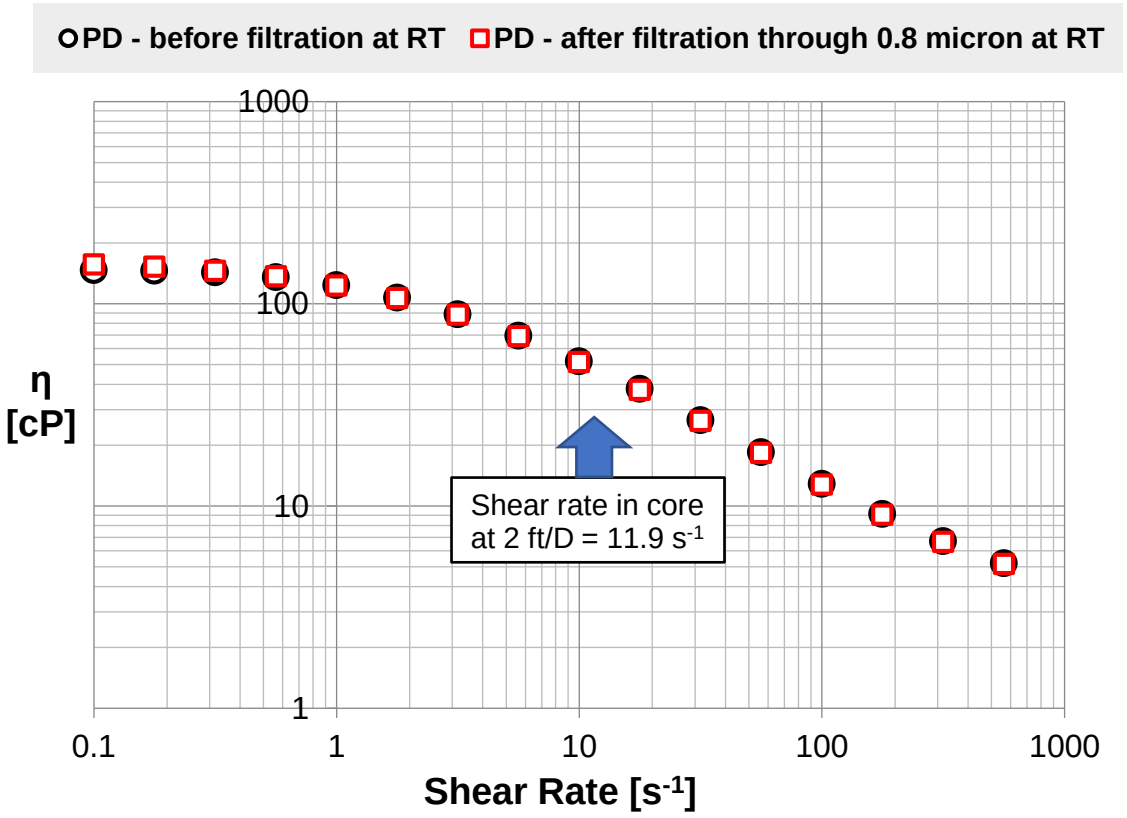

Figure 5-25: SCL-06 slug viscosities

The viscosity at the estimated shear rate in the core (*a priori*, the shear correction factor, *C*, is estimated as 2) is 45.3 cP at 26ºC and 22.1 cP at 78ºC, translating to a predicted viscosity of around 18.8 cP at the core temperature of 95ºC. The predicted whole pressure drop was 3.1 psi. As Figure 5-26 below shows, the pressure plateau that begins after 3 pore volumes of injection was below this predicted level (2.5 psi).

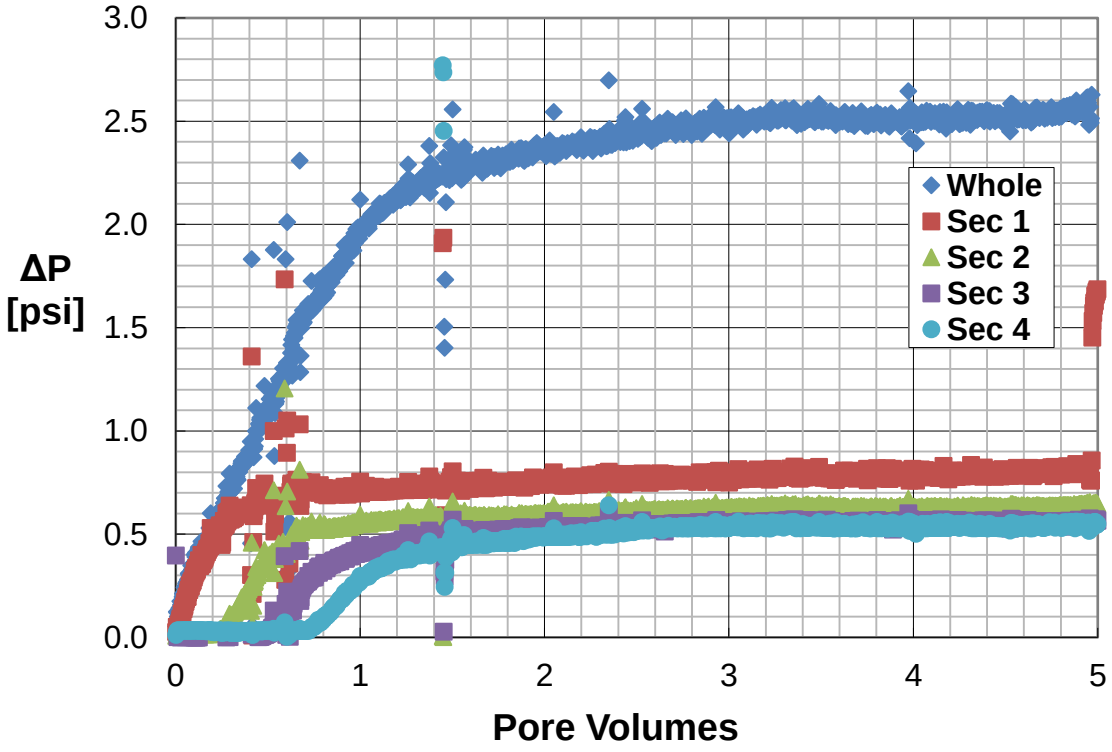

Figure 5-26: SCL-06 pressure drops during polymer flood

The apparent viscosity of the polymer is 15.1 cP, which corresponds to a shear rate of 22.5 s^{-1} in the rheometer, and $C = 3.78$. Unfortunately, mineral oil was injected beginning at 5 pore volumes, so the injection rate could not be modulated to more accurately determine the shear correction factor. However, the level pressure plateau (steady state) in combination with its low value relative to the predicted pressure drop indicates that the scleroglucan solution did not plug the 440 millidarcy Berea sandstone under the conditions tested.

Effluent samples were collected using the fraction collector, and their viscosity measured using the LS-1 rheometer (Figure 5-27, blue data). These viscosities were

converted to polymer concentrations using a second-order polynomial standard curve created from shear viscosity measurements of serial dilutions of 1000 ppm scleroglucan in SSW brine (Figure 5-27, red data).

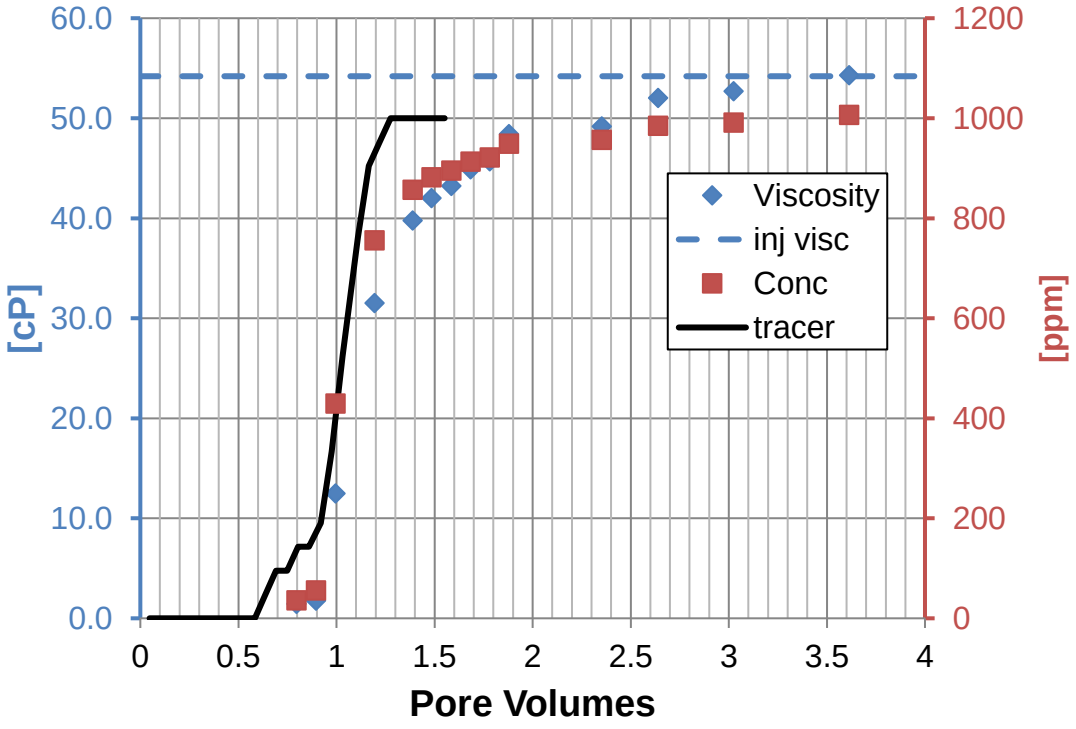

Figure 5-27: SCL-06 retention estimation

By subtracting the total recovered polymer from the amount injected (less one pore volume equivalent) and dividing by the density of the polymer solution (ρ = 1.02 g/cm^3) and the mass of the core, the estimated retention is 17.3 µg/g of rock. This is a low level of retention that is acceptable for EOR applications.

5.3.2 SCL-08

After the success of SCL-06 and a technical failure with SCL-07 that hinted at good transport in a 260 millidarcy Berea core, SCL-08 was designed to probe polymer transport in a core cut from KB-1 block (Berea Sister Grey). The core was initially saturated with 6% KCl (permeability tested by flow rate modulation, 150 millidarcys) and a salinity tracer test was performed using 2% KCl brine, leading to a pore volume estimate of 68.8 mL. The bulk volume of the core was 329.2 mL at a weight of 697.50 g, so the porosity was found to be 20.9% and the matrix density was 2.68 g/cm^3, very similar to the nominal sandstone lithology.

The core was injected with the standard EDTA treatment brine at 2 ft/d for approximately 8 pore volumes, at which point the flood was aborted due to an observed reduction in permeability (down to ~90 millidarcys). EDTA-free reduction brine solution was injected for 1.8 pore volumes and the permeability increased to 114 millidarcys, while the ORP was verified to fall below the target of -700 mV. The core was then flooded at 2 mL/min with 2% KCl + 500 ppm dithionite for ~3.4 pore volumes to displace the carbonate-containing buffer, and permeability appeared to hold. The core oven temperature was set to 105ºC for heating overnight. After heating, the core was flooded with 2.3 pore volumes of SSW brine at 2 mL/min with 30 psi back pressure, and then an additional 1.4 pore volumes in the reverse direction in an effort to rectify any fines migration that was occurring over the course of the previous floods. During that final flood, stable pressure drops were observed and brine permeability was determined to be 105

millidarcys (Table 5-6). The permeability reduction from 150 millidarcys complicates the interpretation of the ensuing polymer flood somewhat.

Table 5-6: SCL-08 brine permeabilities before polymer injection

Section	Brine Permeability (mD) at 105 °C
Section 1	106
Section 2	106
Section 3	108
Section 4	99
Whole	**105**

A 1000 ppm solution of scleroglucan in SSW brine was prepared from a paste using the standard homogenization procedure (IKA Magic Lab). The solution was filtered directly on 0.65 μm cellulose filter paper at 2.5 psi (Figure 5-28). This filter was chosen to be tighter than for the previous successful flood due to the substantial permeability difference between the two cores. From filtration testing with scleroglucan, it can also be shown that filtration at 0.65 μm improves subsequent filtration at 0.45 μm relative to direct filtration at 0.45 μm, indicating that the 0.65 μm filter improves solution quality.

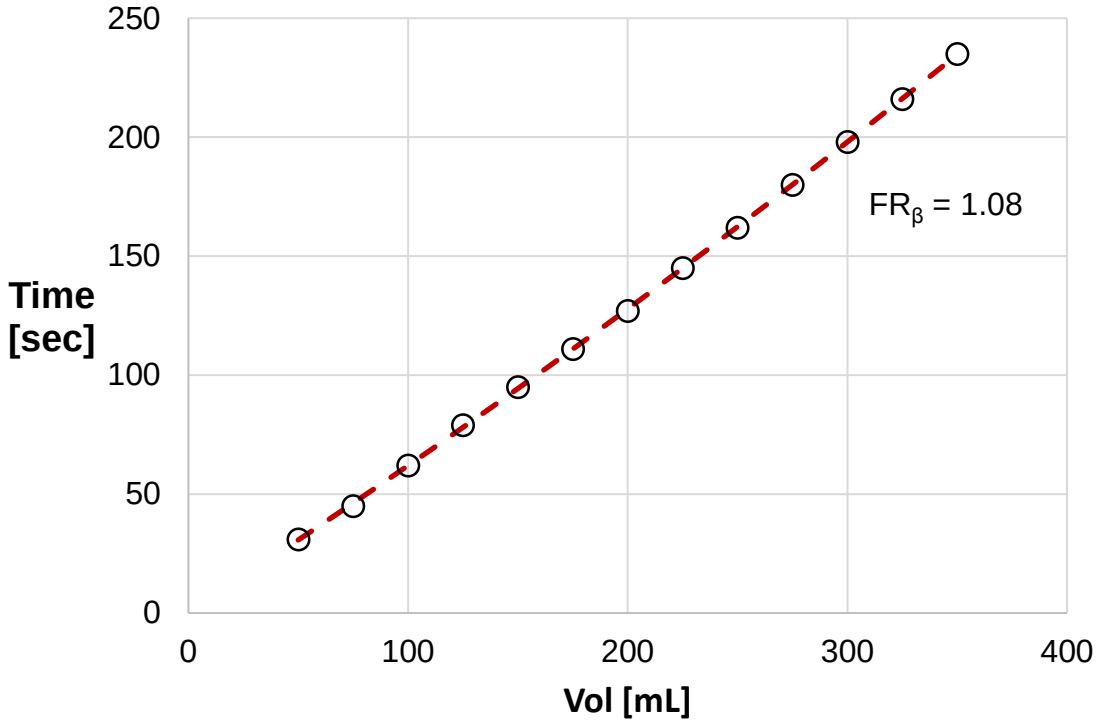

Figure 5-28: Filtration (0.65 microns) of polymer for SCL-08

The beta-estimated filtration ratio of 1.08 was deemed to be acceptable based on comparison to other such filtrations. No viscosity was lost as a result of this filtration or the subsequent heating to 105ºC for 21 hours in a column (prior to loading, the solution was argon bubbled and 500 ppm dithionite was added). The results are shown in Figure 5-29.

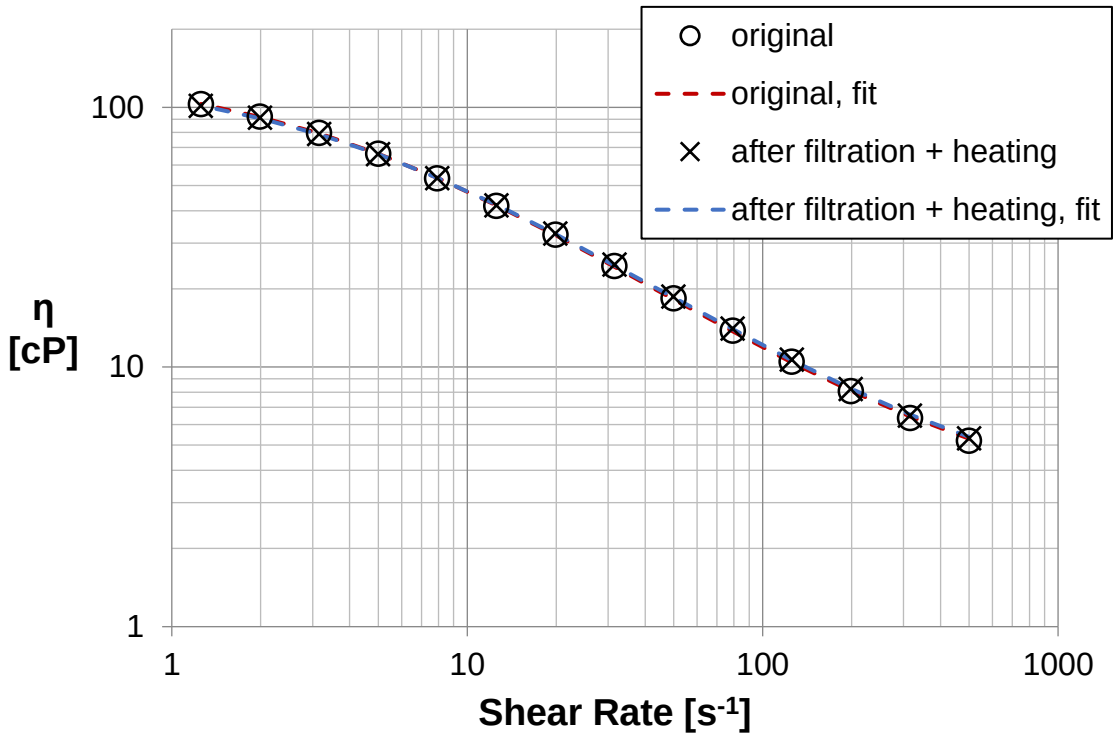

Figure 5-29: SCL-08 slug viscosities

After confirming that the solution viscosity was stable (indicating no oxygen contamination), polymer injection began at a frontal velocity of 2 ft/d. It became clear very quickly that plugging was occurring, as the section 1 pressure drop steadily increased after 1.3 pore volumes injected (5.2 of its sectional pore volumes, see Figure 5-30). The flood was paused to flush the pressure lines to clear them to make sure that the pressure readings were accurate. Unfortunately, at the flood temperature, this had the opposite effect, and the sectional readings were rendered useless after this effort. However, the whole core pressure drop continued to rise steadily for around 5.6 total pore volumes of polymer injected, reaching around 12 psi, well over the 7.1 psi anticipated.

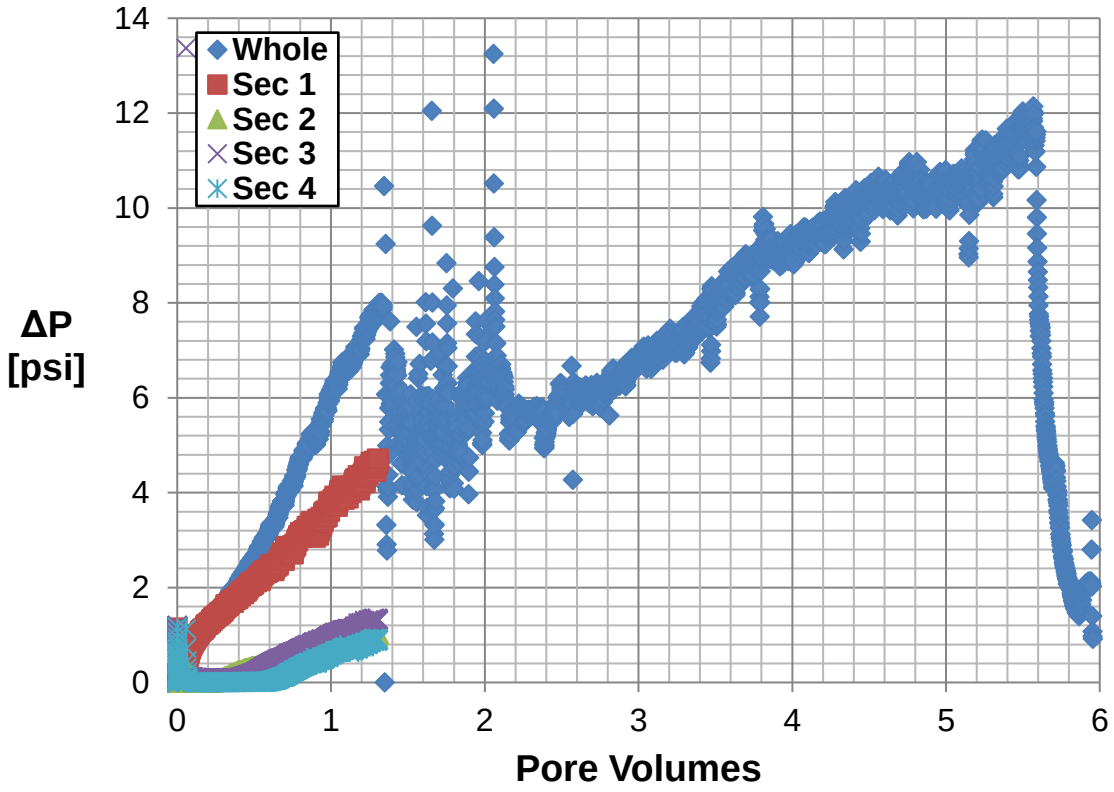

Figure 5-30: SCL-08 pressure drops during polymer flood

The sectional pressure drops were all predicted to be around 1.8 psi, roughly consistent with the data at 1.3 pore volumes injected. The viscosity of the polymer left in the column after the conclusion of the flood was 49.8 cP at 10 s^{-1}, which corresponds to an empirical polymer concentration of 963 ppm based on the correlation developed for the SCL-06 flood. By contrast, the viscosity of late fractions (~4.75 PV) was 41.2 cP, indicating a polymer concentration of 873 ppm, or 90.7% of the late injected. The deep bed filtration model would therefore predict a dimensionless length decay constant of 0.0976 (see Chapter 2: Mechanical Entrapment), which would have polymer concentration falling

rather uniformly through the core. The sectional pressure drops over the first pore volume suggest that this is not the case. The likely explanation is that the model does not presently account for a molecular weight distribution with high molecular weight components that are selectively filtered out at the core face or near the inlet.

A better way to approximate the filtration behavior of the core might be to assume face plugging and to estimate the plugging constant based on the retained eluate viscosity. In separate testing, a 1000 ppm solution of scleroglucan in the same brine filtered on cellulose filter papers of pore sizes 0.65 μm and 0.45 μm produced filtrates of 53.0 cP and 41 cP, respectively, or 98.8%, and 76.4% of the original viscosity. These retained viscosity figures corresponded to plugging constants of 0.00085 mL^{-1} and 0.0691 mL^{-1}, and one may presume that a plugging constant of 0 mL^{-1} maps to 100% retained viscosity. The sandstone reduced the viscosity of the eluate to 82.7% of its injected level; a quadratic interpolation gives an effective filter constant of $\beta = 0.040\ mL^{-1}$. This, in turn, must be corrected for the difference in filter area versus core face area: $\beta A_{filter}/A_{core} = 0.16\ mL^{-1}$. The plugging metric and pressure accumulation are interrelated (see Chapter 2: Filtration of Polymers).

$$\frac{1}{P_o}\frac{d(\Delta P)}{dV} = \boldsymbol{\beta} \qquad [\,5\text{-}1\,]$$

This can be used to solve for the initial (unplugged) pressure drop, P_o. Over the span of 2.5 to 5.5 pore volumes, pressure accumulates at around 2 psi per pore volume, or approximately 0.029 psi/mL. Dividing by the effective filtration constant gives $P_o = 0.18$ psi, which can be used to estimate the thickness of the filter from the expected pressure

gradient in the first core section of 7.3 psi/ft. The predicted thickness is 0.025 ft, or roughly 8 mm.

5.3.3 SCL-09

In light of the plugging observed in SCL-08, a sandstone core of intermediate permeability between SCL-06 (440 millidarcys) and SCL-08 (105 millidarcys) was sought. SCL-09 is a 1.5-inch diameter Buff Berea sandstone core cut from block J1 (Kocurek) with a predicted permeability in the ~250 millidarcy range. The core was initially saturated with 6% KCl brine, and proved to be relatively homogenous with a permeability of 254 millidarcys. A salinity tracer test with 2% KCl indicated a pore volume of 82.8 mL. This put the core porosity at 0.237 and its matrix density at 2.65 g/cm^3, in line with a clean sandstone lithology.

Due to previous experience with iron-rich Buff Berea, an EDTA treatment flood was not used. Instead, the core was simply reduced with EDTA-free reduction solution. This required around 25 pore volumes of reduction solution to reach the target effluent ORP of < -700 mV (-43 mV @ 4.5 PV, -675 mV @ 19.8 PV). The core was heated overnight to 95ºC and then flooded with 4 pore volumes of 2% KCl + 500 ppm dithionite brine, then with 4.6 pore volumes of SSW + 500 ppm dithionite brine, revealing a pre-polymer brine permeability of 218 md across the core (Table 5-7).

Table 5-7: SCL-09 brine permeabilities before polymer flood

Section	Brine Permeability (mD) at 95 °C
Section 1	194
Section 2	206
Section 3	229
Section 4	231
Whole	**218**

A 1000 ppm scleroglucan solution was made from a 100% active powder in lieu of paste, due to a shortage. The preparation protocol was otherwise the same. The polymer solution was filtered directly at 0.65 μm, giving a beta-estimated filtration ratio of 1.17 (Figure 5-31). This was higher than previous filtrations (Figure 5-28), perhaps owing to the use of powder versus paste. The solution was filtered a second time at the same pore size, and the plugging metric fell to 1.08, identical to its previous level (Figure 5-32). The solution was thus deemed fit for use.

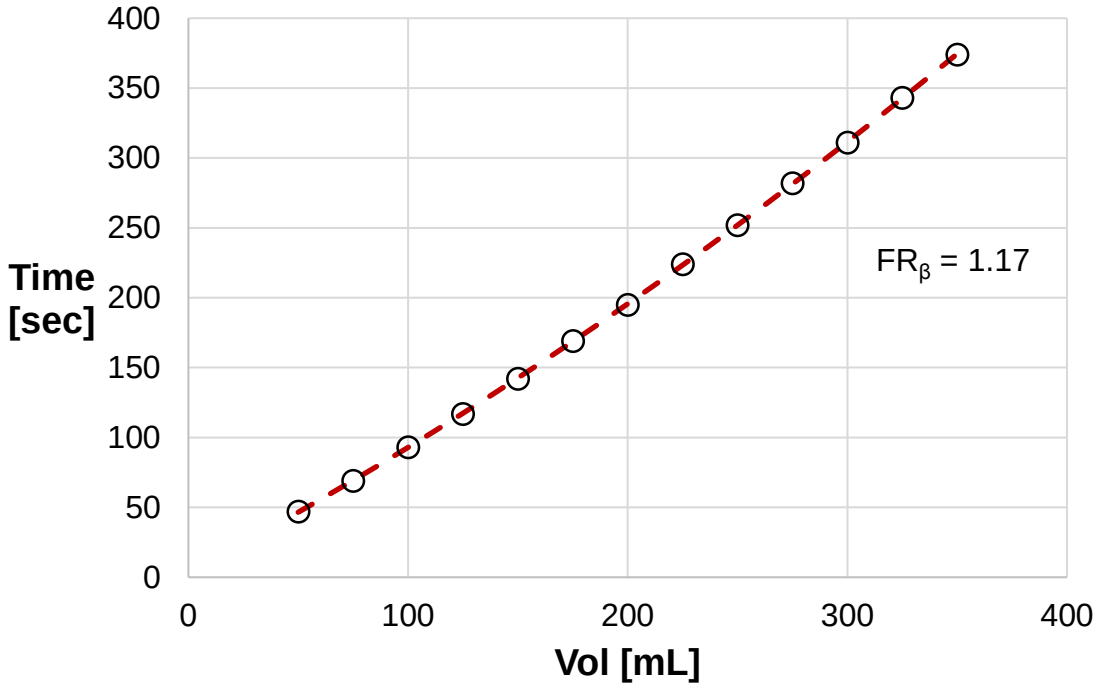

Figure 5-31: First filtration (0.65 microns) of polymer slug for SCL-09

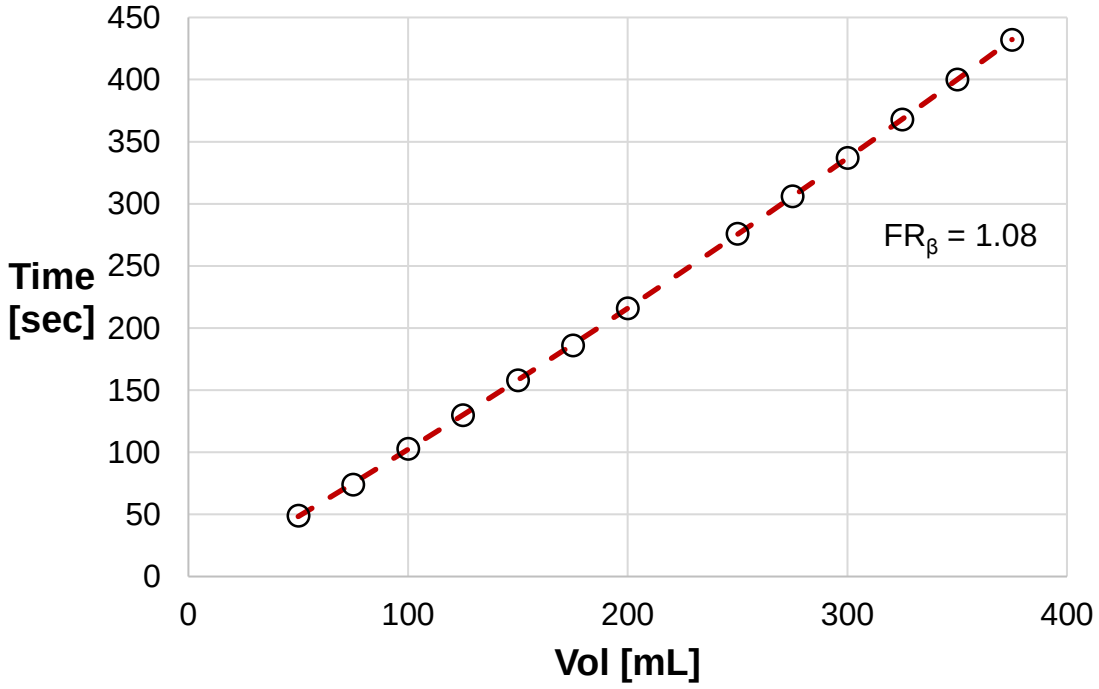

Figure 5-32: Second filtration (0.65 microns) of polymer slug for SCL-09

The scleroglucan solution lost no viscosity through the two filtrations (Figure 5-29, black and blue lines). After argon bubbling, dithionite addition, column loading, and overnight heating at 95ºC, the viscosity of the polymer was checked and found to be slightly higher (45.8 cP versus 43.5 cP @ 10 s^{-1}; Figure 5-29, red line). Evaporation may have been responsible.

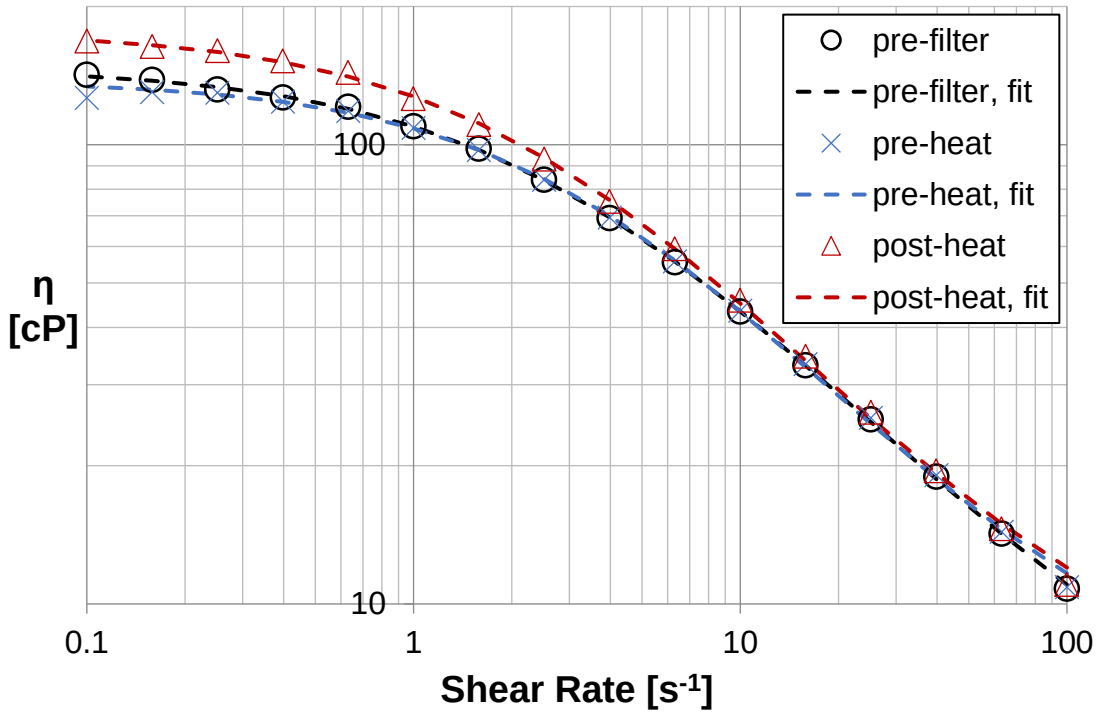

Figure 5-33: Slug viscosities for SCL-09

The heated polymer was injected at a frontal velocity of 3 ft/d (rather than 2 ft/d) to expedite the plugging diagnosis (Figure 5-34). At 3 pore volumes injected, the flow rate was reduced to 2 ft/d to establish the long-time pressure plateau. The column needed replenishing after 5 pore volumes of injection, so the flood was paused for this operation.

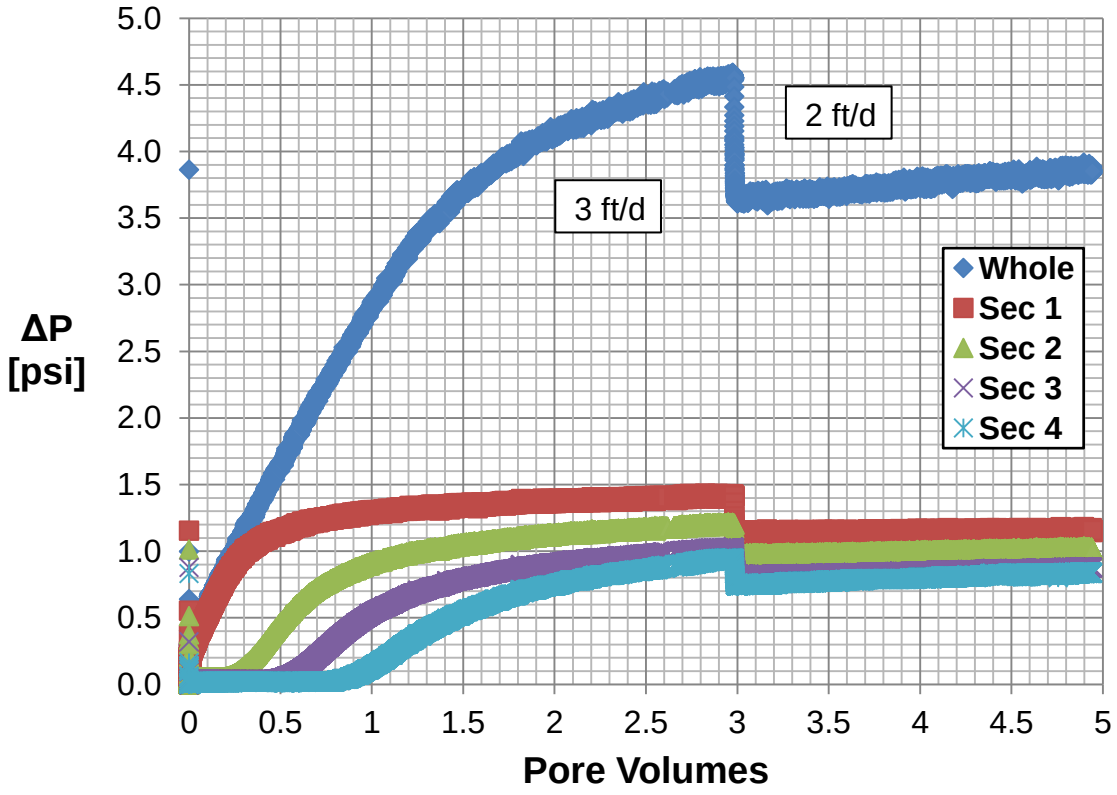

Figure 5-34: SCL-09 pressure drops during injection of polymer slug

After reloading and reheating the column, the flood was resumed at 1 ft/d for 1.7 pore volumes, enough for the pressure to stabilize at 2.56 psi (Figure 5-35). Subsequently, flow was increased to 2 ft/d and 4 ft/d.

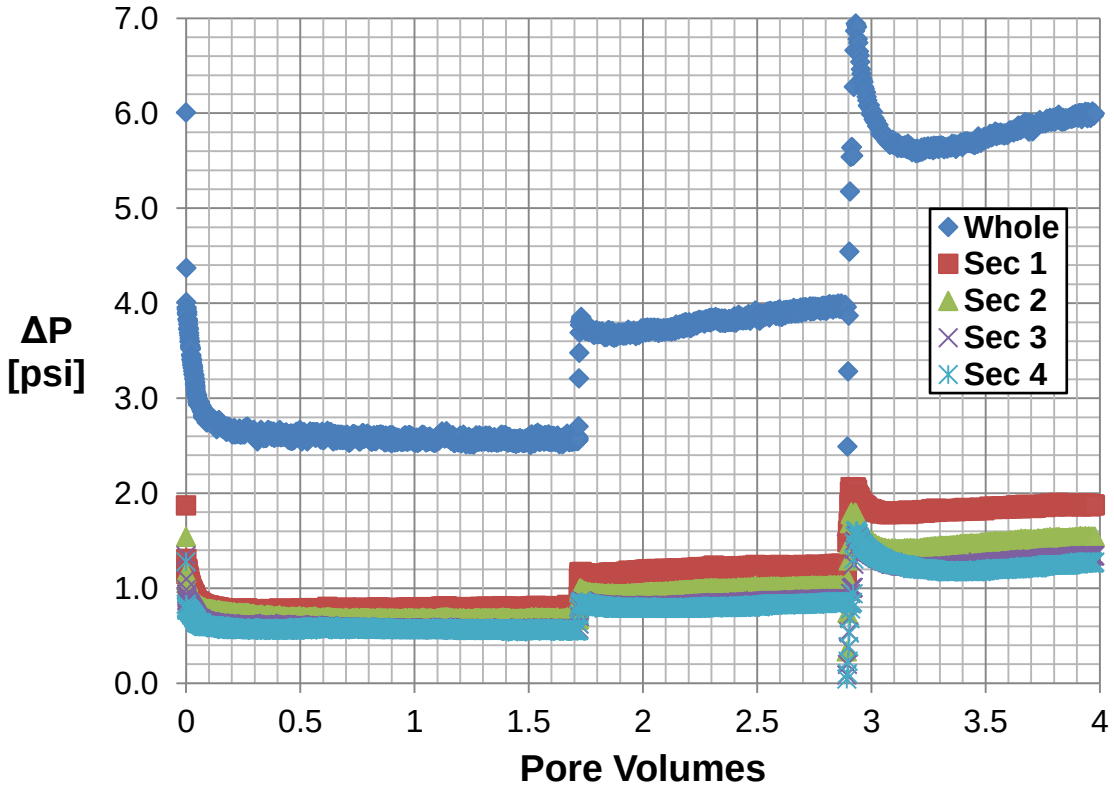

Figure 5-35: SCL-09 pressure drops during continued injection of polymer slug

From these data, effective viscosities were calculated and plotted against those measured in the rheometer (Figure 5-36). A shear correction factor value of C = 2.4 gives a reasonable description of the core rheological behavior.

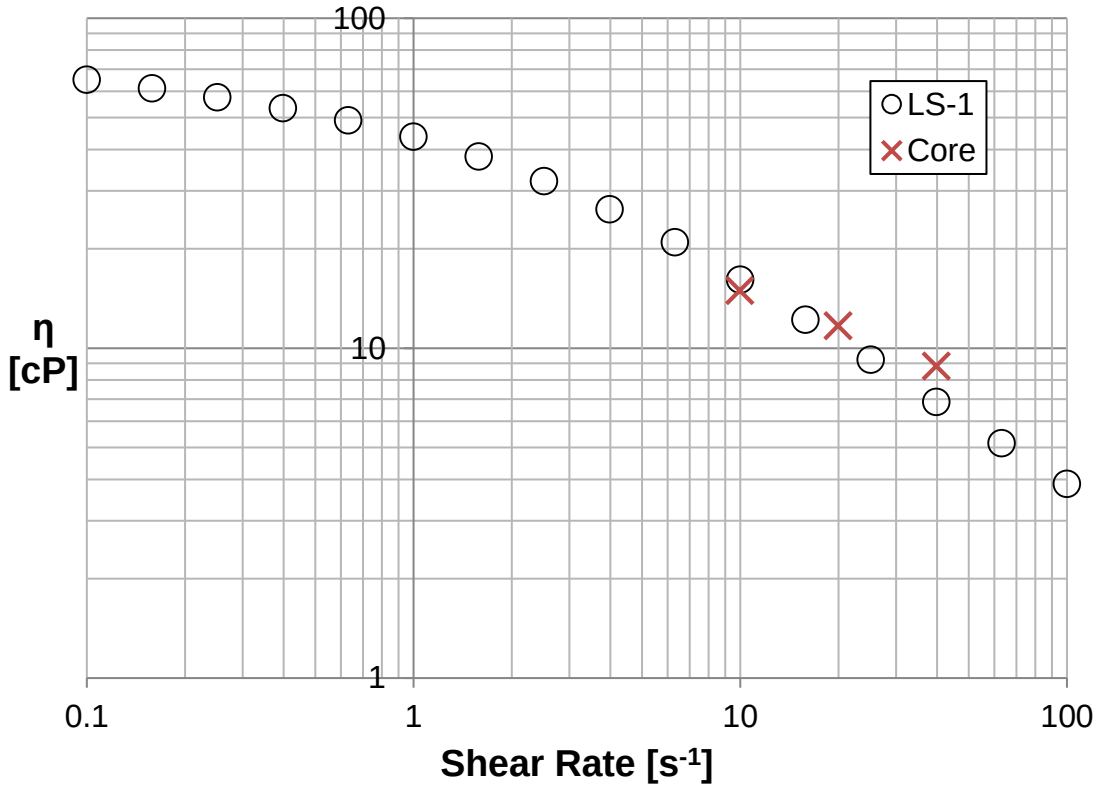

Figure 5-36: SCL-09 apparent viscosities versus LS-1 shear viscosities

Effluent viscosities were measured to estimate the retention (Figure 5-37), with the same viscosity-to-concentration conversion as in SCL-06. The lower initial viscosity relative to SCL-06 accounts for the difference in the estimated concentration (922 ppm versus 1000 ppm), but is justified for comparison to the results of SCL-06. As is clear from the protracted tail in the core pressure drop and effluent viscosity data, the retention in this flood is higher than in SCL-06. The integration procedure estimates 55.9 µg/g. Therefore, while polymer transport was acceptable in this core from the standpoint of mechanical retention, adsorption was higher than desirable. Since the only significant differences between this flood and SCL-06 was the rock and the reduction procedure, the increase in

adsorption is most likely due to differences in the mineralogy and oxidation state presented in the pore space. For instance, the Buff Berea rock used in this flood contains much more iron and perhaps other reducible species as judged from the copious amounts of reduction buffer required to achieve low ORP, and from previous laboratory floods with EDTA-rich reduction buffer that removed tremendous amounts of iron, as detected in effluent samples using colorimetric strips.

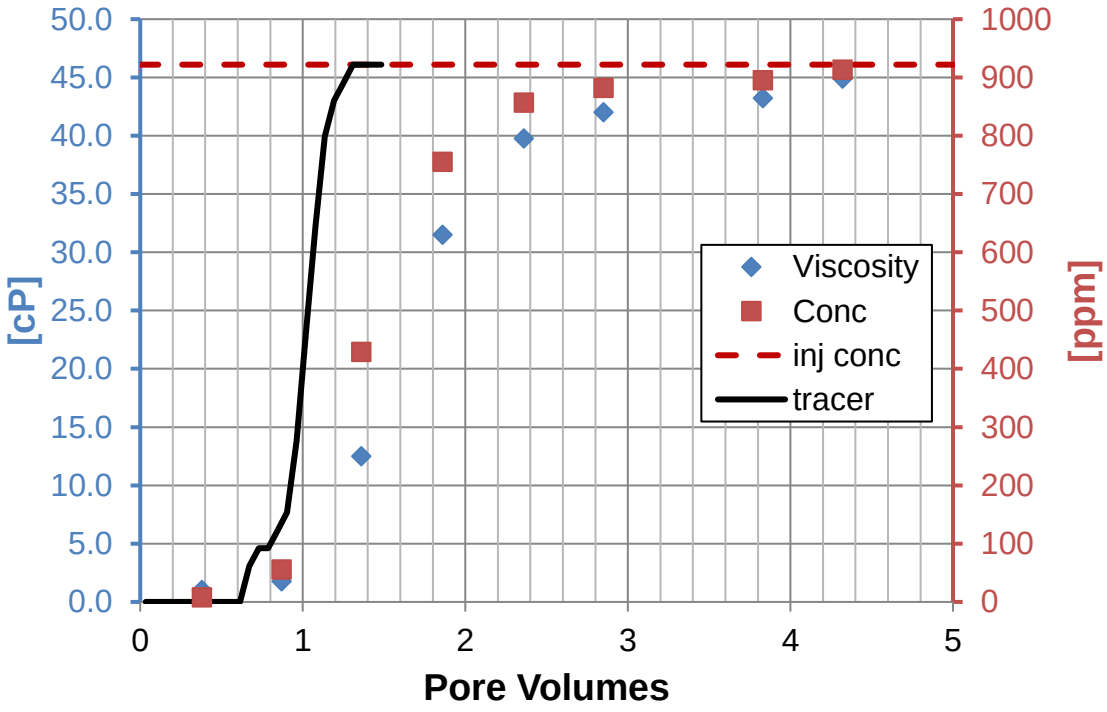

Figure 5-37: SCL-09 retention estimation

5.4 Chapter Conclusions

1. Serial flooding with polymer slugs of ascending viscosity and polymer size is a viable way to determine the limits of polymer injectivity.
2. Pore size distributions inferred from mercury injection data are a better guide to polymer injectivity limits than permeability, as low permeability sandstones with unusually large pores may permit injection of unsheared, high molecular weight polymers (CT-01 flood).
3. A carefully sheared and filtered HPAM solution tailored for excellent transport in a 30 millidarcy sandstone (CT-01 flood) produces no permeability reduction and requires no apparent shear correction from the bundle of capillary tubes model.
4. Shearing optimization of filtrate viscosity can be used to produce highly injectable polymer solutions with viscosities sufficient for ASP floods, even with filters as tight as a 0.10 μm pore size cellulose filter.
5. Optimized, filtered polymer solutions can be injected into very low permeability carbonate reservoir cores with negligible plugging.
6. Scleroglucan has a volume similar to that of FP3330S, though its transport and plugging behavior in porous media has been poor by comparison.
7. With current preparation procedures for homogenization and filtration and at high temperatures (preferably $\geq$ 95°C), the scleroglucan supplied by Cargill will transport well in laboratory sandstone cores of at least ~220 millidarcys, perhaps lower.

8. Plugging can be analyzed and diagnosed via effluent viscosity and sectional pressure drops. For the face plugging encountered in core flood SCL-08, comparison with laboratory filtration data permitted an estimation of the thickness of the rock section responsible for filtration of the high-molecular weight polymer from solution (8 mm).

6 Conclusions, Discussion and Recommendations

6.1 Conclusions

6.1.1 Shearing and Filtration

Filtration of polymer solutions in the laboratory is a powerful technique that is currently underleveraged. Filtration time course measurements yield informative, physically interpretable information about polymer plugging when a simple theory (developed in this thesis) is applied. Filterability with pore size is likely the most pertinent way to determine whether a polymer solution will plug pores of a certain size. Alterations to polymer solutions can be quantitatively assessed using a suite of filtrations across filter pore sizes. Salient points include:

- Mechanical shearing of HPAM solutions for filterability improvement. These experiments reveal the extent of the shift in the high end of the molecular weight distribution as a function of viscosity. Such shifts are useful for predicting filterability both on filter papers and in cores.
- Decreasing salinity causes HPAM to swell, which predictably causes an increase in plugging at small filter pore sizes. Interestingly, there is a pore size threshold above which plugging does not increase, even when some plugging is detected in both high and low salinity solutions.
- Post-synthesis hydrolysis also causes HPAM to swell, and produces similar changes in filterability to the salinity reduction explored. In the particular case investigated, the post-hydrolyzed polymer filtered with a *less* plugging than an

unmodified HPAM of the same viscosity and concentration. Matching viscosity and concentration implicates single-molecule shape as a factor in the pore-size-dependent plugging of filter membranes. Whether this is something that occurs in porous media remains unexplored.

- Scleroglucan filters with quantitatively lower levels of plugging than HPAM of a similar single-molecule volume in solution, as assessed by intrinsic viscosity. Scleroglucan is extremely shear thinning, making filtration flow rates between HPAM and scleroglucan difficult to match in the laboratory. This remains an explanation for the discrepancy. In cores, scleroglucan plugs as a much larger polymer than an equal-volume HPAM.

6.1.2 Core Flooding

Core flooding is the gold standard for evaluating polymer transport (among many other things) in the laboratory. The experiments described in this thesis begin to establish the rational, quantitative application of shearing and filtration to the preparation of polymers for core floods, though much more needs to be done. The experiments described in chapter 5 demonstrate that:

- Pore size distributions inferred from MICP data can be a better guide to predicting polymer plugging than permeability.
- Polymer solutions tailored to transport through low permeability (~30 millidarcy) sandstones using filtration and mechanical degradation can give no permeability

reduction and require no shear correction relative to the bundle of capillary tubes model. We are unaware of another instance of this in the literature.

- The viscosity of filtrates can be preserved by pre-shearing, and optimization for tight filters (even 0.10 μm) can produce solutions that meet the needs of chemical EOR core flood experiments.
- Tight filtration can prepare polymer solutions for injection into reservoir cores of extremely low permeability (approaching 10 millidarcys).
- Scleroglucan can be prepared by high-shear homogenization and tight, low-pressure filtration to transport in sandstone cores of at least 220 millidarcys without plugging, and potentially lower permeability (105 millidarcys plugged). Scleroglucan polymer floods should be conducted at 95°C or higher to combat adsorption.

6.2 Discussion

The experiments presented in this thesis form a practical guide to the preparation and analysis of polymer solutions for injection into laboratory cores. Pore size distribution, inferred from capillary pressure or perhaps by other means, is the best tool for predicting the single-molecule limit of injectivity, which can be used as a point of reference for filter selection. Mechanical shear degradation is very useful for optimizing the molecular weight distribution of a polymer solution for maximum filtrate viscosity. Filtration, in turn, is useful as both a processing and an analytical technique. A suite of filtrations across a range of pore sizes is particularly useful for building a picture of the shape of the high end of the polymer molecular weight distribution, and permits a more nuanced comparison of

different polymer solutions. It can be used to quantitate the extent to which shearing improves filterability, or how changes in polymer swelling affect plugging in a manner dependent on pore size. Naturally, it can also be used to quantitate filterability improvement due to preceding filtrations as well. This is practically important for assessing filter performance between filters of different types.

Mapping out the relationship between a polymer's filterable size and its transport in a laboratory core will require significantly more data than could be undertaken in one thesis study. The core floods presented herein provide interesting and promising fodder for analysis and discussion. They demonstrate that high molecular weight polymers can indeed be injected into low permeability rocks if the pore size distribution permits (Experiment CT-01), and that quantitative plugging metrics on laboratory filters may scale between rocks based on the relative pore size difference (SAMA-13R compared to CT-01). It is also clear that the filterable size of different types of polymers cannot yet be compared directly, as the plugging limit for scleroglucan appears to be as much as ~7x higher (in permeability terms, see SCL experiments) than that for FP3330S, the similarly-sized HPAM product. This is still a step forward for scleroglucan, one that makes it viable for injection in more reservoirs than before, and further improvements and advances should not be ruled out. It is also important to remember that scleroglucan's selling point is its tolerance for harsh reservoir conditions, something that was not emphasized here.

Much of the work in this thesis is subject to a pointed, two-fold criticism: the preparatory techniques used to create injectable polymer solutions cannot be replicated in the field, and empirical evidence suggests that, for some reason, polymer solutions that

plug reservoir cores in the laboratory may have acceptable injectivity in the field. However, laboratory core floods are the pertinent experimental design for oil recovery deep in the reservoir away from the near wellbore. Core flood experiments are also essential for other reasons such as testing of surfactants in reservoir cores, and such tests cannot be properly interpreted without good polymer transport.

It is likely that filtration of the polymer solution occurs near the wellbore when the formation permeability is low and/or the quality of the injected polymer solution is not high. For this as well as other reasons, it makes sense to test polymer solutions in core floods after they have been filtered and/or sheared in the laboratory. Such tests are at the moment an indispensable laboratory procedure. These experimental results provide a clue as to why field injectivity sometimes appears to be better than in the laboratory. Specifically, the experimental results in this thesis clearly show that if a polymer solution is filtered with tight filter A and loses a significant portion of its viscosity, that it can be filtered with a less tight filter B before filtration by A and lose less viscosity than by filtration through A alone. This is illuminating, and one could imagine what might happen with a continuum of filters rather than a discrete pairing. Polymer that first passes through reservoir layers of greater permeability and pore size before flowing into lower permeability layers may experience a graded filtration that cannot be easily replicated in the laboratory. It is also notable that polymer injectivity is nearly always augmented in the field in the traditional sense (flow rate that can be achieved ignoring plugging), most likely due to the formation of small fractures and deconsolidation of grains near the wellbore in response to stresses induced by the highly non-Newtonian polymer (Ma & McClure, 2017).

Such mechanical responses may help to maintain injectivity even when mild plugging occurs during injection. Furthermore, some degree of shear degradation almost always occurs in the mixing and injection facilities. This reality should also be taken into account when designing laboratory experiments.

As decades pass and conventional oil fields continue to age, interest in enhanced oil recovery techniques should only intensify. With this intense interest come intense demands on where these recovery techniques will be used and the percentage of remaining oil they will be able to recover to compete with other means of oil production. To stay relevant, polymers must venture into increasingly inhospitable environments and rocks. As with virtually any venture in the oil and gas industry, stasis eventually ensures obsolescence.

6.3 Recommendations for Future Work

The ultimate goal of predicting the plugging behavior of any given polymer solution in any given laboratory core needs much more experimental support. The problem is still best handled with single-phase injectivity testing as the cleanest, most interpretable experimental design. The simplest way to characterize the filtration behavior of a core is to measure the concentration of polymer in the eluate, and to compare that to the concentration of polymer in filtrates from filters over the range of pore sizes used in the pore size assay to generate an "effective" filter pore size of the core. A suggested workflow:

- Measure pore size distribution in plugs (ideally multiple) from a candidate rock.

- Measure plugging of a polymer solution likely to plug cores from the rock in the serial filtration pore size assay. Measure filtrate viscosity and polymer concentration as well.
- Cut a core or cores from the candidate rock for polymer flooding. Use polymer concentration in the eluate to establish an effective filter pore size of the rock.
- Repeat many times for many cores from many sources. Develop correlations between pore size distribution and effective filter pore size.
- Examine data from previous core floods with pore size information for plugging or lack thereof. Use pore size information to predict effective filter pore size. Recreate polymer solutions used in those floods to quantitate in the filtration pore size assay. Correlate plugging behavior of polymer solutions on filters to the predicted effective filter pore size of the rocks.
- Only one HPAM polymer was tested in this research. This particular polymer has been used extensively in both the laboratory and field and is one of the highest quality polymers of its type that is commercially available. The behavior of other HPAM polymers cannot be assumed to be the same let alone other co-polymers or ter-polymers of acrylamide. The same methods developed and illustrated in this thesis can and should be applied to other polymers as part of their basic testing and characterization for chemical EOR.

7 Works Cited

Al Hashmi, A. R., Al Maamari, R. S., Al Shabibi, I. S., Mansoor, A. M., Zaitoun, A., & Al Sharji, H. H. (2013). Rheology and mechanical degradation of high-molecular-weight partially hydrolyzed polyacrylamide during flow through capillaries. *Journal of Petroleum Science and Engineering, 105*, 100-106.

Bird, R. B., Stewart, W. E., & Lightfoot, E. N. (1960). *Transport Phenomena.* New York: John Wiley and Sons, Inc.

Burdine, N. T., Gournay, L. S., & Reichertz, P. P. (1950). Pore Size Distribution of Petroleum Reservoir Rocks. *Journal of Petroluem Technology, 2*(7), 195-204.

Cannella, W. J., Huh, C., & Seright, R. S. (1988). Prediction of Xanthan Rheology in Porous Media. *SPE Annual Technical Conference and Exhibition.* Houston. doi:10.2118/18089-MS

Carreau. (1972). Rheological Equations from Molecular Network Theories. *Transactions of the Society of Rheology, 16*(1), 99-127.

Davison, P., & Mentzer, E. (1982). Polymer Flooding in North Sea Reservoirs. *SPE Journal, 22*(3), 353-362.

de Gennes, P. G. (1971). Reptation of a Polymer Chain in the Presence of Fixed Obstacles. *Journal of Chemical Physics, 55*(2), 572-579.

Dillon, P., Pavelic, P., Massmann, G., Barry, K., & Correll, R. (2001). Enhancement of the Membrane Filtration Index (MFI) Method for Determining the Clogging Potential of Turbid Urban Stormwater and Reclaimed Water Used for Aquifer Storage and Recovery. *Desalination, 140*(2), 153-165.

Farajzadeh, R., Bedrikovetsky, P., Lotfollahi, M., & Lake, L. (2016). Simultaneous sorption and mechanical entrapment during polymer flow through porous media. *Water Resources Research, 52*, 2279-2298.

Flory, P. J. (1953). *Principles of Polymer Chemistry.* Ithica: Cornell University Press.

Gogarty, W. B. (1967). Mobility Control with Polymer Solutions. *SPE Journal, 7*(2), 161-173.

Hiemenz, P. C., & Lodge, T. P. (2007). *Polymer Chemistry, 2nd Ed.* Boca Raton: CRC Press.

Hirasaki, G. J., & Pope, G. A. (1974). Analysis of Factors Influencing Mobility and Adsorption in the Flow of Polymer Solution Through Porous Media. *SPE Journal, 14*(4), 337-346.

Horn, A. F., & Merrill, E. W. (1984). Midpoint scission of macromolecules in dilute solution in turbulent flow. *Nature, 312*, 140-141.

Jouenne, S., Chakibi, H., & Levitt, D. (2015). Polymer Stability Following Successive Mechanical Degradation Events. *18th European Symposium on Improved Oil Recovery.* Dresden: EAGE. doi:10.3997/2214-4609.201412151

Kalpakci, B., Jeans, Y. T., Magri, N. F., & Padolewski, J. P. (1990). Thermal Stability of Scleroglucan at Realistic Reservoir Conditions. *SPE/DOE Enhanced Oil Recovery Symposium* (pp. 603-613). Tulsa: SPE. doi:10.2118/20237-MS

Koh, H., Lee, V. B., & Pope, G. A. (2017). Experimental investigation of the effect of polymers on residual oil saturation. *SPE Journal*. doi:10.2118/179683-PA

Kohler, N., & Chauveteau, G. (1981). Xanthan Polysaccharide Plugging Behavior in Porous Media - Preferential Use of Fermentation Broth. *Journal of Petroleum Technology, 33*(2), 349-358.

Kulawardana, E. U., Koh, H., Kim, D. H., Liyanage, P. J., Upamali, K., & Huh, C. (2012). Rheology and Transport of Improved EOR Polymers under Harsh Reservoir Conditions. *SPE Improved Oil Recovery Symposium.* Tulsa: SPE. doi:10.2118/154294-MS

Lee, V. B. (2015, August). The Development and Evaluation of Polymers for Enhanced Oil Recovery. *MS Thesis*. University of Texas at Austin.

Levitt, D. B. (2009, May). The Optimal Use of Enhanced Oil Recovery Polymers Under Hostile Conditions. *PhD Dissertation*. University of Texas at Austin.

Levitt, D. B., & Pope, G. A. (2008). Selection and Screening of Polymers for Enhanced-Oil Recovery. *SPE Symposium on Improved Oil Recovery.* Tulsa: SPE. doi:10.2118/113845-MS

Levitt, D. B., Pope, G. A., & Jouenne, S. (2011). Chemical Degradation of Polyacrylamide Polymers Under Alkaline Conditions. *SPE Reservoir Evaluation & Engineering, 14*(3), 281-286.

Ma, Y. W., & McClure, M. W. (2017). The effect of polymer rheology and induced fracturing on injectivity and pressure-transient behavior. *SPE Reservoir Evaluation and Engineering, 20*(2), 394-402.

Maerker, J. M. (1975). Shear Degradation of Partially Hydrolyzed Polyacrylamide Solutions. *SPE Journal, 15*(4), 311-322.

Mansour, A. M., Al-Maamari, R. S., Al-Hashmi, A. S., Zaitoun, A., & Al-Sharji, H. (2014). In-Situ Rheology and Mechanical Degradation of EOR Polyacrylamide Solutions under Moderate Shear Rates. *Journal of Petroleum Science and Engineering, 115*, 57-65.

Martin, F. D., & Sherwood, N. S. (1975). Effect of Hydrolysis of Polyacrylamide on Solution Viscosity, Polymer Retention and Flow Resistance Properties. *SPE Rocky Mountain Regional Meeting.* Denver: SPE. doi:10.2118/5339-MS

Morel, D., Vert, M., Jouenne, S., & Nahas, E. (2008). Polymer Injection in Deep Offshore Field: The Dalia Angola Case. *SPE Annual Technical Conference and Exhibition.* Denver: SPE. doi:10.2118/116672-MS

Noik, C., Delaplace, P., & Muller, G. (1995). Physico-Chemical Characteristics of Polyacrylamide Solutions after Mechanical Degradation through a Porous Medium. *SPE International Symposium on Oilfield Chemistry* (pp. 93-100). San Antonio: SPE. doi:10.2118/28954-MS

Pope, G. A. (1980). The Application of Fractional Flow Theory to Enhanced Oil Recovery. *SPE Journal, 20*(3), 191-205.

Purcell, W. R. (1949). Capillary Pressures - Their Measurement using Mercury and the Calculation of Permeability Therefrom. *Petroleum Transactions, AIME, 1*(2), 39-48.

Qi, P., Ehrenfried, D. H., Koh, H., & Balhoff, M. T. (2017). Reduction of Residual Oil Saturation in Sandstone Cores by Use of Viscoelastic Polymers. *SPE Journal, 22*(2), 447-458.

Rajapkesha, S., Britton, C., McNeil, R. I., Kim, D. H., Unomah, M., Kulawardana, E., . . . Pope, G. A. (2014). Restoration of Reservoir Cores to Reservoir Condition before Chemical Flooding Tests. *SPE Improved Oil Recovery Symposium.* Tulsa: SPE. doi:10.2118/169887-MS

Rehm, B. H. (2009). *Microbial Production of Biopolymers and Polymer Precursors: Applications and Perspectives.* Norfolk: Caister Academic Press.

Rivenq, R. C., Donche, A., & Noik, C. (1992). Improved Scleroglucan for Polymer Flooding under Harsh Reservoir Conditions. *SPE Reservoir Engineering, 7*(1), 15-20.

Smith, F. W. (1970). The Behavior of Partially Hydrolyzed Polyacrylamide Solution in Porous Media. *Journal of Petroleum Technology, 22*(2), 148-156.

Sodeifian, G., Daroughegi, R., & Aalaie, J. (2015). Study of Adsorptive Behavior of Sulfonated Polyacrylamide onto Carbonate Rock Particles to Enhance Oil Recovery. *Korean Journal of Chemical Engineering, 32*(12), 2484-2491.

Sorbie, K. S. (1991). *Polymer-Improved Oil Recovery.* Boca Raton: CRC Press.

Southwick, J. G., & Manke, C. W. (1988). Molecular Degradation, Injectivity, and Elastic Properties of Polymer Solutions. *SPE Reservoir Engineering, 3*(4), 1193-1201.

Wellington, S. L. (1983). Biopolymer Solution Viscosity Stabilization. *SPE Journal, 23*(6), 901-912.

Wreath, D. G. (1989, December). A Study of Polymer Flooding and Residual Oil Saturation. *MS Thesis*. University of Texas at Austin.

Yerramilli, S. S., Zitha, P. L., & Yerramilli, R. C. (2013). Novel insight into polymer injectivity for polymer flooding. *SPE European Formation Damage Conference & Exhibition.* Noordwijk: SPE. doi:20.2118/165195-MS

Zaitoun, A., Makakou, P., Blin, N., Al-Maamari, R. S., Al-Hashmi, A. R., Abdel-Goad, M., & Al-Sharji, H. H. (2012). Shear Stability of EOR Polymers. *SPE Journal, 17*(2), 335-339.

Zentz, F., Verchere, J.-F., & Muller, G. (1992). Thermal denaturation and degradation of schizophyllan. *Carbohydrate Polymers, 17*, 289-297.

Zhang, G., & Seright, R. (2014). Effect of Concentration on HPAM Retention in Porous Media. *SPE Journal, 19*(3), 373-380.